PRECISION DETERMINATION

OF PHOTONEUTRON THRESHOLDS

by
Milton Birnbaum

Thesis submitted to the Faculty of the Graduate School
of the University of Maryland in partial
fulfillment of the requirements for the
degree of Doctor of Philosophy

1953

ProQuest LLC.
789 East Eisenhower Parkway
P.O. Box 1346
Ann Arbor, MI 48106 - 1346

ACKNOWLEDGEMENTS

It is a pleasure to thank Professor Jules R. de Launay for his supervision of this work; Dr. Leo Seren, not only for suggesting the problem but also for helpful guidance; Dr. Erich M. Harth for many stimulating discussions and helpful suggestions; Dr. Warren L. Bendel for carefully reading the manuscript and suggesting numerous improvements; Mr. Ralph A. Tobin for maintaining the betatron; and the entire Naval Research Laboratory organization for their generous cooperation.

TABLE OF CONTENTS

Chapter		Page
1.	MEASUREMENT OF THE PHOTONEUTRON REACTION THRESHOLD	1
	1.1 Introduction	
	1.2 Significance of the Photoneutron Threshold Measurements	
	1.3 Method of Measurement of the Photoneutron Threshold	
	1.4 Photoneutron Threshold Measurements of Baldwin and Koch	
	1.5 Photoneutron Threshold Measurements of McElhinney, et al.	
	1.6 Photoneutron Threshold Measurements of Sher, et al.	
	1.7 Purpose of Present Work	
2.	APPARATUS	15
	2.1 Description of Betatron and Control Circuits	
	2.2 Equipment for Measurement of Sample Activity	
	2.3 Samples, Sample Holders and Considerations of Geometry	
	2.4 Monitoring the x-ray Beam	
	2.5 Control of the Peak x-ray Energy	
3.	EXPERIMENTAL PROCEDURE	34
	3.1 Alignment of the Sample	
	3.2 Performance of Counting Equipment	
	3.3 Irradiation and Counting Schedule	
	3.4 Calculation of Effect of x-ray Intensity Variations	

Chapter Page

3.5 Reproducibility of Geometry

3.6 Reproducibility of Activations

3.7 Monitoring the Peak x-ray Energy

3.8 Other Factors Affecting the Peak x-ray Energy

4. PHOTONEUTRON THRESHOLD DETERMINATION OF Cu^{63} . 48

4.1 Introduction

4.2 Half-life of Cu^{62}

4.3 Correction for Different Exposure Times

4.4 Cu^{62} Activation Curve

4.5 Threshold determination by log-log Analysis

4.6 Other Cu^{63} Threshold Determinations

5. PHOTONEUTRON THRESHOLD DETERMINATION OF Ag^{109} . 62

5.1 Introduction

5.2 Half-lives of Ag^{108} and Ag^{106}

5.3 Correction for 24 min. Ag^{106} Activity

5.4 Ag^{108} Activation Curve

5.5 Threshold Determination by log-log Analysis

5.6 Repeat Determination of Ag^{109} Threshold

5.7 Summary of Cu^{63} and Ag^{109} Threshold Determinations

6. PHOTONEUTRON THRESHOLDS OF C^{12}, N^{14}, O^{16} . . . 76

6.1 O^{16} Threshold Determination

6.2 N^{14} Threshold Determination

6.3 C^{12} Threshold Determination

Chapter Page

6.4 Summary

7. EXPERIMENTAL RESULTS 102

7.1 Photoneutron Threshold Values of Cu^{63} and Ag^{109}

7.2 Proof of method of Cu control activity

7.3 Non-linearity of Energy Scale

7.4 Summary

APPENDIX 113

LITERATURE CITED 119

LIST OF TABLES

Table		Page
1.	Disc Thickness Data.	26
2.	Effect of x-ray Beam Intensity Variations.	40
3.	Effect of x-ray Beam Intensity Variations.	41
4.	Cu^{63} Threshold Determination No. 2.	55
5.	Cu^{63} Threshold by log-log Analysis.	58
6.	Cu^{63} Threshold Determination No. 1.	60
7.	Cu^{63} Threshold Determination No. 3.	61
8.	Control Data for Ag^{109} Threshold No. 1.	67
9.	Ag^{109} Threshold Determination No. 1.	70
10.	Ag^{109} Threshold by log-log Analysis.	73
11.	Ag^{109} Threshold Determination No. 2.	75
12.	Comparison of Values of Exponent.	69
13.	O^{16} Threshold Determination No. 1.	80
14.	O^{16} Threshold Determination No. 2.	83
15.	N^{14} Threshold Determination No. 1.	87
16.	N^{14} Threshold Determination No. 2.	90
17.	Half-Lives of Polyethylene Discs near Threshold.	94
18.	C^{12} Threshold Determination No. 1.	98
19.	C^{12} Threshold Determination No. 2.	101
20.	Thresholds Based on N^{14}, O^{16}, C^{12} Determinations No. 1.	103
21.	Thresholds Based on N^{14}, O^{16}, C^{12} Determinations No. 2.	104
22.	Cu^{63} and Ag^{109} Threshold Values.	105
23.	Validity of Method of Cu Control Activity.	107

LIST OF FIGURES

Figure		Page
1.	Experimental Arrangement used by Sher, Halpern and Mann (10).	10
2.	Naval Research Laboratory 22-Mev Betatron.	17
3.	Betatron Control Panel.	18
4.	Apparatus for Measurement of Sample Activity.	19
5.	Sample Holders.	21
6.	Position of Disc during Irradiation.	23
7.	Samples and Sample Receptacles.	24
8.	2050 Thyratron Trigger Circuit.	31
9.	8000-volt Alternating Current Power Supply.	33
10.	Autoradiograph of Irradiated Cu Disc.	35
11.	Reproducibility of Cu^{62} Activity near Threshold.	44
12.	Cu Control Activation Curve.	46
13.	Cu^{62} Decay Curve.	50
14.	Cu^{62} Activation Curve.	56
15.	Cu^{62} Activation Curve near Threshold.	57
16.	Log-log Analysis of Cu^{62} Activation Curve.	59
17.	Ag^{108} Decay Curve.	64
18.	Ag^{106} Decay Curve.	65
19.	Ag^{108} Activation Curve.	71
20.	Ag^{108} Activation Curve near Threshold.	72
21.	Log-log Analysis of Ag^{108} Activation Curve.	74
22.	O^{15} Decay Curve.	77

Figure		Page
23.	O^{15} Activation Curve.	81
24.	O^{15} Activation Curve near Threshold.	82
25.	N^{13} Decay Curve.	85
26.	N^{13} Activation Curve.	88
27.	N^{13} Activation Curve near Threshold.	89
28.	C^{11} Decay Curve.	92
29.	C^{11} Activation Curve.	99
30.	C^{11} Activation Curve near Threshold.	100
31.	Effect of Magnet Amplitude on Cu Activity at Fixed Helipot Setting	109
32.	Flux Integrator Stack Arrangement.	117
33.	Block diagram of Expander System.	118

CHAPTER I

MEASUREMENT OF THE PHOTONEUTRON REACTION THRESHOLD

1.1 Introduction

The threshold energy for the photoneutron reaction is identical with the binding energy of a neutron in an atomic nucleus. Among the reactions from which neutron binding energies can be obtained, are: (p, d), (d, t), (γ, n), (d, p) and (n, γ).[1] In the first three reactions, a neutron is removed from the target nucleus; in the latter two a neutron is added. Harvey (1) has summarized the data for 80 isotopes. Of these 38 have been investigated by the photoneutron reaction (2, 3, 4, 5, 6, 7, 8, 9). In general, those reactions in which the incident particles are charged yield either upper or lower limits because it is difficult to be sure that direct transitions to the ground state are involved. The (γ, n) reaction offers the possibility of greater precision, a fact which is indicated by the summary of Harvey (1).

1.2 Significance of the Photoneutron Threshold Measurements

The measurement of the neutron binding energy is a method of establishing mass differences with great accuracy. In conjunction with other data, it permits the assignment of mass values to intermediate

---

[1] Nuclear reactions are often written symbolically in the form Cu^{63} (γ, n) Cu^{62}. This is a shorthand way of stating that Cu^{63} is the target nucleus; γ-rays (photons) are the bombarding particles, neutrons are the ejected particles and the residual nucleus is Cu^{62}.

and heavy nuclei. In the case of photoneutron reactions, the only data required is the mass of the target nucleus.

Considerable evidence has been obtained which definitely indicates a shell structure model for the nucleus (11). The shell model implies that when a shell is completed a nucleus of high stability is formed (high binding energy) and when a new shell is begun, the binding energy of the newly added particles will be less than that of the particles which completed the shell. The experimental results show sharp decreases of about 2 Mev at the 127th neutron and 51st neutron. There is also a drop in the region of 82 neutrons. The evidence for a closed shell of 28 neutrons is not very conclusive. Thus, the neutron binding energies offer direct experimental evidence for the shell structure model with closed shells at 50, 82 and 126 neutrons.

Much information concerning the structure of the nucleus and the mechanism of photonuclear reactions can be obtained from the activation curves which are used in determining the photoneutron thresholds. It has been found that the activation curves for C^{11} and O^{15} consist of straight line sections (12, 23). The discontinuous changes in slope are interpreted as evidence for energy levels in the C^{12} and O^{16} nuclei.

1.3 Method of Measurement of the Photoneutron Threshold

Thresholds can be measured by observing the yield of induced activity or neutrons as a function of the peak x-ray energy. Betatrons were used, in most experiments, to produce the required x-rays. A description of the production of x-rays by means of a betatron is described

in Section 2.1.

When the x-rays have an energy greater than the photoneutron threshold energy, neutrons are ejected from the bombarded nuclei. In many cases, the daughter nucleus will be radioactive. Thus, the activation curves may be obtained by plotting the yield of activity or neutrons as a function of the peak x-ray energy. In the present work, the first method was used.

1.4 Photoneutron Threshold Measurements of Baldwin and Koch

The first measurements of photoneutron thresholds were obtained by Baldwin and Koch (2) at the University of Illinois using the first 22 Mev betatron.[2] The yield of activity was plotted as a function of the peak x-ray energy which resulted in a curve from which the threshold was obtained by inspection. The method involved the problems of (a) accurate control of peak x-ray energy (b) monitoring the x-ray intensity (c) detection of the reaction (d) calibration of the energy scale of the betatron.

In order to control the peak x-ray energy, Baldwin and Koch made use of the fact that the energy acquired by the electrons during acceleration in the betatron is proportional to the magnetic flux linking their orbit, which, in turn, is proportional to the flux linking the main coils (13, 14). A series resistance and capacitance was placed across one of the main coils with a time constant large compared with the period of the

---

[2] A betatron, so called because it accelerates electrons, was first successfully built by D. W. Kerst in 1940 at the University of Illinois (13, 14).

180 cycle/second alternating flux. The capacitor voltage was proportional to the flux linkage and hence to the energy. This voltage was applied in series with an adjustable bias. A trigger circuit was actuated at a chosen critical input voltage and this in turn actuated the orbit expander.[3] The trigger point was found reproducible to within 0.2 volt which corresponded to about 50 kev at an energy of 11 Mev.

The samples were irradiated in a standard position in the x-ray beam, 46 cm from the target, ordinarily to half-saturation. The x-ray beam intensity, monitored by an ionization chamber, was recorded in roentgens per minute at 1 meter from the target. The different irradiation times used were corrected to the standard irradiation time by consideration of the process of radioactive growth with decay.[4]

Samples were usually thick cylinders which fitted snugly over the counters. The counters were designed to count beta rays and were coupled to a Neher-Harper circuit followed by a scale-of-16 counting circuit. Background was reduced to 15 counts per minute by enclosure in a lead shield 10 cm thick.

The x-ray energy control circuit was calibrated by a search coil in the orbit plane. It was known that the magnet flux was an accurate

---

[3]The method is entirely analogous to the more accurate circuits used at Nav. Res. Lab. A more complete description of the method of control of the peak x-ray energy and the basic principles of operation are given in Appendix I.

[4]See Section 3.4.

sine wave - the third harmonic amounting to only 0.07 percent at the highest amplitude. The flux within the search coil could thus be determined by a voltage measurement. This voltage could be compared simultaneously with flux integrator response (voltage on the capacitor) and with the magnet voltage, read on a voltmeter connected to a 2-turn coil about the magnet yoke. The latter reading was made a permanent substandard to which each setting was referred by determining the magnet voltage at which the integrator circuit would cause orbit expansion at peak flux. From these calibration data, the momentum of the electrons in gauss-cm, and hence the energy with which the electrons struck the target could be computed. The total error in most cases did not exceed 2%. Thus the calibration error at 10 Mev amounted to approximately 200 kev.

There was a systematic error in the energy values because of a phase shift in the integrating circuit which was appreciable when expansion occurs well below peak flux. The correction at about 11 Mev was found to be not more than 0.1 Mev.

In all, nine photoneutron thresholds were determined including C^{12}, N^{14}, O^{16}, Cu^{63} and Ag^{109}. The uncertainty of these determinations was about ± 0.4 - 0.5 Mev, except for Cu^{63} which was reported to ± 0.3 Mev. On irradiation, Cu^{63} produced the strongest activity observed in a photoneutron reaction.

The major sources of error were uncertainties in the calibration of the energy scale, poor yield of activity in the neighborhood of

threshold and fluctuations in the peak x-ray energy. Accurate determination of the thresholds of carbon, nitrogen and oxygen would have served as a test of the method since their thresholds were known accurately from the mass data. However, low activities precluded an accurate measurement of these thresholds.

1.5 Photoneutron Threshold Measurements of McElhinney et al.

The same general considerations apply to this work as above and it may, in fact, be regarded as a continuation of the work of Baldwin and Koch. However, several improvements in the design of the betatron had made available for these experiments an increase in the x-ray intensity by a factor of 20. In addition, the samples to be irradiated were taped onto the doughnut at the exit point of the x-ray beam.[5] The study also included a number of photoneutron thresholds in which the emitted neutrons were detected by means of a rhodium foil.[6] This permitted the thresholds of H^2 and Be^9 to be determined. An attempt was made to base an energy scale on photoneutron thresholds which could be calculated from the mass data.

Among the factors considered which could contribute errors in the energy scale were the effects of electron beam expansion and delays in the expansion process. Estimates of the correction for the additional

---

[5]The acceleration chamber of the betatron has the shape of a doughnut (torus). A portion of it is visible in Fig. 2.

[6]Upon absorption of neutrons, the rhodium foils become radioactive. The beta rays from the rhodium foils are counted.

flux introduced by the expander were of the order of 0.02 Mev. These corrections were small compared to the uncertainties in determining the actual threshold energies and so were neglected.

A constant time delay between the actuating of the trigger circuit and the triggering of the expander circuit could introduce a non-linearity in the energy scale. These time delays were accurately measured and were taken into account in the estimated errors made in the process of expansion. However, a similar error could be introduced by a slight phase shift between the effective integrator signal and the actual magnetic field of the betatron. It should have been possible to detect any significant error of this type by measuring the change in the integrator bias voltage corresponding to a photoneutron threshold upon changing the amplitude of the exciting current in the main coils of the magnet. Actual tests of this type using the threshold of Cu^{63} were not conclusive. Individual runs indicated changes in the bias setting for copper of from 0 to 0.3%.[7] It was concluded from the foregoing that the non-linear corrections were small and somewhat uncertain.

In order to establish a relationship between peak x-ray energy and integrator bias, it was decided to use the known thresholds of H^2 and Be^9 at low energies and those of N^{14} and C^{12} at the higher energies. The thresholds of Be^9 and C^{12} could be accurately defined. This scale places

---

[7] This effect has been successfully measured in the course of this thesis. The results are described in Section 7.3.

the threshold for Cu^{63} at 10.9 ± 0.2 Mev which is the same as that used by Baldwin and Koch (2).

By measurement of the magnetic field, the value obtained for the Cu^{63} threshold was 11.0 ± 0.2 Mev. A direct comparison of the Cu^{63} threshold with that of N^{14} indicated a value of 10.76 ± 0.2 Mev if the N^{14} threshold is taken as 10.51 Mev. It was concluded that the value chosen for the Cu^{63} threshold, 10.9 ± 0.2 Mev, was a fair compromise between the various data and should serve until more reliable values of some of these thresholds became available.

Twenty photoneutron thresholds were determined. Most of them were measured with reference to an energy scale calibrated using the fixed point of Cu^{63} at 10.9 Mev and the assumption of scale linearity. Although different trigger circuits were used at various times, it was stated that these introduced errors comparable to the errors involved in estimating the actual thresholds from the observed activities. The precision claimed for the majority of the determinations was ± 0.2 Mev.

It was found that all the activation curves were similar in shape and could be represented by a function of the form $Y = k(E-E_t)^2$, where Y is the activity per unit of x-ray intensity, k is a constant, E is the peak x-ray energy[8] and E_t is the observed threshold energy. This representation was valid for a region of 3 Mev.

---

[8]The phrases peak x-ray energy, peak gamma ray energy, peak photon energy and peak bremsstrahlung energy all have the same meaning.

Hanson et al. (4), in a continuation of the above work, have measured several additional photoneutron thresholds which were again referred to an energy scale calibrated by taking the Cu^{63} threshold at 10.9 Mev. It was found that in nearly all cases the activation curves could be represented by a function of the form $Y = k(E-E_t)^2$ valid for a 3 Mev interval in the neighborhood of threshold.

1.6 Photoneutron Threshold Measurements of Sher et al.

In this study, a new technique was used for measurement of the photoneutron threshold. The emitted neutrons were detected directly with boron trifluoride proportional counters imbedded in paraffin. The primary advantage of detecting neutrons rather than residual activity is the possibility of determining photoneutron thresholds where the reaction leads to either stable nuclei or nuclei with very long or short half-lives. However, a disadvantage is that the identification of isotopes becomes more difficult when elements having several isotopes are bombarded.

A diagram of the apparatus and geometry is shown in Fig. 1. The x-rays from the betatron consisted of pulses of about 0.5 microsecond duration at a repetition rate of 180 cycles/second. A gate circuit controlled the counting time of the BF_3 counters in order to avoid saturation during the initial pile-up of secondary electrons and to give the best possible ratio of sample counts to background. The control of the peak x-ray energy was accomplished in a manner similar to that used in the present work (Appendix I) and was similar to that described by Katz et al. (15). The total number of roentgens striking the sample at a given

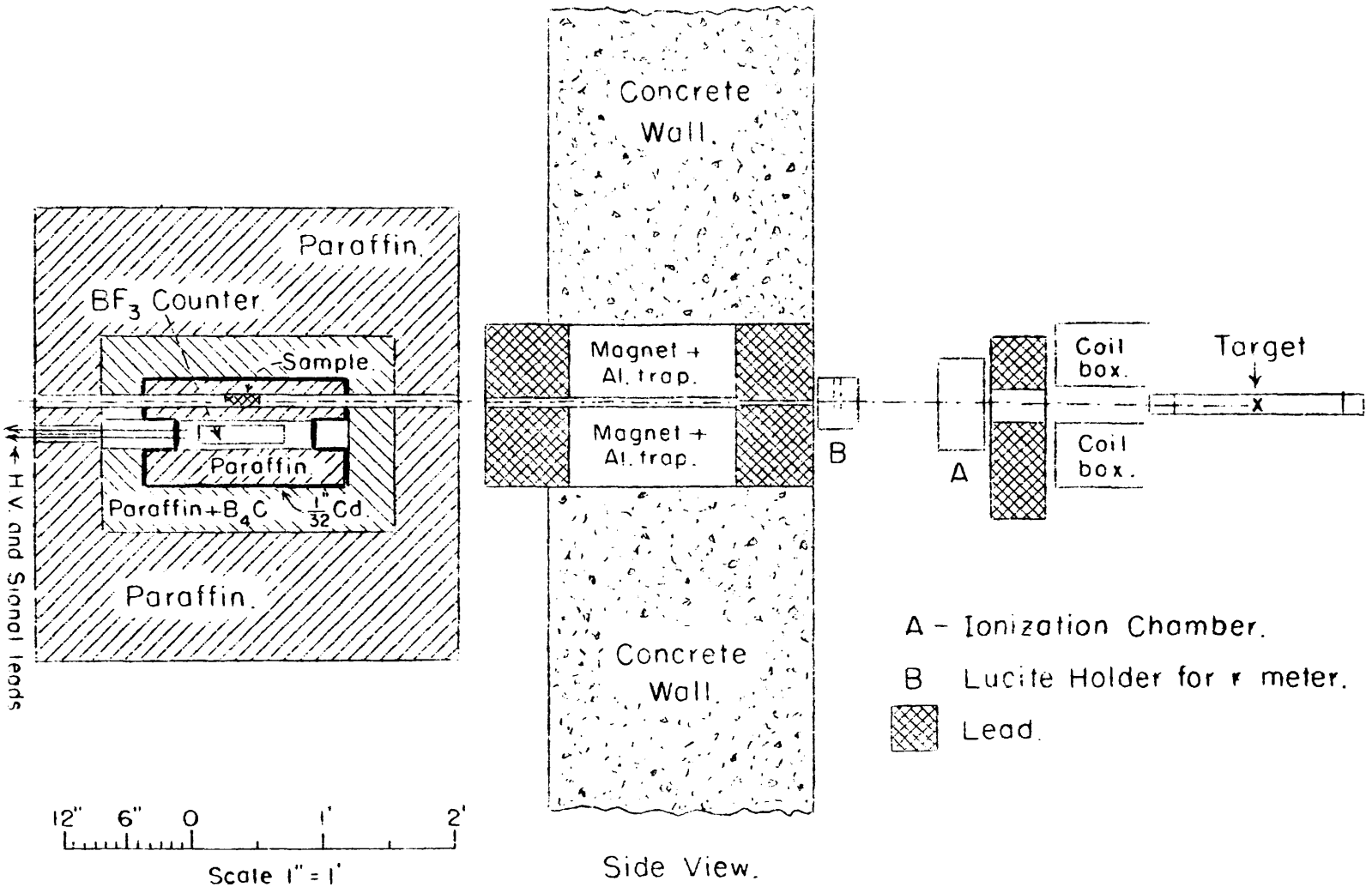

Fig. 1. Experimental Arrangement used by Sher, Halpern and Mann (10).

helipot setting[9] was determined with a 250 r Victoreen thimble imbedded in a lucite cylinder of 8 cm diameter and located 3 feet from the betatron target. The absolute measurement of the number of roentgens was not required.

The thresholds were determined by measurement of the neutron yield corresponding to the various peak x-ray energies. It was found that the resultant data could always be fitted by an expression of the form $Y = k(E-E_t)^m$ for a 3-Mev interval near threshold, where Y is the yield per roentgen, k a constant, E the peak x-ray energy, E_t the threshold energy, and m a constant. The values of E_t and m which gave the best fit were determined graphically by trial. The value of E_t found in this manner was taken to be the threshold energy for the reaction. This method has the advantage of providing a unique extrapolation to zero yield.

The energy scale was determined by the thresholds of photoneutron reactions which could be accurately calculated from the mass values. The thresholds used were those of Be^9, H^2 and Li^7. As a check on the overall performance of the equipment and the reproducibility of the energy scale, daily threshold measurements were taken on Mn^{55} and Bi^{209} during the entire course of the experiment.

About 77 isotopes were measured; 31 were repetitions of previously

---

[9]The helipot setting determines the peak x-ray energy.

reported values, and 46 were either new or more precise determinations. In most cases the uncertainties quoted for thresholds were 0.2 Mev and in no case larger than 0.3 Mev. The contributions of the various sources of uncertainty to the total uncertainty were as follows. The daily threshold measurements on Mn^{55} and Bi^{209} exhibited a maximum spread of 0.15 Mev. A mean deviation of 0.1 Mev was assigned to the absolute threshold due to the fluctuations in the energy scale. In general, the statistical errors contributed an uncertainty in the value of a threshold determination of about half that due to the energy scale fluctuation or about 0.075 Mev.

The relationship between yield and energy could be calculated if the energy dependence of the cross section for the reaction, the bremsstrahlung spectrum and the efficiency of the detecting apparatus were known. However, these factors are too complex for individual determination. The justification of the method was taken to be the agreement of the results with thresholds previously determined by the activation method.

1.7 Purpose of Present Work

The situation revealed by the experiments described in Sections 1.4, 1.5 and 1.6 was as follows. In both techniques, only a small amount of data was gathered in the neighborhood of threshold. In the work of Sher et al. (10) points were taken at intervals of about 350 kev so that the closest approach to threshold was about 175 kev on the average. Thresholds were found by extrapolation to zero yield of the activation curves which in all cases could be represented by a function of the form $Y = k(E-E_t)^m$

for a 3-Mev interval. The exponent m varied in an unpredictable manner from 0.7 to 3.1. In the work of the Univ. of Illinois group (2, 3, 4, 5), points were taken at intervals of about 200 kev. The activation curves were found, in almost all cases, to fit a function of the form $Y = k(E-E_t)^2$ for a 3-Mev interval. Thresholds were determined in most cases by inspection of the activation curves but in the work of (4) by parabolic extrapolation of the yield curves. For both methods, a precision of about ± 0.2 Mev was given for the determination.

The Univ. of Pennsylvania group (10) calibrated the betatron by using photoneutron reactions whose thresholds could be accurately calculated from the mass data. The calibration was checked by the agreement of the threshold values with thresholds previously determined by the Illinois group.

The Illinois group had attempted to calibrate the energy scale by using known photoneutron thresholds. However, the electrical method (2) gave 11.0 ± 0.2 Mev for the Cu^{63} threshold while direct comparison to the N^{14} gave 10.76 ± 0.2 Mev for this threshold. A compromise choice of 10.9 ± 0.2 Mev was taken for the Cu^{63} (γ, n) threshold. An energy scale was obtained using this value for Cu^{63} and assuming a linear relationship between the peak x-ray energy and the helipot setting.

The major factors which limited the precision with which a threshold could be determined were the fluctuations in the peak x-ray energy and the low counting rates encountered in the neighborhood of threshold.

The purpose of the present work was to investigate the possibility

of precise determination of photoneutron thresholds. The careful determination of the activation curves in the immediate neighborhood of threshold might provide the data for a unique extrapolation of the activation curve to zero yield. This would result in a considerable improvement in the reliability of the threshold measurements.

One of the major difficulties encountered was that of calibration of the energy scale. Thus, the compromise value of 10.9 Mev for the Cu^{63} threshold was widely used as a substandard for the calibration of the energy scale and 38 thresholds had been determined relative to it. If the thresholds for C^{12}, O^{16} and N^{14} could be determined accurately, they would serve to calibrate the energy scale. It would then be possible to determine precisely the threshold for Cu^{63}.

An improvement in precision would result in entirely new information about the shape of the activation curves in the neighborhood of threshold. This, in conjunction with other data, could be used to obtain information on the dependence of the cross-section for the reaction on the x-ray energy.

CHAPTER II

APPARATUS

2.1 Description of Betatron and Control Circuits

The source of x-rays for these experiments was the Naval Research Laboratory 22-Mev betatron - an early model of the standard 22-Mev betatron manufactured by Allis-Chalmers. The fundamental principle involved in the acceleration of electrons in a betatron is that of Faraday's Law of electromagnetic induction. A changing magnetic flux through the surface bounded by the electron orbit produces an electric field at the orbit. It is this electric field which provides the accelerating force on the electrons. By a suitable design of the magnet structure, the electrons can be constrained to move in a circle of approximately constant radius during the entire acceleration cycle (13, 14).

The source of electrons consisted of an electron gun assembly mounted within the doughnut, so as to inject the electrons in a direction tangent to the orbit at approximately the orbit radius. The electrons were injected at a time in the magnetic cycle when the injection energy corresponds to that required by the magnetic field. The number of electrons captured in this process depends very critically upon the timing.

In order to provide for control of the peak x-ray energy, orbit expansion coils were mounted above and below the doughnut. The coils consisted of a single turn with a radius almost equal to that of the electron orbit. At an appropriate time in the acceleration cycle, a pulse of current

is initiated in these coils. The additional flux produced thereby caused the electrons to spiral outward until they struck a platinum target mounted on the electron gun structure. A block diagram of the expander system is shown in Fig. 33.

The acceleration of the electrons in the coulomb field of nuclei in the target produces x-rays. Whenever x-rays are produced in this manner, there results a characteristic spectrum known as bremsstrahlung (16). The peak x-ray energy which can be produced in this manner is determined by the peak kinetic energy possessed by the electrons. The x-rays were produced in short bursts with a repetition rate of 180 cycles per second.

A view of the Naval Research Laboratory betatron is shown in Fig. 2. In view are part of the magnet assembly, the coil boxes containing the coils which energize the magnet and the two air ionization chambers which are used to monitor the x-ray beam. The doughnut may be seen in the space between the coil boxes.

Fig. 3 shows a view of part of the betatron control panel containing the electronic equipment which requires periodic attention and adjustment by the operator.

2.2 Equipment for Measurement of Sample Activity

In Fig. 4 is shown the equipment and experimental arrangement used in order to measure the radioactivity induced in the sample by exposure to the x-ray beam. At the far right may be seen the Lead Shield Model No. AL14A manufactured by Technical Associates, Inc. Inside the

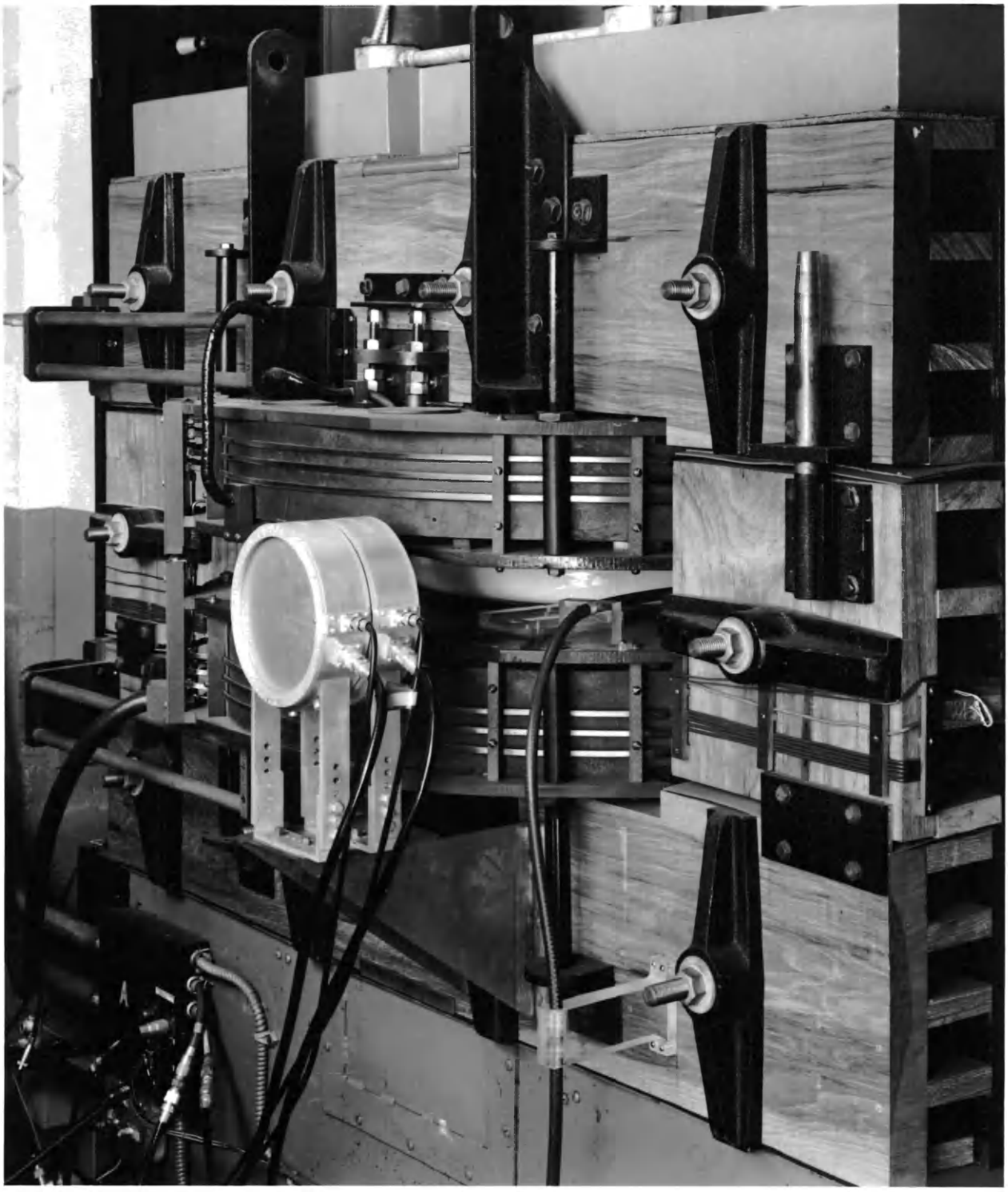

Fig. 2. Naval Research Laboratory 22-Mev Betatron.

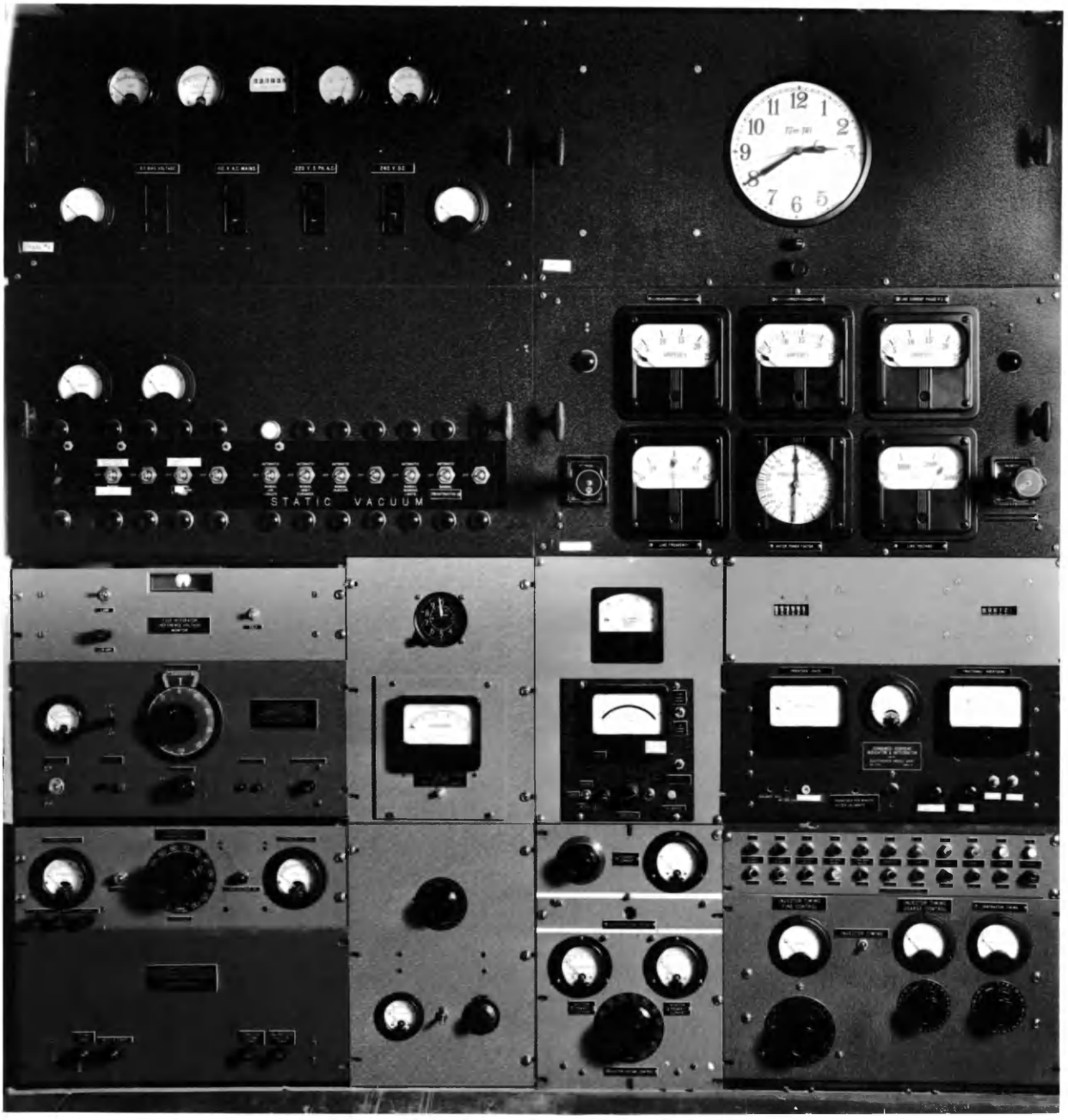

Fig. 3. Betatron Control Panel.

Fig. 4. Apparatus for Measurement of Sample Activity.

lead shield, the lucite stand may be seen which supports the sample-holding receptacles just under the mica window of the Geiger counter. Clamped to the top of the lucite stand is an Amperex Beta counter, end mica window type, number 120C. It is filled with argon and a quenching admixture. The mica window has an average thickness of 5.6 mg/cm^2 and will pass beta radiation in excess of 57 kev when the source is close to the window. The window diameter was somewhat less than 1.9 in. and, for this reason, the diameter of the samples was made 1.75 in.

The discharges of the Geiger tube were amplified by a Scaling Unit Model 162, shown in the center of Fig. 4, manufactured by Nuclear Instrument and Chemical Corp. The scaler output served as the input for the unit at the left of Fig. 4, a Streeter-Amet Co. "Ametron" counter, No. SCI626. The Streeter-Amet counter contains a counting unit, a printing unit and a set of electric timing clocks. At preset intervals ranging from 30 seconds to 12 hours, the number on its counter, together with the date and time, is printed on a 5-in. wide tape. The number of counts was recorded by the printing mechanism at one minute intervals, synchronized with the electric clock in the betatron control room. The number of disintegrations was obtained by multiplying the number of counts recorded by the Ametron counter by the scale-factor setting of the scaler.

2.3 Samples, Sample Holders and Considerations of Geometry

In Fig. 5 is shown the betatron sample holder and two types of disc holders. The one on the left consisted of a cover and receptacle, and

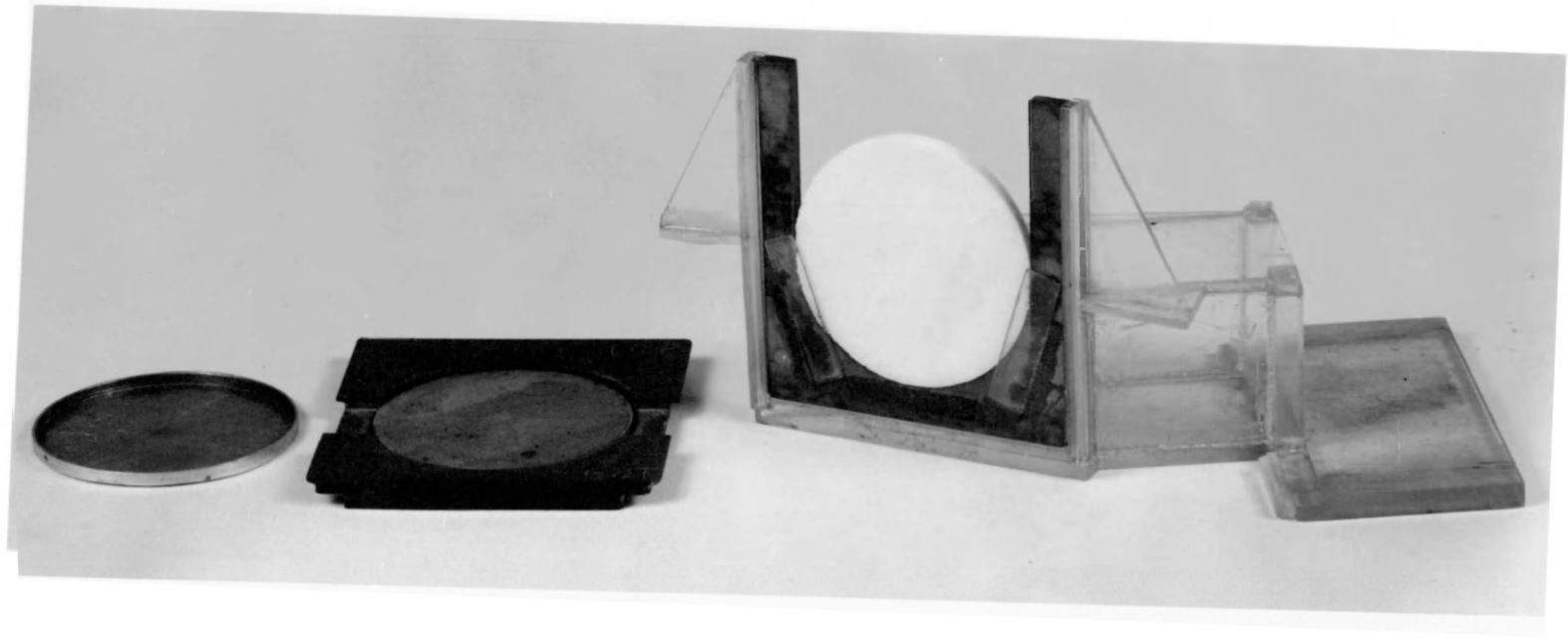

Fig. 5. Sample Holders.

completely surrounded the sample with 1/32-in. thickness of cadmium. The cadmium, which has a very large cross-section for absorption of slow neutrons, is thus able to shield the discs from the slow neutrons present. Whenever the betatron x-ray energy is in excess of 6 Mev, neutrons are ejected from the Pt target, so that a flux of neutrons accompanies the x-ray beam. The cadmium shield reduces the amount of activity, usually of a half-life different from the photo-induced activity, which the disc can acquire through neutron absorption. The other type of disc holder, which does not provide for a cadmium shield, is shown with a disc in the sample holder.

In Fig. 6, the ionization chambers have been removed to afford a view of the sample position during irradiation. The lucite rail assembly, which positions the sample holder, was attached to the coil box by means of 4 brass machine screws in recessed slots. When these screws were loosened the rails could be rotated, permitting the lining-up of the sample with respect to the x-ray beam. At the end of the rails were lucite blocks which limited the forward (toward the doughnut) motion of the sample holder. The sample holder was attached to the rails with a piece of Scotch tape which prevented the magnet vibration from moving the sample holder during an irradiation.

An array of discs of each of the materials irradiated is shown in Fig. 7.[1] In back of the samples are shown the two types of receptacles

---

[1]From left to right they are Cu, Ag, melamine (N), boric acid (O), polyethylene (C).

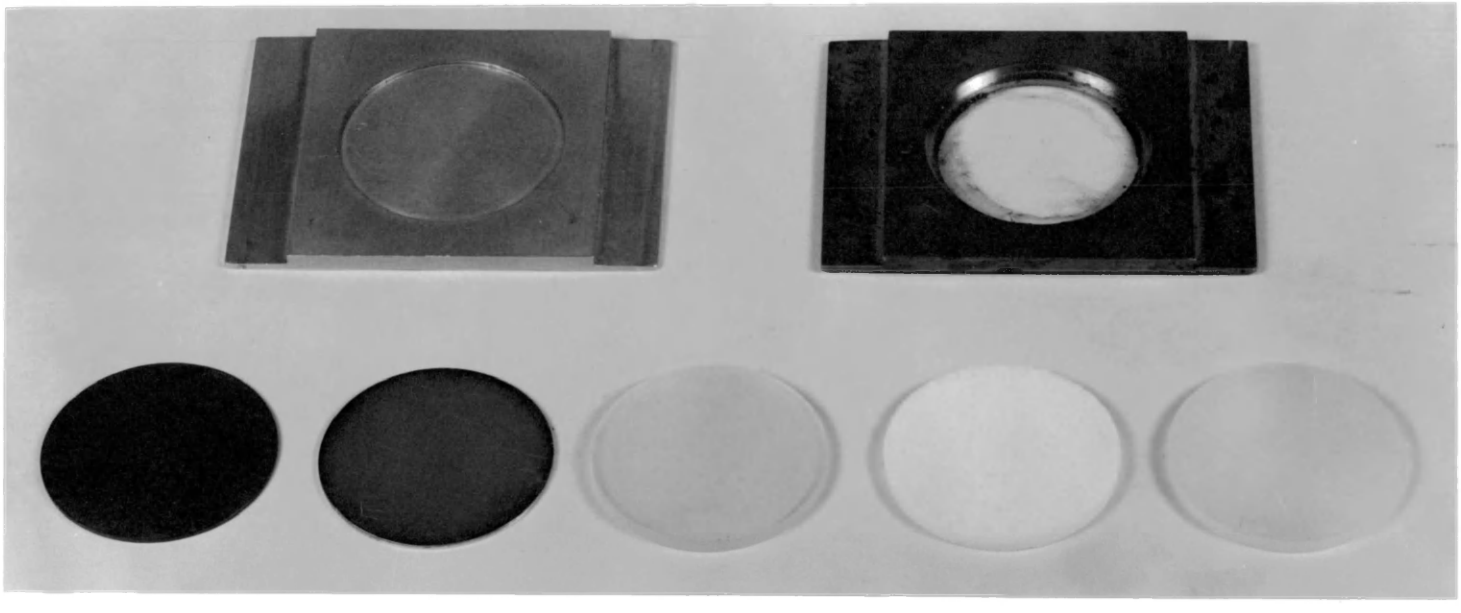

Fig. 7. Samples and Sample Receptacles.

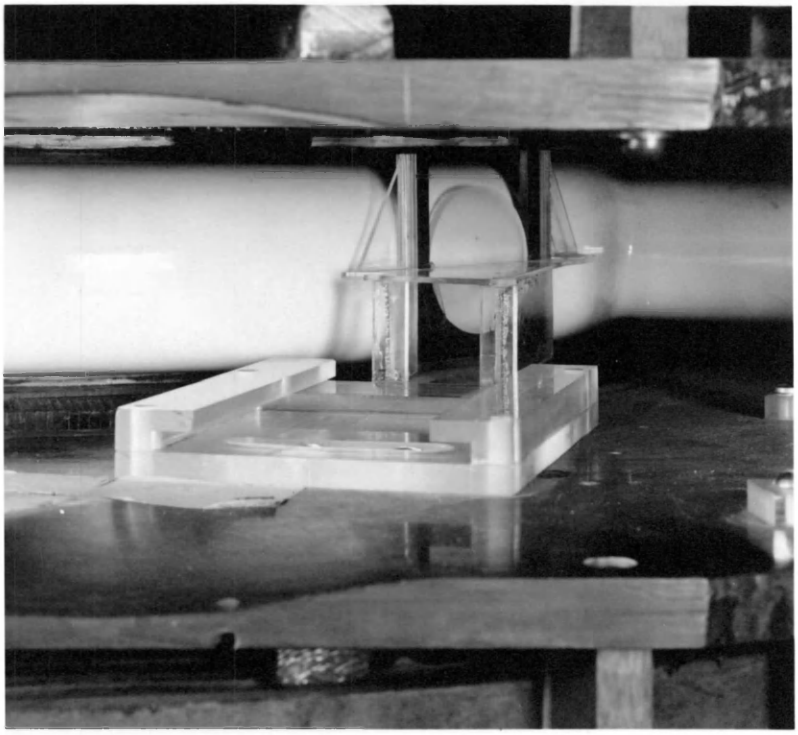

Fig. 6. Position of Disc during Irradiation.

designed to accommodate samples of 0.040-inch and 0.125-inch thickness. The discs were machined to a tolerance of 0.001 inch in all dimensions to make them as nearly identical (and therefore interchangeable) as possible.

The samples fitted the disc holders and the receptacles for counting to within 0.001 in. The receptacles were a loose push fit with the lucite stand in the lead shield and, similarly, for the sample holder and the lucite rails on the betatron coil box. By all these devices, the effects due to non-reproducibility of geometry were kept to a minimum and, as will be shown later, the uncertainty, which could be introduced by a non-reproducible geometry was negligible.

Reference to Fig. 6 shows that the sample was held approximately tangent to the doughnut at the exit point of the beam. The angle of incidence of the beam on the sample was about 70°. This geometry was advantageous in two ways. Firstly, it placed the sample as close as possible to the origin of the gamma rays and thus insured irradiation at the highest flux density. Secondly, since in all cases, the activity counted originated mainly from the surface layer, the beam intercepted 3 times more surface than it would if the disc were perpendicular to the beam. For threshold work, it was desirable to employ conditions which produce the highest activity in the sample.

It was desirable, in order to obtain the highest yield of activity, to use a sample whose thickness was of the order of the absorption thickness of the maximum energy beta particle which would be emitted. The

thickness of sample to be used was computed from the formula $R = 0.536 E - 0.165$ where R is the range in grams per square centimeter and E is the energy of the beta ray in Mev (17).[2] Results are summarized in Table 1 below.

TABLE 1. Disc Thickness Data

Material	Max. Beta Ray Energy (MEV)	Range (gm/cm^2)	Range (in.)	Sample Thickness
Cu	2.9	1.39	0.061	0.040
Ag	1.47	0.62	0.023	0.040
Melamine (N)	1.24	0.50	0.123	0.125
Boric Acid (O)	1.68	0.74	0.207	0.125
Polyethylene (C)	0.99	0.37	0.156	0.125

The mechanical design of all sample holders was such as to permit rapid handling of the discs. The half-lives of the radioactivities encountered in these experiments ranged from 2 minutes to 13 hours. When counting a sample with a 2 min. half-life it was imperative to start the counting as soon as possible after the irradiation. It was found possible to de-energize the betatron magnet, carry the sample from the betatron room to the counting room, remove the disc from the sample holder, place it in the counting receptacle and load the receptacle into the lead shield in a little less than 1 min.

---

[2]This equation is for aluminum absorbers, and is approximately true for the materials used in these experiments.

2.4 Monitoring the x-ray Beam

The x-ray beam intensity and the x-ray dosage were monitored by identical air ionization chambers mounted as shown in Fig. 2. The ionization chambers were of conventional design, not hermetically sealed and consisted of 3 parallel plates of which the center plate was maintained at ground potential and the outside plates at about 320 volts above ground. The design incorporated a guard ring in order to reduce the effects of leakage currents.

The ionization current of the ion chamber closest to the betatron was amplified by a direct current amplifier consisting of a single tube, a 6C8G. The amplified current was read on a microammeter calibrated to read roentgen/min. at one meter for a peak x-ray energy of 20 Mev. Over a period of many months, the drifts and transient effects were found to be less than 1/1000 of the maximum signal reading. Taking as an average the half-scale reading, the unit has a long period stability of the order of 1 part in 500 or 0.2% (18).

The current developed by the x-ray beam in the second ionization chamber was fed into a current integrator and indicator circuit. The basic circuit was that of a very stable direct current amplifier such as that described in (19). The circuit operated two registers and a microammeter on which were read respectively roentgens at one meter and fraction of a roentgen at one meter. The calibration of both ionization chambers was accomplished by comparison with the reading of a Victoreen Roentgen Meter at a peak x-ray energy of 20 Mev. The reading was

obtained by means of a standard Victoreen thimble imbedded in the center of a 4 in. cubical block of lucite. It has already been pointed out that an absolute measurement of the number of roentgens was not required for these experiments.

The linearity of the current integrator, that is the number of roentgens recorded as a function of the roentgen rate, was checked by operating it from an accurate potentiometer circuit. The linearity checked to better than 1% over a much larger range in operating rates than would be encountered in practice. The stability was tested by noting the drift in the amplifier, which is indicated as a certain number of roentgens, over an interval comparable with that of an average irradiation time. The results indicated that in all cases, errors resulting from amplifier drift would not be in excess of 0.5%. In actual operation the amplifier was balanced for zero drift before each irradiation.

A factor which might contribute an error in the measurement of the dosage was the change in efficiency of the ionization chambers with changes in the atmospheric pressure and temperature, since the chambers were not hermetically sealed. To a first order of approximation the efficiency (the number of ion pairs produced per incident photon) should depend only on the number of molecules in the chamber. At constant volume, the number of molecules will depend directly on the pressure and inversely on the temperature.[3] The temperature in the betatron

---

[3]This is merely a statement of the perfect gas law: $PV = NRT$.

room was maintained constant to about $\pm 3^{o}C$ by means of an air conditioning unit. On the absolute scale of temperature, this temperature variation amounted to $\pm 1\%$. The barometric pressure was recorded at the beginning of each day and also several times during the day with an accurate aneroid barometer. The pressure readings were found to agree with the readings of a standard mercury pressure gauge in the same room. Over a 3 month period the pressure fluctuated between 29.5 and 30.5 inches of mercury, a variation of about $\pm 1.6\%$. However, on any given day a much smaller pressure variation was encountered usually of the order of $\pm 0.2\%$.

It was concluded that the overall long time reliability of the instruments for measuring the number of roentgens should be of the order of 1.8%. However, on any given day the fluctuations due to the above mentioned effects should be less than 1%.

2.5 Control of the Peak x-ray Energy

The necessity for accurate control of the peak x-ray energy has been explained in Section 1.7. The integrator amplifier containing the energy control circuit was in most respects similar to that of Katz et al. (15). An exposition of the basic principles underlying this method is contained in Appendix I.

In order to improve the stability of the circuit, the a.c. line voltage was regulated with a Sorensen line voltage regulator, which maintained the root-mean-square line voltage constant to within $\pm 0.1\%$.

The reference voltage power supply was checked both before and

during an irradiation by means of the reference voltage test circuit.[4] The reference voltage test circuit consisted of a bridge circuit with a sensitive galvanometer as detector which compared a fraction of the reference voltage with that of a Weston Standard Cell No. 4. The reference voltage was checked in this manner and maintained constant to 0.01%.

Several improvements in the electronics were incorporated in order to improve the stability of operation. In particular, it was found that the method which had been employed to trigger the 5C22 hydrogen thyratron both in the injector and expander circuits was inadequate. To achieve stable triggering of these thyratrons, the circuit shown in Fig. 8 was designed and installed. Essentially, the circuit used the signal which formerly triggered the 5C22 thyratron to trigger a 2050 thyratron. The pulse produced by the 2050 tube was, in turn, used to trigger the 5C22 thyratron. The circuit produced a pulse of over 200 volts across a 100 ohm load with a rise time of less than 0.01 microsecond.

About 60 watts were dissipated in the 1 megohm resistor of the integrator stack. Bench tests indicated a change in resistance of several tenths of a percent until reaching thermal equilibrium. The variation in the peak x-ray energy due to this change in the integrator characteristics

---

[4] The helipot is used to tap off a fraction of the reference voltage. When the integrator amplifier input voltage exceeded this voltage, the expansion process was initiated. Thus the stability of the peak x-ray energy is directly connected with the stability of the reference voltage power supply.

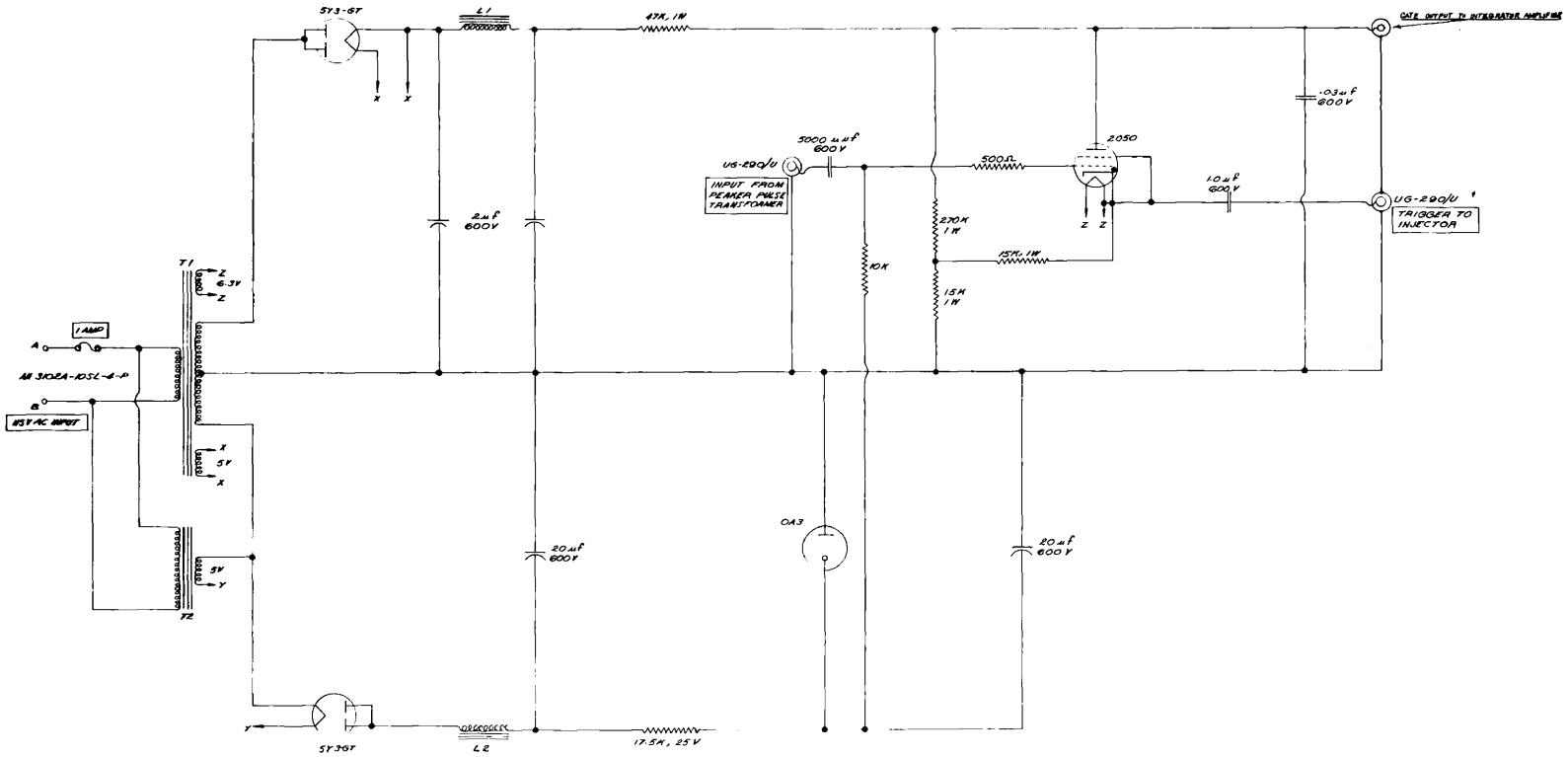

Fig. 8. 2050 Thyratron Trigger Circuit.

was estimated to be of the order of 20 kev at a peak energy of 10 Mev. If the change in capacity of the integrator capacitor is also considered, then the total instability might be about 30 ~ 40 kev.

In order to reduce the variations in the peak x-ray energy due to the above effect, the circuit shown in Fig. 9 was designed and installed. It consisted of a 60 cycle per second alternating current power supply which put a voltage across the stack, equal to that present when the magnet amplitude was set for a peak x-ray energy of 21 Mev. The other components were for switching and interlocking with the betatron magnet controls so that when the magnet current switch was closed the integrator stack was switched from the supply of Fig. 9 to the betatron magnet and vice versa. By this means, the integrator stack was always maintained at an equilibrium condition for a 21-Mev magnet amplitude.

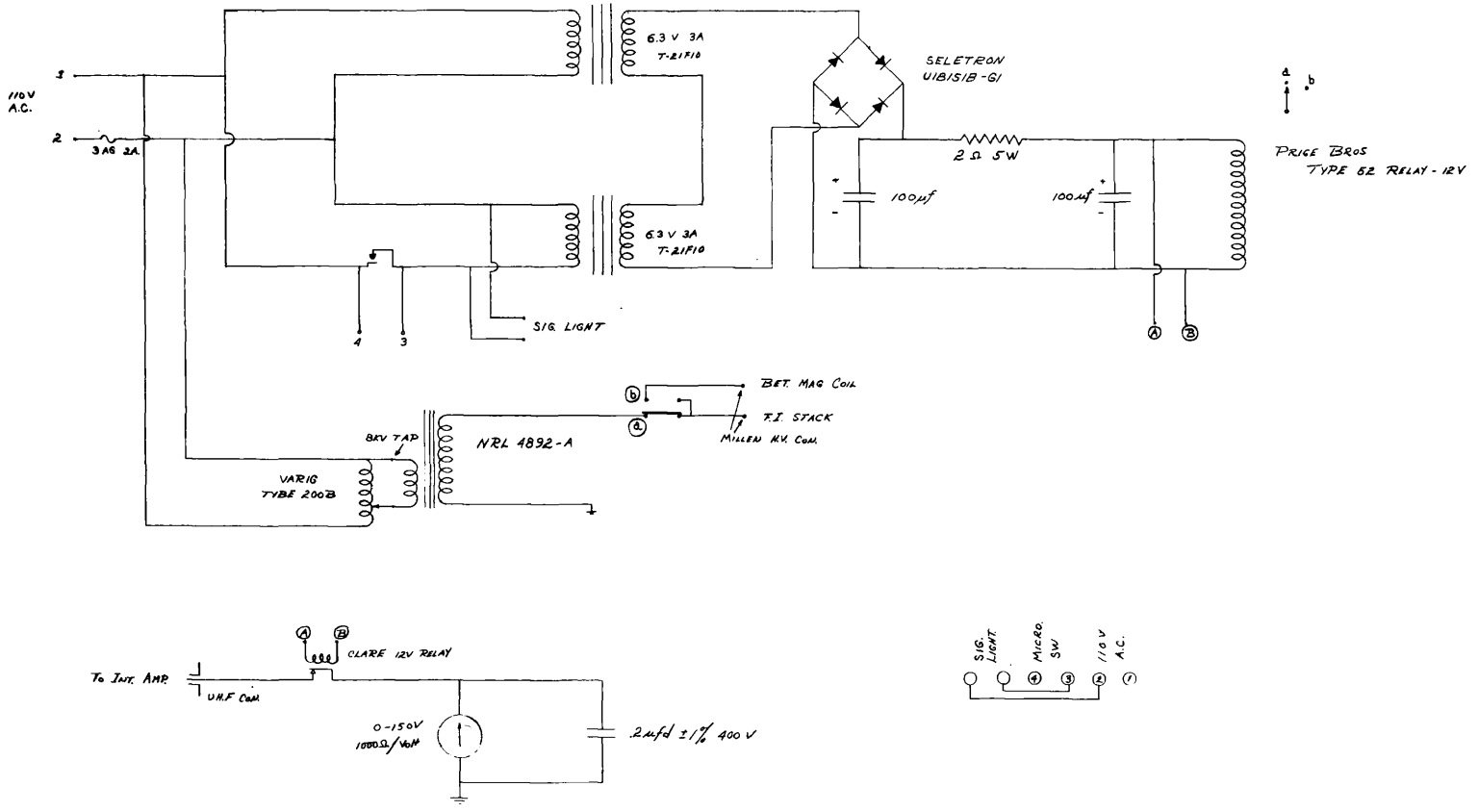

Fig. 9. 8000-volt Alternating Current Power Supply.

CHAPTER III

EXPERIMENTAL PROCEDURE

3.1 Alignment of the Sample

Before proceding with the threshold experiments, it was necessary to test the sample alignment with respect to the x-ray beam. Unless the most intense portion of the x-ray beam were to go through the disc, a lower x-ray intensity would be used to irradiate the sample with a consequent loss in sensitivity. Furthermore, if the x-ray beam center and the disc center coincide, it should reduce the sensitivity of the experimental arrangement to small errors as regards the reproducibility of the geometry.

The method of autoradiography was used for this test. A Cu disc in the standard irradiation position (shown in Fig. 6) was given a 4 min. irradiation at a peak x-ray energy of 20 Mev. The disc, having received about 15,000 roentgens, was immediately taken to the counting room and placed flat on a table. On top of the disc was placed a packet of Eastman Kodak dental x-ray film (Occlusal Super Speed) and a weight on the film to hold it in position. Care was taken to have the side of the film packet without the Pb foil face the Cu disc. The exposure time was 10 minutes and blackening occurred through the action of the beta particles ejected by the radioactive Cu.

After exposure, the film was developed and fixed. A print of the resulting autoradiograph is shown in Fig. 10. The light parts of the print

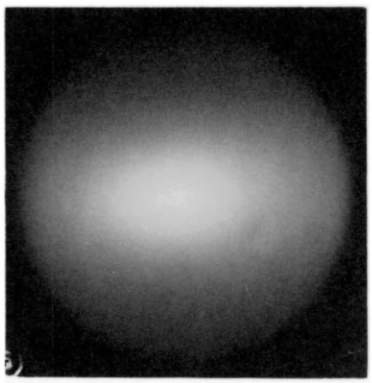

Fig. 10. Autoradiograph of Irradiated Cu Disc.

correspond to the regions exposed to the highest intensity of x-rays. The outline of the disc together with the central light spot are clearly discernible. Adjustments were made on the sample holder and in the position of the tracks (Fig. 6) until the light spot occurred in the center of the disc as shown in Fig. 10. The central light spot was elliptical rather than circular because the sample was positioned at an angle of incidence of 70°.

3.2 Performance of Counting Equipment

The activity of the irradiated sample was determined by counting the discharges produced in a Geiger tube. In order to determine the optimum voltage for the Geiger tube, a counting rate versus Geiger tube voltage curve (a "plateau" curve) was obtained. The Geiger tube operating voltage was then set at about 100 volts above the knee in the plateau curve. The Nuclear scaler, used in conjunction with the Geiger tube, was powered from a Solar electronic line voltage regulator to improve the stability of operation.

The background counting rate was determined each day by the counts accumulated during the preceding 8 - 24 hours. Ordinarily the number of counts accumulated was between 10,000 and 30,000 depending upon the time interval, and gave a background counting rate of about 21 counts/min. The total variation in background counting rate was less than ± 1 c/min. over a 9 month period.[1]

Each day, prior to the start of irradiations, the entire apparatus

---

[1] The abbreviation "c" will always stand for the work count.

for counting was checked by means of a standard beta ray source. A Bureau of Standards RaD and E Radium Standard, No. 1266, was placed in the top step of the lucite rack inside of the lead shield (Fig. 4) in the same position as that used for counting the samples. The number of c/min. was recorded by the Ametron recorder for about 20 min. About 75,000 counts were recorded in this interval so that the resultant statistical error was about 0.3%. The total spread in the measurements of the counting rate of the Ra source, over the 57 days during which most of the data presented in this thesis were gathered, was about $\pm 1.3\%$. However, all but six of the measurements fell within the limits of $\pm 0.7\%$. Thus the long period reliability and reproducibility of the counting apparatus was $\pm 0.7\%$.

It is well known that Geiger tubes exhibit hysteresis and other effects difficult to account for. By way of illustration, it was found that if the Ra source is counted immediately after counting a hot source (100,000 c/min. or higher), the result of the measurement will invariably be high.[2] Furthermore, at high counting rates, it is necessary to correct for dead time of the Geiger tube. In order to eliminate the effects of these variables, the counting rate, in the course of the threshold work, was not permitted to exceed 10,000 c/min. At counting rates of 10,000 c/min. and less, dead-time corrections were negligible and hysteresis

---

[2]The adjectives hot and cold as applied to radioactive samples are colloquial expressions which indicate in a loose way a strong or weak activity, respectively, of the samples.

effects were not encountered.

3.3 Irradiation and Counting Schedule

The following procedure was employed in order to insure good reproducibility of the irradiation and counting schedules. The electric clock in the control room of the betatron was synchronized with that of the Ametron counter so that whenever the second hand of the betatron control room clock swept past the 60 second position, the automatic printing mechanism of the Ametron would be actuated and would print the number on its register together with the time and date. For radioactive nuclei with half-lives of from 5 - 20 min., the irradiation was started at the 30 second point and counting was begun 1.5 min. after an irradiation. For nuclei with half-lives less than 5 min., counting was begun at one minute after the end of an irradiation; this was the shortest time interval with which the transfer of the sample from the betatron room to the counting room could be accomplished without altering the experimental arrangement.

It was clear that with this system the only place where some uncertainty could occur in the sequence of exposures was in timing the length of irradiation. Most of the irradiation times were 4 minutes or longer and the timing could be held to within 1 second or about $\pm$ 0.4%. However, a consideration of the effect of these errors upon the induced radioactivity indicated that they were much smaller than the error in timing and, in fact, were negligible.

3.4 Calculation of Effect of x-ray Intensity Variations

In order that the irradiations be directly comparable in terms of the number of roentgens received by the sample, it was necessary to insure that the intensity waveform of the irradiation be the same for all the irradiations. The simplest waveform to use in practice was a square wave, that is, the flux of x-rays was maintained at a constant value during the irradiation. This was accomplished by means of an injector timing switch and injector timing control. Ordinarily it was found possible to keep the flux of gamma rays constant to about ± 0.5 roentgen/min. The following calculation was performed in order to obtain an estimate of the error due to departures of the actual intensity waveform from a square wave. The calculation resulted in a comparison of the activities induced by a square wave with that due to different waveforms. The square wave calculation is given in Case 1. The activity resulting from simple waveforms consisting of periods of high and low intensity is considered in Cases 2 and 3.

Case 1. Radiate with a constant flux of x-rays, ϕ, for a time T. Let dn_1 be the number of radioactive atoms formed in the time dt, dn_2 be the number of radioactive atoms which decay in the time dt. Then

$$dn_1 = s\phi dt$$

$$dn = dn_1 + dn_2 = \left[s\phi - \lambda n(t)\right] dt$$

$$dn = dn_1 + dn_2 = \left[s\phi - \lambda n(t)\right] dt \qquad (3\text{-}1)$$

where n(t) is the number of radioactive atoms present at time t, λ is the decay constant and s is a constant which depends on the cross-section

for the particular reaction considered. Solving equation (3-1) subject to the initial condition that $n(t) = 0$ for $t = 0$, there results

$$n(T) = (s\phi/\lambda)(1-e^{-\lambda T}) \tag{3-2}$$

The number of counts, $N_1(T)$, recorded in an interval $(t_2'-t_1')$ after the irradiation will be proportional to $n(T)\left(e^{-\lambda t_1'} - e^{-\lambda t_2'}\right)$ or

$$N_1(T) = k\phi\,(1-e^{-\lambda T}) \tag{3-3}$$

where t' is counted from the end of irradiation and k is independent of ϕ and T.

Case 2. Radiate for a time T/2 with a flux 10% low, followed immediately by irradiating with a flux 10% high for a time T/2. The sample receives the same number of roentgens in Case 2 as in Case 1. Calculating as above, there results

$$N_2(T) = k\phi\,(1-e^{-\lambda T/2})(0.9e^{-\lambda T/2} + 1.1) \tag{3-4}$$

Comparison of Cases 1 and 2 as a function of the irradiation time, T, in units of the half-life is shown in Table 2 below.

TABLE 2. Effect of x-ray Beam Intensity Variations.

T in units of half-life	$(N_2-N_1)/N_1$
0.5	0.009
1.0	0.017
2.0	0.033
Infinity	0.10

Case 3. The same as Case 2, except that the flux is 10% high initially and then 10% low. Calculating as above there results

$$N_3(T) = k\phi\,(1-e^{-\lambda T/2})(1.1e^{-\lambda T/2}+0.9) \qquad (3-5)$$

Comparison of Case 3 with that of Case 1 is tabulated below in Table 3.

TABLE 3. Effect of x-ray Beam Intensity Variations.

T in units of half-life	$(N_1-N_3)/N_1$
0.5	0.009
1.0	0.017
2.0	0.033
Infinity	0.10

The results of the above calculation indicate that the activity will be least sensitive to fluctuations in the beam intensity for irradiation times short compared to the half-life. However, the error introduced from this source will, in general, be very small since in practice the flux of x-rays can be maintained constant to about 3 or 4%. In Section 3.6 of this chapter, it will be shown that with an irradiation time of 0.4 half-life (a value which is favorable from the above considerations) excellent reproducibility was achieved which indicated that the error due to this effect must indeed be practically negligible.

3.5 Reproducibility of Geometry

The following experiment was performed in order to check the reproducibility of the experimental procedure. Two discs of Cu were

irradiated simultaneously at a peak x-ray energy of 21 Mev for 8 minutes. After waiting until the samples cooled sufficiently (initial counting rate about 14,000 c/min.), the disc closest to the doughnut was counted from 86 - 106 min. after the end of irradiation and the other for 75 - 85 min. For each disc about 100,000 counts were obtained and the experiment was repeated 4 times. The ratio of the number of counts of the rear disc to the front disc should depend only on differences in the samples and in the geometry. The ratios obtained were 1.096, 1.088, 1.096 and 1.085. The total spread was about $\pm$ 0.5% of which $\pm$0.4% was due to statistics. It was concluded that the geometry was reproducible to better than $\pm$0.3%.

3.6 Reproducibility of Activations

It had been realized throughout the course of this work that the peak x-ray energy of the betatron would be one of the most difficult factors to control with a high degree of stability over a long time interval. It was for this reason that the additional circuits described in Section 2.5 were incorporated into the Naval Research Laboratory control circuits. In fact, the instability of the peak x-ray energy was one of the major factors which limited the precision of the threshold determinations in previous work.

A test of the stability of the peak x-ray energy was obtained by the reproducibility of Cu activations at helipot 730, approximately 800 kev above threshold. Reference to Fig. 12 indicated a slope of approximately

20 counts/roentgen per helipot unit.[3] Thus at helipot 730 a change in the peak x-ray energy of 0.1% produces a 3.6% change in the Cu activity. It is for this reason that the activity induced in a Cu disc can be used to monitor the peak x-ray energy near the Cu^{63} threshold.

For a 4 min. irradiation and a 20 min. counting period about 75,000 counts were obtained, resulting in a statistical precision of ± 0.36%. Taking into account all of the factors previously discussed, a short time stability (8 - 10 hours) of the order of 0.7% could be expected.

In order to test the peak x-ray stability, a series of Cu discs were irradiated and counted as described above. The dispersion in the resulting values would indicate the degree of stability in the peak x-ray energy. The results of 11 irradiations of Cu at helipot 730 are shown in Fig. 11. The total spread in activity was 1.3%. Using the above figure of 0.7% for the other effects, the spread of the c/r due to fluctuations of the peak x-ray energy was about 1.1%, corresponding to ± 0.8 h.u. At a peak energy of 11 Mev, the peak x-ray energy was stable to within ±10 kev. In most cases, the fluctuations of the peak x-ray energy over the course of a day were somewhat greater than this, about ±20 kev.

3.7 Monitoring the Peak x-ray Energy

Since, at helipot 730, the largest error by far in the reproducibility of an activation was due to the peak energy fluctuation, for simplicity, from now on all of the observed changes in activity of Cu at helipot 730

---

[3]The abbreviations c/r and h.u. will stand respectively for counts per roentgen and helipot unit.

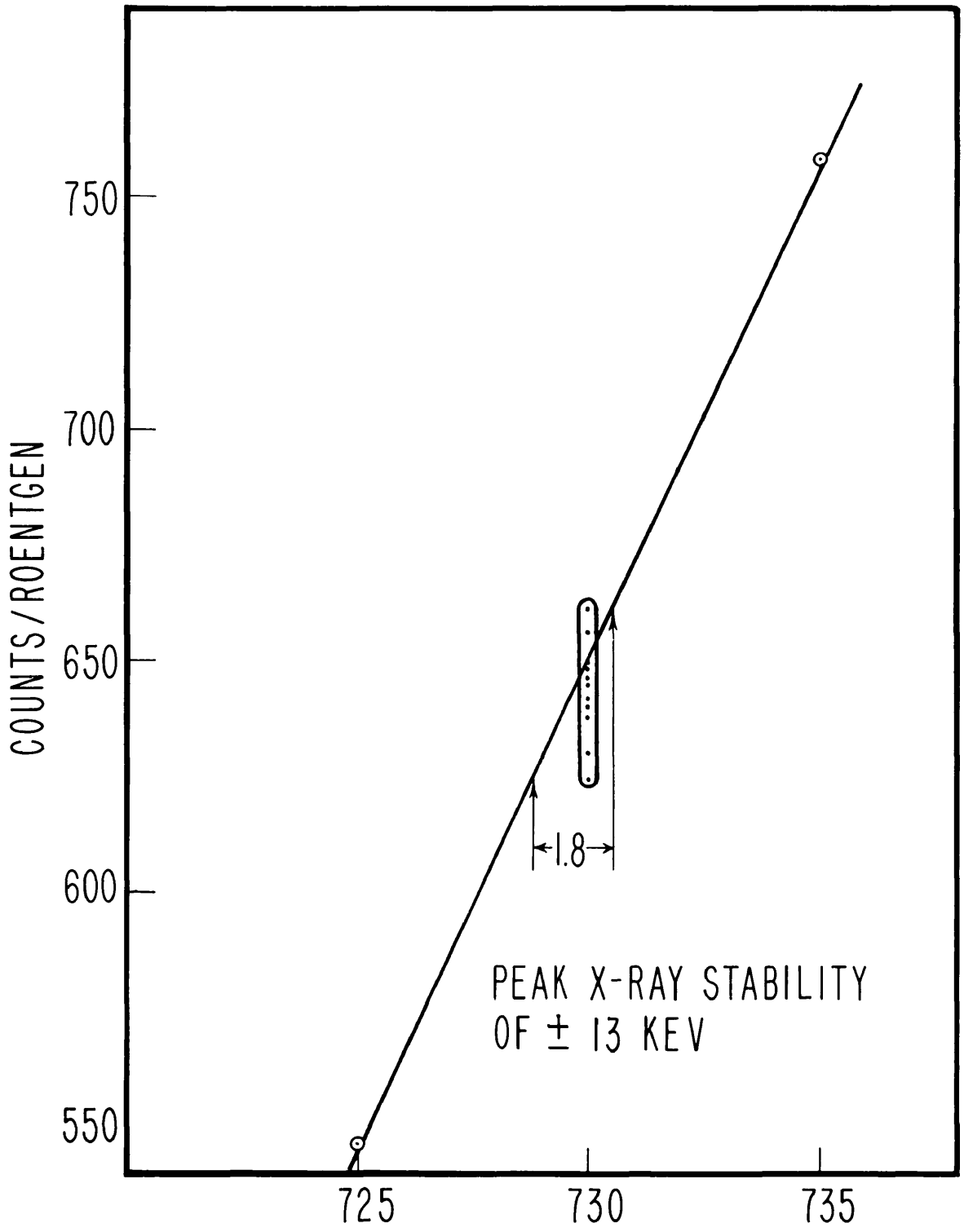

Fig. 11. Reproducibility of Cu^{62} Activity near Threshold.

will be ascribed to this cause. It is now evident that the activation of Cu at helipot 730 can be used to monitor the peak x-ray energy. Suppose, for example, that on one day the Cu control activity[4] was 600 c/r and on another 500 c/r. Reference to Fig. 12 shows that the peak x-ray energy has shifted by 5 h.u. To normalize the latter to the former, it would be necessary to subtract 5 h.u. It will be shown later, Section 7.2, that this method can be rigorously justified.

A portion of the activation curve of Cu^{62} about 800 kev above threshold is shown in Fig. 12. The peak x-ray energy stability of the betatron for this determination was comparable to that of Fig. 11, which indicated that the shape of the activation curve was free from distortions due to fluctuations in the peak x-ray energy. The activation curve of Fig. 12 was used throughout the threshold determinations to correct for fluctuations and shifts in the peak x-ray energy as indicated by the Cu control activity.

3.8 Other Factors Affecting the Peak x-ray Energy

Many days were occupied with sequences of Cu activations at a fixed helipot setting in order to secure data concerning the peak x-ray energy fluctuations. On a number of days, it appeared that there was a trend towards lower activations towards the end of the sequence. The effect was attributed to a temperature rise of the betatron magnet, but

---

[4]Activation of Cu at helipot 730 for the purpose of monitoring the peak x-ray energy will be referred to as Cu control activity.

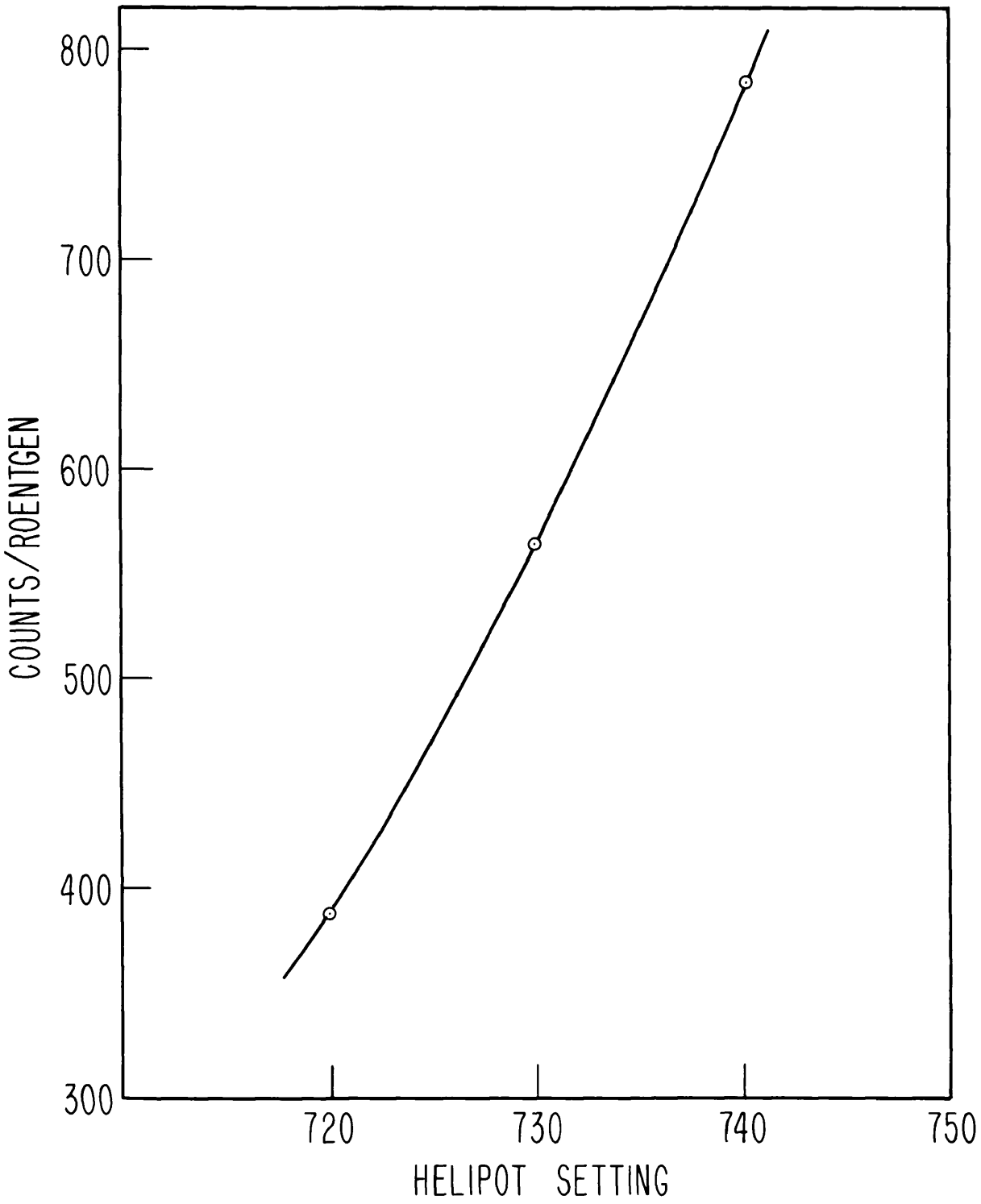

Fig. 12. Cu Control Activation Curve.

it was not possible to reproduce this effect consistently. The main conclusion drawn from all of these tests indicated that to minimize the energy fluctuations, it would be desirable to adopt an irradiation schedule in which the duty cycle of the magnet (the ratio of the magnet energized time to the total time) would be as low as possible consistent with adequate statistics in the neighborhood of threshold.

The photoneutron thresholds of Cu^{63}, Ag^{109}, C^{12}, N^{14}, O^{16} were obtained with a control Cu activity of about 700 c/r. This was followed by a period of rather violent energy fluctuations of the order of 70 - 100 kev. After some thought, it was decided that the instability was most probably an effect of the clamping diode in the integrator amplifier (Appendix I). A new diode was installed and tests indicated stability comparable to the results shown in Fig. 11, but now the control Cu activity was 480 c/r. Other diodes were substituted and found to result in different activities at the same helipot setting. However, it was possible to repeat the entire set of threshold measurements with a control Cu activity of about 480 c/r. These experiments have indicated a probable source of instability in the control of the peak x-ray energy. A more thorough investigation of this effect is currently in progress.

CHAPTER IV

PHOTONEUTRON THRESHOLD DETERMINATION OF Cu^{63}

4.1 Introduction

Naturally occurring Cu consists of the two isotopes, Cu^{63} and Cu^{65}, present in the proportions 69% and 31% respectively. On irradiation with x-rays of energy in excess of 11 Mev, the beta emitters Cu^{62} and Cu^{64} are produced with half-lives of 10 min. and 13 hours respectively (20).[1] The threshold for Cu^{64} was known to be lower than that of Cu^{62}, with the result that the 13 hour activity would be present in all determinations of the Cu^{63} threshold.

About 25 Cu discs could be irradiated and counted in the course of a day. However, several days were usually required for the 13 hour activity to practically disappear. In order to insure a plentiful supply of "cool" discs, over 60 discs were employed. They were 0.040-inch thick and 1.750-inch in diameter, were machined from sheet stock of very pure electrolytic Cu, and were numbered consecutively in order to keep a record of when they were irradiated. A simple test of the residual activity was obtained by determining the background counting rate with the Cu disc to be used the next day. This should also result in a more reliable background counting rate determination.

---

[1] "Beta emitter" refers both to electron and positron emission.

4.2 Half-life of Cu^{62}

A very sensitive test of sample purity from the point of view of a threshold determination could be obtained by plotting a radioactive decay curve of the induced sample activity. If the plot of log (c/min.) versus the time is accurately represented by a straight line, then it may be concluded that there is no or very little activity of other half-lives present. Furthermore, the agreement of the measured half-life with that given by other investigators, identifies positively the nucleus under investigation. The half-life on irradiation of Cu was found to be 10.0 min., as shown in Fig. 13, in agreement with the value 9.9 min. for Cu^{62} (20).

4.3 Correction for Different Exposure Times

The standard exposure and counting schedule consisted of a 4 min. irradiation and a 20 min. counting interval beginning 1.5 min. after the x-ray bombardment. The Cu discs were supported during exposure by the holder which completely enclosed them with 1/32-in. of Cd (Fig. 5). The x-ray dosage was about 100 r at one meter or about 5900 r at the sample position.

For Cu irradiations at helipot settings above 730, the induced activities were too strong for counting 1.5 min. after the exposure if the initial counting rate was not to exceed 10,000 c/min. Both time of exposure to the x-ray beam and beam intensity were reduced to obtain lower counting rates. In order to normalize these runs to those obtained with the standard procedure, the following method was employed.

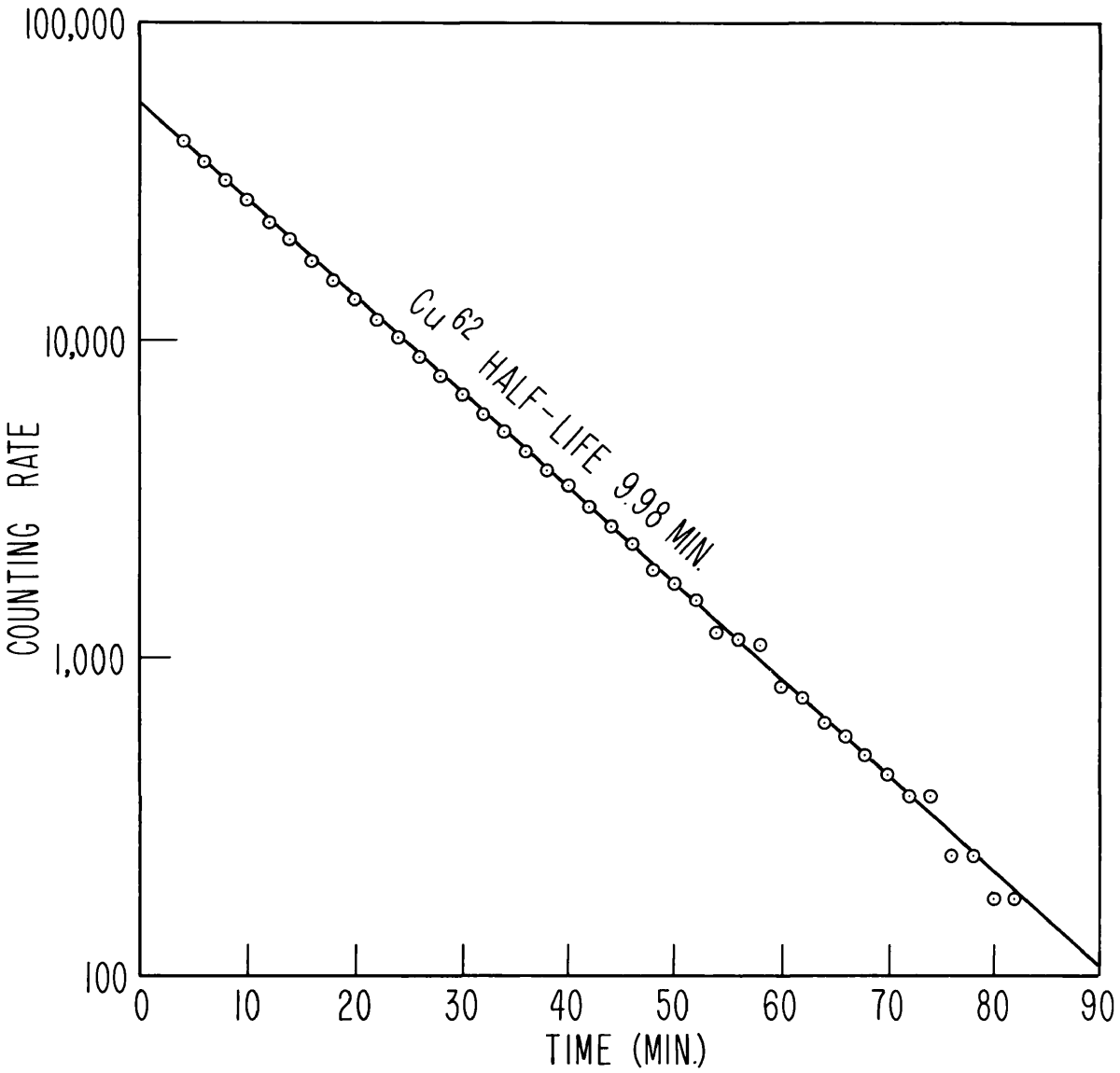

Fig. 13. Cu^{62} Decay Curve.

According to equation 3-3 (Section 3.4) the number of counts due to an exposure of T min. will be

$$N = k\emptyset\,(1-e^{-\lambda T}) \qquad (4\text{-}1)$$

In an exposure with a constant flux of radiation, $\emptyset = R/T$ where R is the total number of roentgens. The number of c/r is therefore

$$C = (k/T)(1-e^{-T}) \qquad (4\text{-}2)$$

Let C_4 and C_x denote the c/r in a 4 min. and x min. exposure. The ratio from (4-2) is

$$\frac{C_x}{C_4} = \frac{4}{x}\,\frac{(1-e^{-\lambda x})}{(1-e^{-4\lambda})}$$

or

$$C_4 = C_x\,\frac{x}{4}\,\frac{(1-e^{-4\lambda})}{(1-e^{-\lambda x})} \qquad (4\text{-}3)$$

By means of equation (4-3) the activation of the x min. exposure can be expressed in terms of the equivalent 4 min. exposure.

4.4 Cu^{62} Activation Curve

Usually about 3 control Cu activations were obtained at the beginning of each day. If there was good agreement among the Cu control activations, the threshold measurement was started. This consisted of irradiating a series of discs at various peak x-ray energies (helipot settings). A control run was taken for every one, two or three data runs.[2] The decision on the distribution of control runs with respect to the data

---

[2] "Run" refers to the entire process of irradiating and counting a sample.

runs depended on the agreement of the control runs.

The activation curve for the reaction Cu^{63} (,n) Cu^{62} is shown in Fig. 14. The ordinates represent the observed activity in c/r corrected for cosmic-ray background and normalized to a 4 min. exposure time. The dotted-line portion of Fig. 14 is shown on an expanded scale in Fig. 15. Inspection of the curve of Fig. 15 indicated threshold at 670 ± 1 h.u. In Fig. 14 and 15 there is shown an upper abscissa scale which is in helipot units and a lower one in peak bremsstrahlung energy. The method of conversion of the arbitrary helipot unit scale to the peak x-ray energy scale is described in Section 7.1. Table 4 contains the data displayed in Fig. 14 and 15.

It will be noticed that some of the points on the curve of Fig. 15 are represented by the intersection of a vertical and horizontal bar. The vertical bar represents the standard error in the c/r due only to counting statistics. The horizontal bar represents the precision to which the helipot setting was known as obtained from the control Cu runs.[3] About 22 control Cu runs were obtained for the data in Table 4 which were referred to a Cu control of 565 c/r, since most of the data near threshold was obtained with this value for the control. The spread in control activations was from 585 - 536 c/r or ± 1.25 h.u.

The presence of an appreciable activity below threshold is due to the reactions Cu^{65} (γ,n) Cu^{64}, Cu^{65} (n,γ) Cu^{66}, and Cu^{63} (n,γ)Cu^{64}.

---

[3]The crosses on the activation curves which follow will have the same meaning.

The Cu^{64} and Cu^{66} activities have 13 hour and 5 min. half-lives respectively (20). The contribution of the former was determined by counting the discs after the 10 min. activity had practically disappeared. The Cu^{64} activity[4] amounted to 0.15 c/r at helipot 670 and so contributed only a very small fraction of the observed activity. Analysis of the data taken at helipot settings below 670 indicated a 5 min. half-life. The activity was therefore attributed to Cu^{66} through neutron capture in Cu^{65}.

4.5 Threshold Determination by log-log Analysis

In Fig. 16 is shown the log-log analysis of the Cu^{62} activation curve shown in Fig. 14. The data, corrected by subtracting the 13 hour and 5 min. components, is shown tabulated in column 2, Table 5. The ordinates are $\log_{10}(H-H_0)$ and the abscissas are $\log_{10}$ (c/r). The points for the line $H_0 = 667$ represent the numbers listed in column 3, Table 5. However, to the abscissas of the points for $H_0 = 668$ have been added 0.5, to those of $H_0 = 669$, 1.0 and so on. This has been done in order to display on a single graph the behavior of the log-log analysis as a function of the threshold parameter H_0. The log-log analysis is an attempt to fit the activation curve with a function of the form $Y = k(H-H_0)^x$. H_0 is said to be the threshold because when $H = H_0$ the yield is zero and this is what is meant by threshold. One of the main advantages of this type of analysis is the fact that the yield data is uniquely extrapolated to zero yield.

---

[4] All the activities, unless otherwise stated, have been corrected for cosmic-ray background.

It is evident from inspection of Fig. 16 that the best fit to a straight line is obtained with $H_0 = 669$ and $x = 2.23$. A choice of H_0 different by 1 h.u. from 669 gave a much poorer fit to the data. The threshold was therefore taken to be 669 ± 1 h.u. in agreement with that obtained by inspection of Fig. 15, 670 ± 1 h.u. The agreement obtained with these two methods showed that the sensitivity of the determination was such that practically no part of the activation curve near threshold was obscured by the remanent activity.

An advantage of the log-log analysis is that the threshold determination is made to depend upon a 3-Mev interval of the activation curve. The accuracy of the determination, however, depends upon the ability to get reliable data close to the threshold.

4.6 Other Cu^{63} Threshold Determinations

Not illustrated are the results of the threshold data tabulated in Tables 6 and 7. In the Cu^{63} threshold determination of Table 6 a precision of $\pm$ 1 h.u. (about 14 kev) was achieved for the first time. The data of Table 7 yielded a threshold of 674 ± 1 h.u. referred to a control of 480 c/r. Six control runs were taken during this determination with a dispersion of Cu control activities of 487 - 473 c/r or ± 0.4 h.u.

TABLE 4. Cu^{63} Threshold Determination No. 2

Run No.	Helipot	Activity (c/r)
715	654	2.6
703	660	2.0
721	662	2.3
713	664	2.2
719	666	2.7
711	669	2.9
727	669	3.0
701	670	2.8
710	671	3.0
706	672	3.3
707	673	4.5
709	674	4.9
705	675	6.7
734	676.4	8.3
736	678.4	11.1
699	680	16
702	685	31
698	690	54
695	700	132
697	710	239
693	720	389
695	730	565
739	740	784
723	749	992
724	769	1632
733	791	2504
738	820	4176

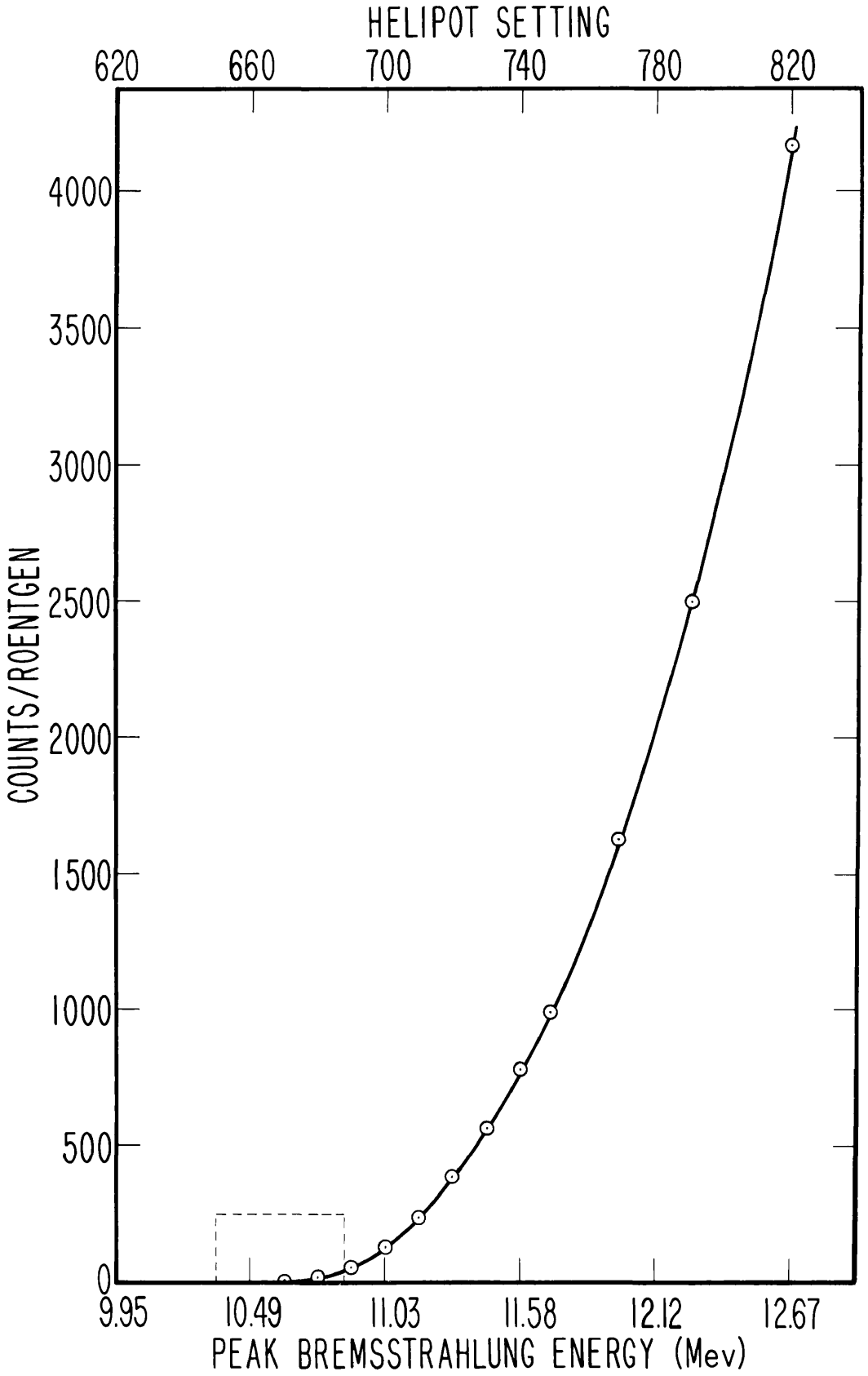

Fig. 14. Cu^{62} Activation Curve.

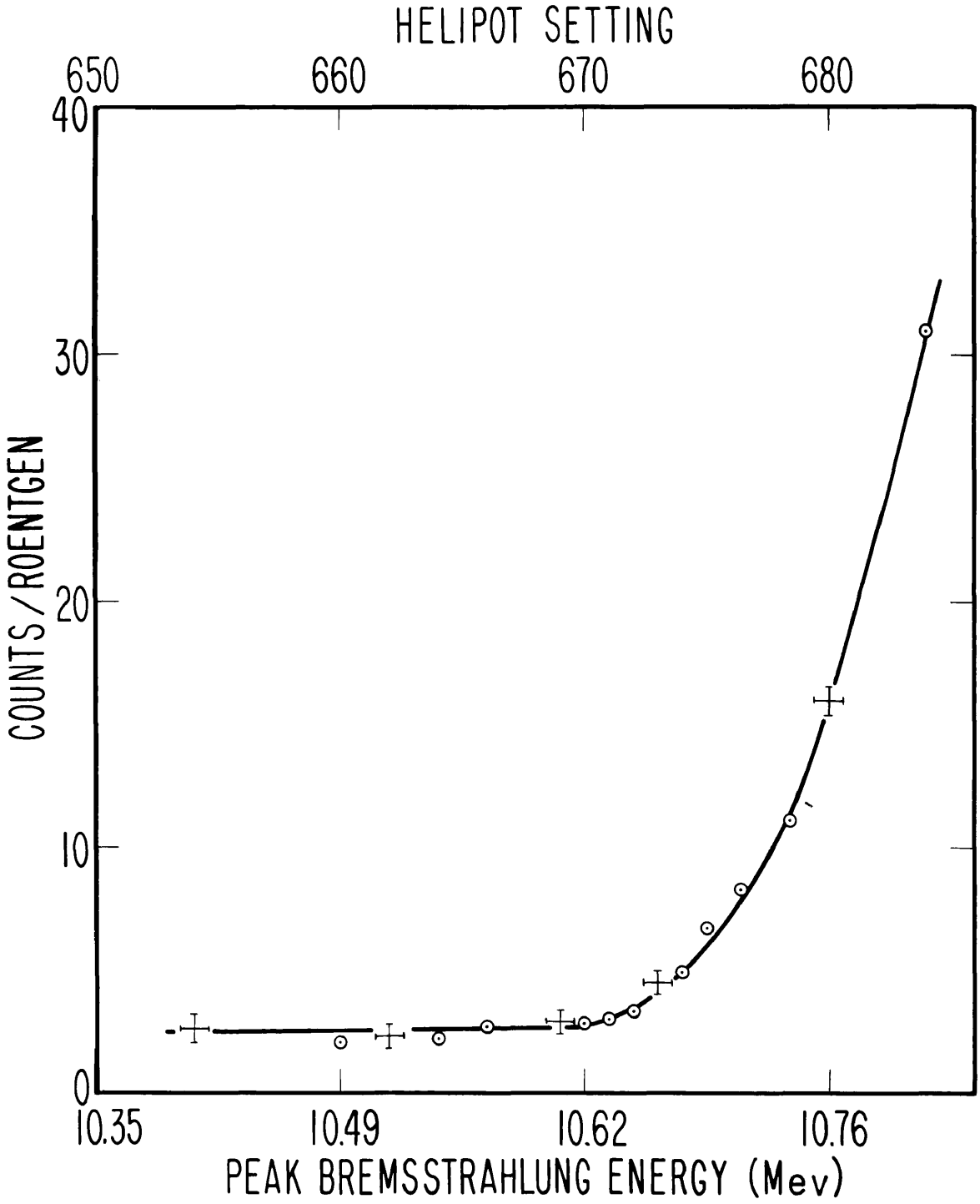

Fig. 15. Cu^{62} Activation Curve near Threshold.

TABLE 5. Cu^{63} Threshold by log-log Analysis.

Helipot	Corrected Activity (c/r)	Log_{10} (c/r)
673	1.4	0.146
674	1.8	0.255
675	3.5	0.544
676.4	5.1	0.708
678.4	7.8	0.892
680	12.5	1.10
685	27.3	1.44
690	50	1.70
700	127.5	2.105
710	233.9	2.369
720	382.4	2.582
730	558.9	2.747
749	985	2.99
769	1623	3.21
791	2494	3.395
820	4166	3.62

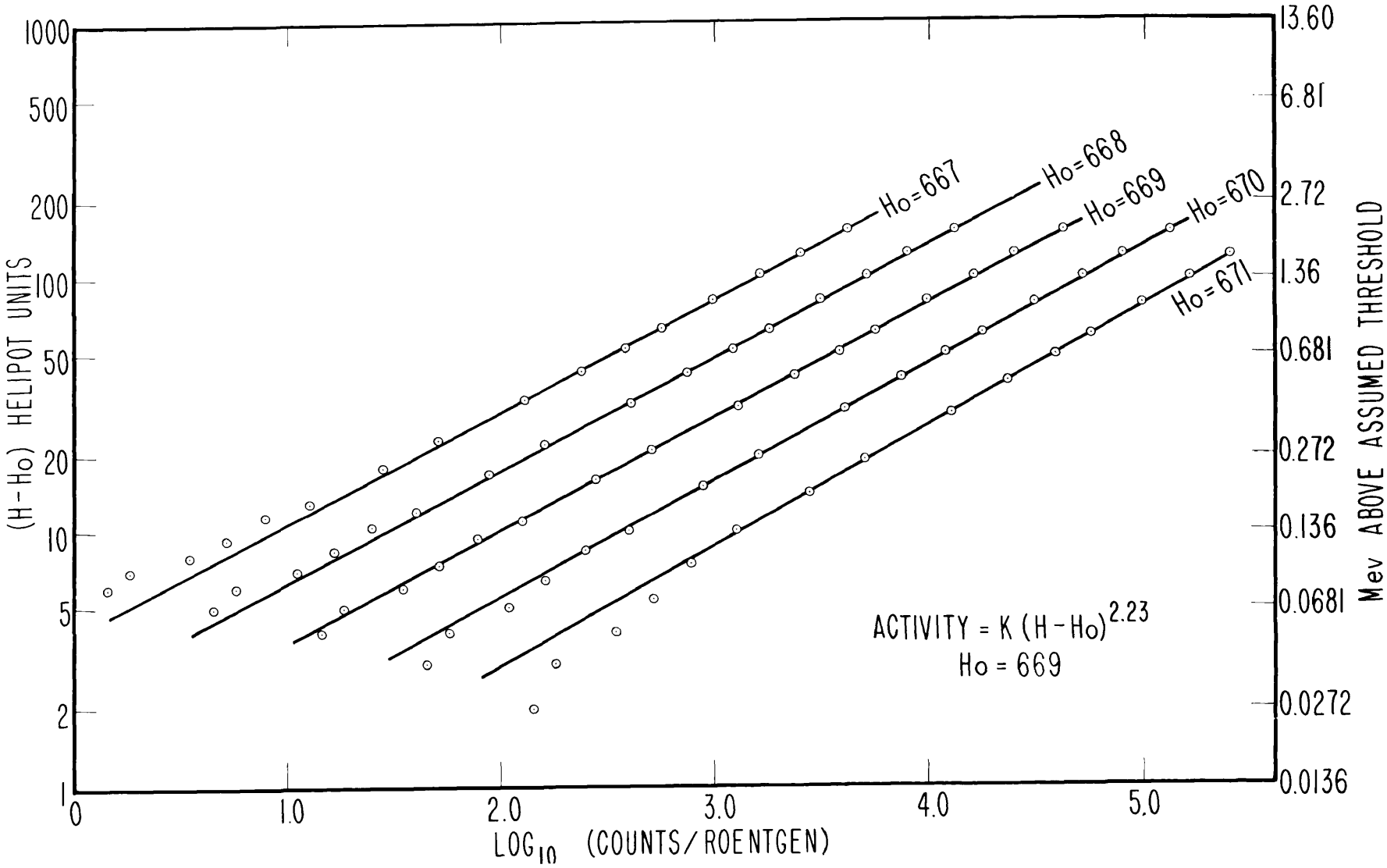

Fig. 16. Log-log Analysis of Cu^{62} Activation Curve.

TABLE 6. Cu^{63} Threshold Determination No. 1

Run No.	Helipot	Activity (c/r)
316	710	2.66
312	715	3.42
311	720	3.14
310	725	3.19
314	728	3.57
309	730	8.38
322	733	12.0
307	735	22.0
324	738	32.3
306	740	46.0
323	743	66.4
305	745	82.6
303	750	129
302	760	280
301	770	479
320	780	727
319	790	989
318	800	1368
326	825	2370
327	850	4000
328	875	5910
329	900	7940

TABLE 7. Cu^{63} Threshold Determination No. 3

Run No.	Helipot	Activity (c/r)
1229	672	2.5
1232	673	2.1
1230	674	2.5
1223	675	2.75
1228	676	3.30
1224	677	3.98
1237	678	3.65
1234	679	5.14
1219	680	5.71
1225	682	9.11
1235	684	12.6
1220	685	14.0
1233	687	19.9
1227	688	25.2
1222	690	30.5

CHAPTER V

PHOTONEUTRON THRESHOLD DETERMINATION OF Ag^{109}

5.1 Introduction

The photoneutron threshold for Ag^{109} was measured to test the method used for Cu^{63} on a different nucleus. The following considerations led to the choice of Ag^{109}. Naturally occurring silver has an isotopic constitution consisting of the two isotopes Ag^{107} and Ag^{109} in nearly equal abundance. It was known that the threshold for Ag^{109} was at least 0.2-Mev below that of Ag^{107}. The photoneutron reactions lead to Ag^{108} and Ag^{106} with half-lives of 2.3 and 24.5 min. respectively (20). Thus the threshold of Ag^{109} could be obtained free from the interfering activity of the Ag^{106}. Furthermore, the short half-life of Ag^{108} indicated that, with an irradiation and counting schedule similar to that used for Cu, almost saturated activation would be achieved and that the experiment approached optimum conditions for a threshold determination.

From a sheet of Ag with a known purity of better than 99.9%, 40 discs were machined which were identical, in all dimensions, to those of Cu. A set of runs at a constant helipot setting indicated that the discs were completely interchangeable, a result which could have been inferred from their physical similarity.

5.2 Half-lives of Ag^{108} and Ag^{106}

In Fig. 17 and 18 are shown the decay curves of the beta emitters Ag^{108} and Ag^{106}. These curves were obtained from the decay of activity

of a single irradiation. The decay curve for Ag^{106} is shown with the first point at 24 min. after exposure at which time the 2.4 min. activity had practically disappeared. The decay curve of the 24 min. Ag^{106} was extrapolated back to zero time and was subtracted from the initial counting rate. The net counting rates are plotted in Fig. 17. The measured half lives from Fig. 17 and 18 were 2.46 min. and 24.4 min. in agreement with the values 2.33 min. for Ag^{108} and 24.5 min. for Ag^{106} (20).

5.3 Correction for 24 min. Ag^{106} Activity

For helipot settings of about 24 h.u. (about 330 kev) above that which corresponded to the Ag^{109} threshold, the 24 min. Ag^{106} activity was observed. In order to estimate the number of counts recorded in the first 9 min. due to this activity, the decay of the sample activity was followed for about 40 to 60 min. It had been noted in earlier work with Ag that the 2.4 min. activity is virtually absent at about 20 min. after exposure. Thus the decay curve for the 24 min. Ag^{106} activity was plotted and extrapolated back to the time at which the counting started. The number of Ag^{106} counts in the first 9 min. was obtained as follows.

The counting rate is given by

$$C = C_0 e^{-\lambda t} \qquad (5\text{-}1)$$

where C_0 is the initial counting rate, and is the decay constant for the 24 min. Ag^{106}. The number of counts, N, is obtained by integrating the above equation.

$$N = \int_0^T C\,dt = (C_0/\lambda)(1-e^{-\lambda T}) \qquad (5\text{-}2)$$

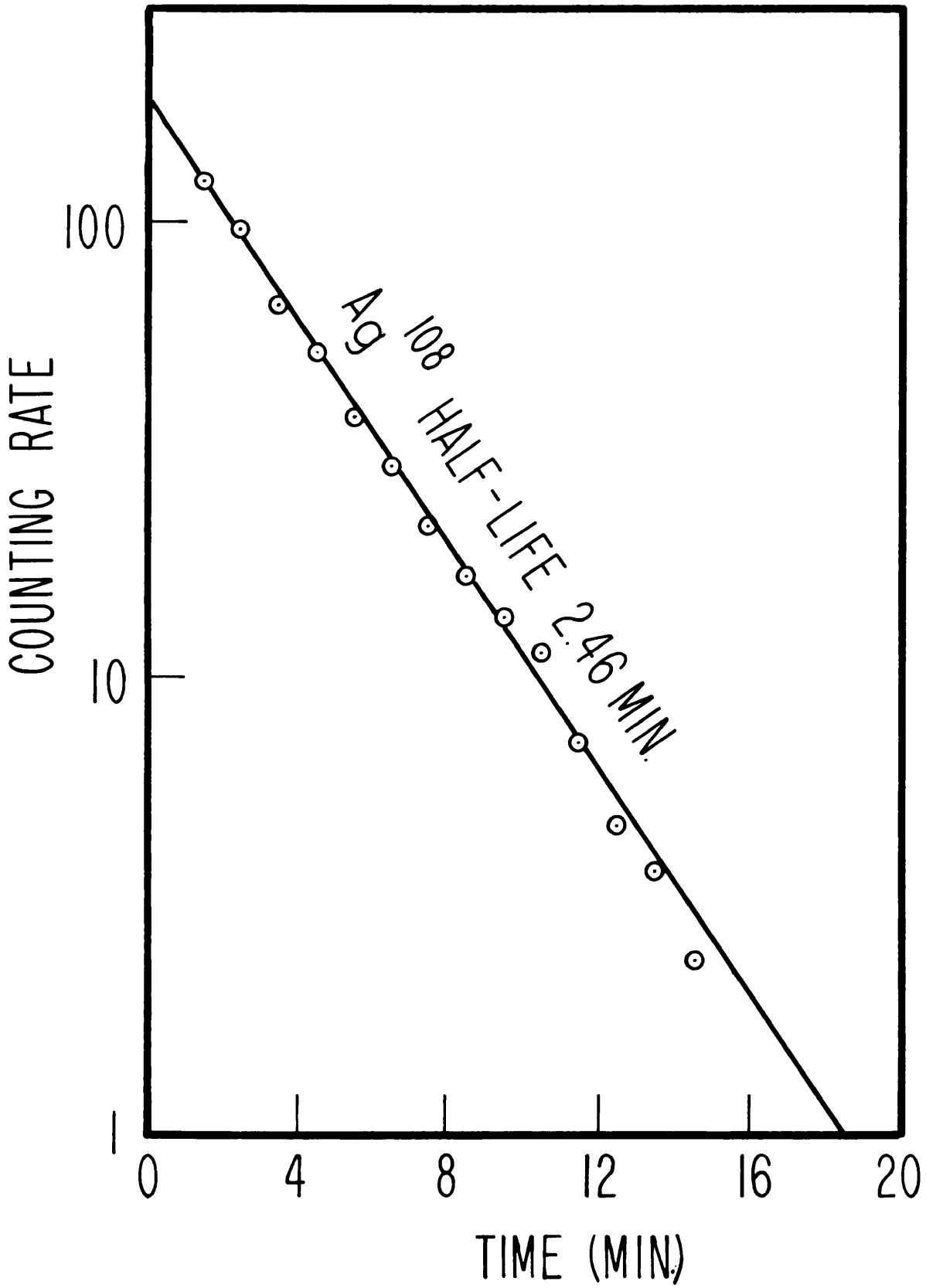

Fig. 17. Ag^{108} Decay Curve.

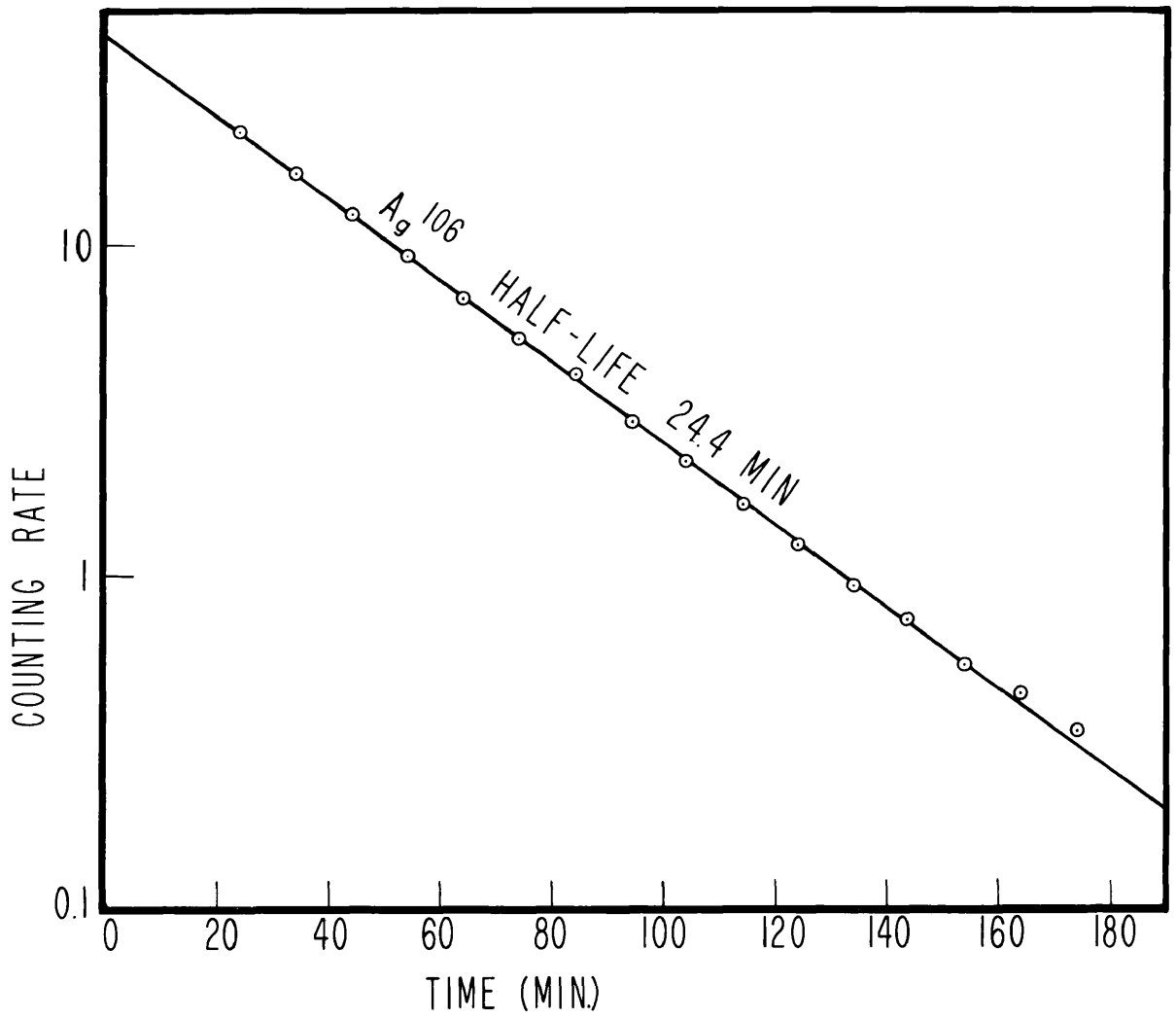

Fig. 18. Ag^{106} Decay Curve.

The initial counting rate was obtained by the extrapolation of the Ag^{106} decay curve. Substituting this value and T = 9 min. in equation (5-2), the number of counts due to the 24 min. activity was obtained.

For irradiations at helipot 630 and above (data of Table 9), the standard exposure of 5 min. would result in too high an initial counting rate. To avoid this condition, shorter exposure times were used. This procedure was beneficial in another way: it discriminated against the 24 min. activity. Correction to the standard 5 min. exposure was done in the same way as for Cu, Section 4.3; the activities were first corrected by subtracting counts due to the 24 min. activity and the cosmic-ray background.

5.4 Ag^{108} Activation Curve

The general procedure for the determination of the Ag^{109} (γ, n) threshold was similar to the method used for Cu. In order to reduce as much as possible the activities induced by neutron absorption, the silver disc was surrounded with cadmium using the sample holder shown in Fig. 5. Near threshold, each Ag disc was irradiated for 5 min., receiving about 4500 r. Counting was started 1 min. after the exposure and terminated on the tenth minute.

The results of threshold determination No. 1 of Ag^{109} are tabulated in Table 9. The activities in column 3 have been corrected for cosmic-ray background, 24 min. Ag^{106} activity and the different exposure times employed. The activation curve is shown in Fig. 19. The portion of the curve enclosed in the dashed lines of Fig. 19 is shown enlarged in

Fig. 20. Inspection of Fig. 20 indicated a threshold of 551 1 h.u.

It is also apparent from Fig. 20 that there is still a residual activity below threshold. This was analyzed by following the decay of activity of the discs. This residual activity showed a half-life of about 2 min. However, there were only about 400 counts in each run and so the statistics were necessarily poor. The activity was identified as that of Ag^{108} with a half-life of 2.4 min. (2) produced through neutron capture in Ag^{107}.

The helipot settings shown in column 2, Table 9 have been normalized to a Cu control activity of 680 c/r. Most of the data near threshold was obtained with a control Cu of 680 c/r and required no correction. The corrected helipot settings are given in most cases to the nearest helipot unit. The estimated precision of the helipot settings in most cases was $\pm$ 0.6 h.u. The data shown in Table 9 was gathered over a 5 day interval during which time 43 control runs were taken. These showed a spread in activity of from 709 - 648 c/r or $\pm$ 1.5 h.u. The control data in terms of individual days are shown below in Table 8.

TABLE 8. Control Data for Ag^{109} Threshold No. 1.

Day	No. of Control Runs	Spread in Activities (c/r)	Spread in h.u.
1	5	702-678	0.5
2	13	681-648	0.75
3	5	684-674	0.25
4	12	682-665	0.5
5	8	709-690	0.5

The Cu control data of Table 8 illustrates a characteristic already mentioned, namely, that on a given day the stability of the peak x-ray energy will usually be better than the day-to-day stability.

5.5 Threshold Determination by log-log Analysis

The log-log analysis of the Ag^{108} activation data is shown in Fig. 21. The same considerations apply here as described for Cu^{62} in Section 4.5. The data plotted in Fig. 21 are tabulated in Table 10. The line denoted by $H_0 = 549$, in Fig. 21 has abscissas which are log (c/r) + 0.2; $H_0 = 550$, log (c/r) + 0.7; $H_0 = 551$, log (c/r) + 1.2, and so on. As in the previous case, this is done in order to display the entire analysis on a single sheet. The threshold obtained by this method was 551 ± 1 h.u. in exact agreement with that obtained by inspection of the activation curve of Fig. 20.

5.6 Repeat Determination of Ag^{109} Threshold

Not shown analyzed by means of figures are the results of the Ag^{109} threshold data summarized in Table 11. The threshold as determined by inspection of the activation curve and analysis by means of a log-log plot were in agreement. The threshold for this determination was found to be 560 ± 1 h.u. referred to a Cu control activity of 520 c/r. Eight control runs were taken with a spread of 548 - 520 c/r or ± 0.7 h.u.

5.7 Summary of Cu^{63} and Ag^{109} Threshold Determinations

The thresholds of Cu^{63} and Ag^{109} have been determined with a precision that exceeds by almost a factor of ten that obtained by previous investigators. It has been found both for Cu^{63} and Ag^{109} that the

activation curves can be represented by a function of the form $Y = k(H-H_0)^x$ over a 3-Mev interval which is in agreement with the results of other investigators (3, 10). However, the method used by Sher et al. (10) is so different as to make comparison difficult. The results are tabulated in Table 12 below.

TABLE 12. Comparison of Values of Exponent.

Target Nucleus	Exponent		
	Birnbaum	McElhinney (3)	Sher (10)
Cu^{63}	2.23	2	1.5
Ag^{109}	1.90	2	2.5

TABLE 9. Ag^{109} Threshold Determination No. 1

Run No.	Helipot	Activity (c/r)
805	530	7.0
806	535	7.0
776	540	6.5
808	540	7.4
812	543	7.4
774	545	6.4
809	545	7.9
811	547	6.4
813	549	7.7
840	549	7.7
773	550	7.7
839	551	7.9
778	552	8.5
815	552	7.2
842	553	8.8
844	553	7.8
816	554	8.3
772	555	9.2
838	555	8.9
818	556	9.3
836	556	8.9
781	557	11.4
823	557	9.6
825	558	12.0
835	558	10.9
770	560	13.0
834	560	12.6
832	562	15.5
769	565	20.0
831	567	24.0
767	570	32.5
762	575	50.3
782	579	61.1
784	584	87.2
786	589	110.0
788	599	158
790	609	233
792	630	368
793	650	535
798	670	712
800	700	1177

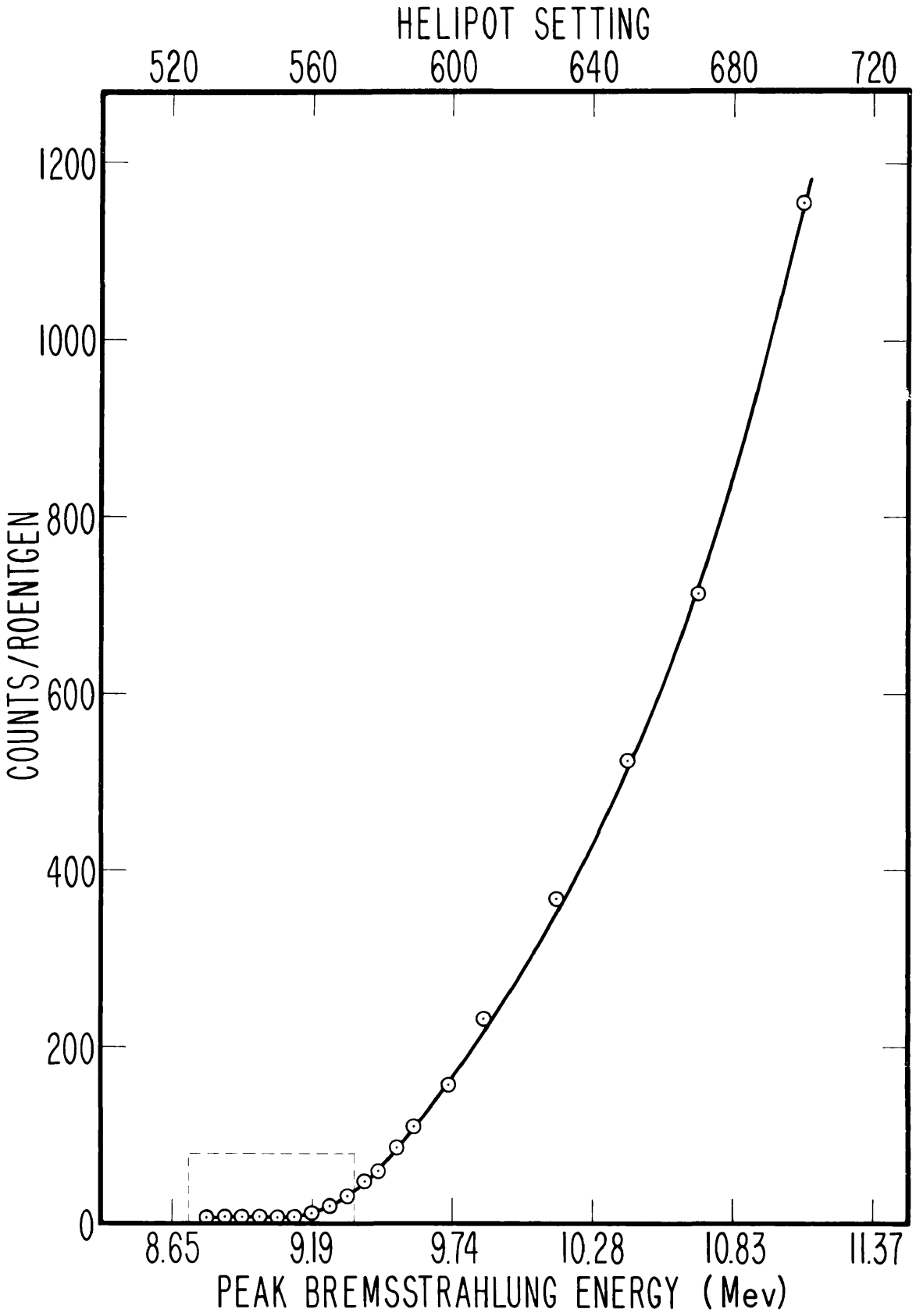

Fig. 19. Ag^{108} Activation Curve.

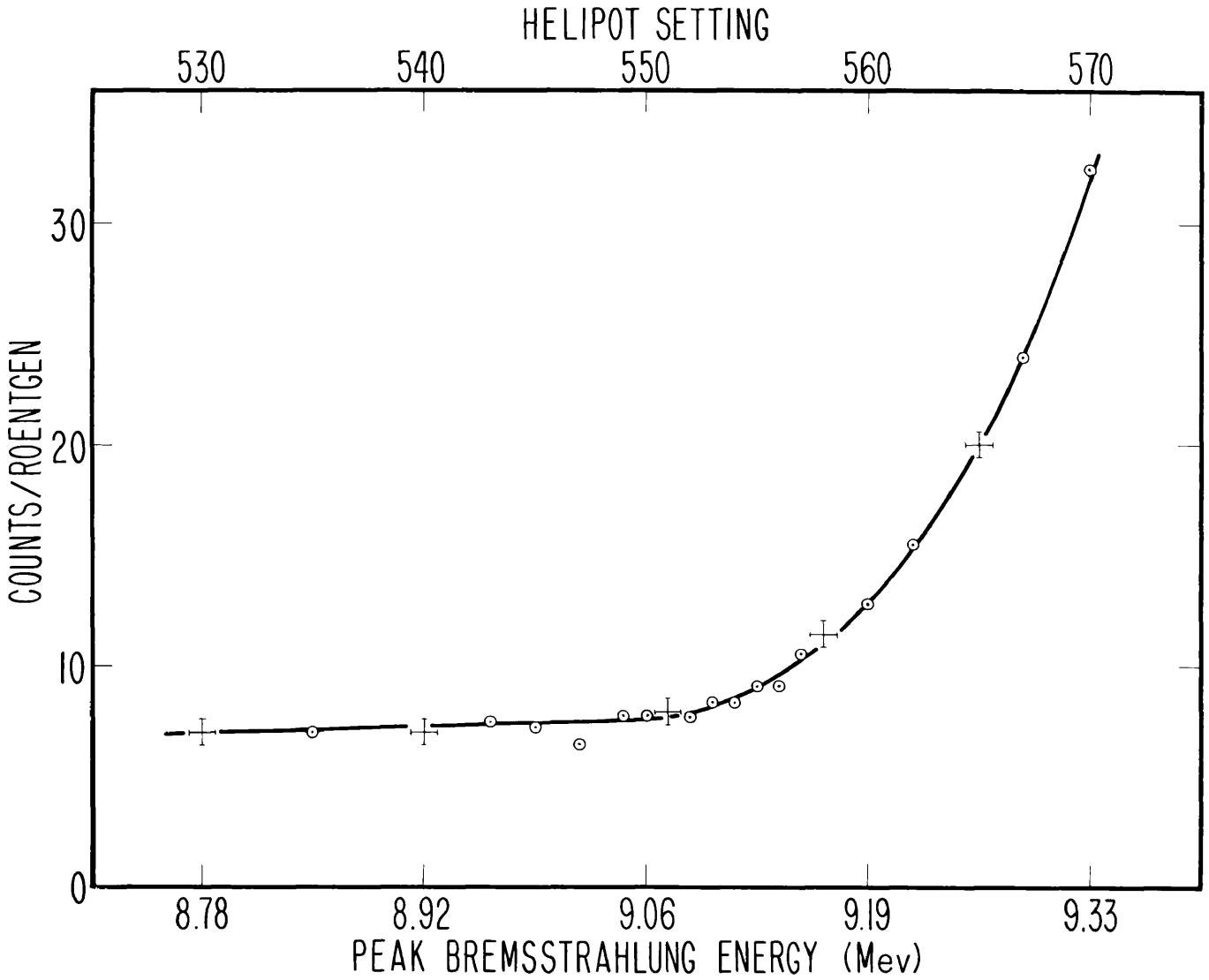

Fig. 20. Ag^{108} Activation Curve near Threshold.

TABLE 10. Ag^{109} Threshold by log-log Analysis.

Helipot	Corrected Activity (c/r)	log (c/r)
554	0.7	-0.155
555	1.4	0.146
556	1.5	0.176
557	2.9	0.462
558	3.8	0.580
560	5.1	0.707
562	7.8	0.892
565	12.2	1.086
567	16.2	1.2095
570	24.6	1.393
575	42.4	1.627
579	53.1	1.725
584	79.1	1.898
589	101.9	2.008
599	150	2.176
609	225	2.352
630	359	2.555
650	525	2.720
670	702	2.846
700	1165	3.071

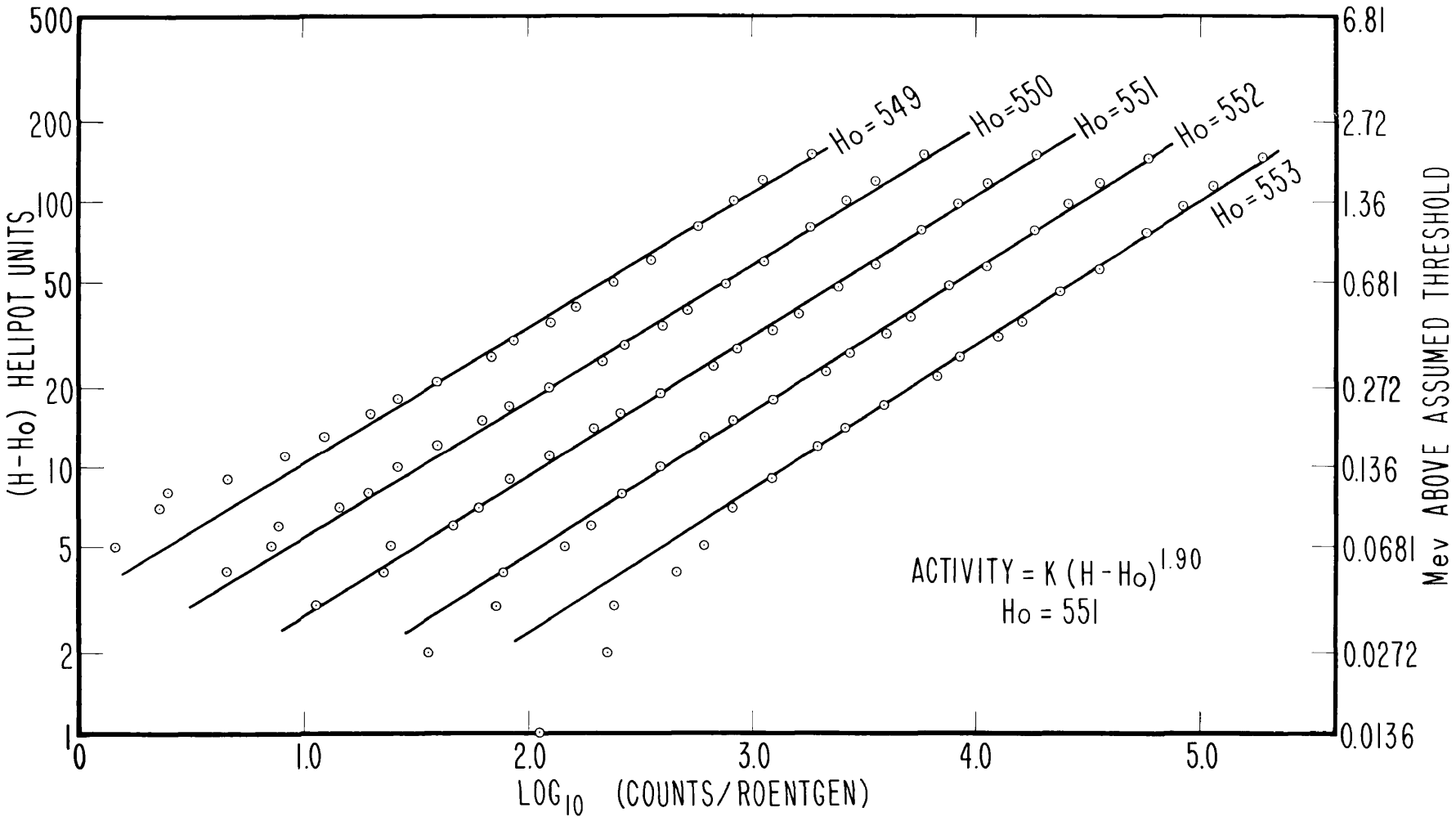

Fig. 21. Log-log Analysis of Ag^{108} Activation Curve.

TABLE 11. Ag^{109} Threshold Determination No. 2

Run No.	Helipot	Activity (c/r)
1192	545	6.05
1194	550	5.75
1195	555	6.84
1196	560	6.84
1211	562	7.25
1203	563	8.10
1213	564	8.3
1198	565	9.0
1205	567	10.2
1215	568	11.8
1199	570	13.4
1207	572.5	15.5
1200	575	23.3
1208	577.5	25.9
1202	580	34.1
1209	583	39.9
1204	585	42.9
1212	586	52.2

CHAPTER VI

PHOTONEUTRON THRESHOLDS OF C^{12}, N^{14}, O^{16}

6.1 O^{16} Threshold Determination

The photoneutron threshold of O^{16} was determined because its threshold is known very accurately from the mass data (21) and thus could serve as a calibration point for the energy scale. Naturally occurring oxygen has an isotopic constitution consisting of 99.76% O^{16} with very small amounts of O^{17} and O^{18}. The 2 min. half life of O^{15} indicated that, with an irradiation and counting schedule similar to that employed for Cu and Ag, saturated sample activation would be achieved and again the experimental conditions would approach optimum for a threshold determination. It was decided to use boric acid (H_3BO_3) for the oxygen determination because it was a solid which contained a very high percentage of oxygen by weight and no other nuclei which would produce interfering activities upon irradiation. The photoneutron reaction in B^{10} leads to a product with a half-life too short to be determined. Neutron capture in B^{11} produces B^{12} which decays with a half-life of 0.02 sec.

About 20 discs of boric acid were prepared by compressing chemically pure boric acid powder in a mold. The discs were then machined to the standard sample size of 1.750 in. diameter and 0.125 in. thickness. As a check on the similarity of the discs, they were all weighed on a chemical balance. Discs numbered 17, 19 and 20 weighed respectively 7.156, 7.151 and 7.146 grams. In view of the presence of a single

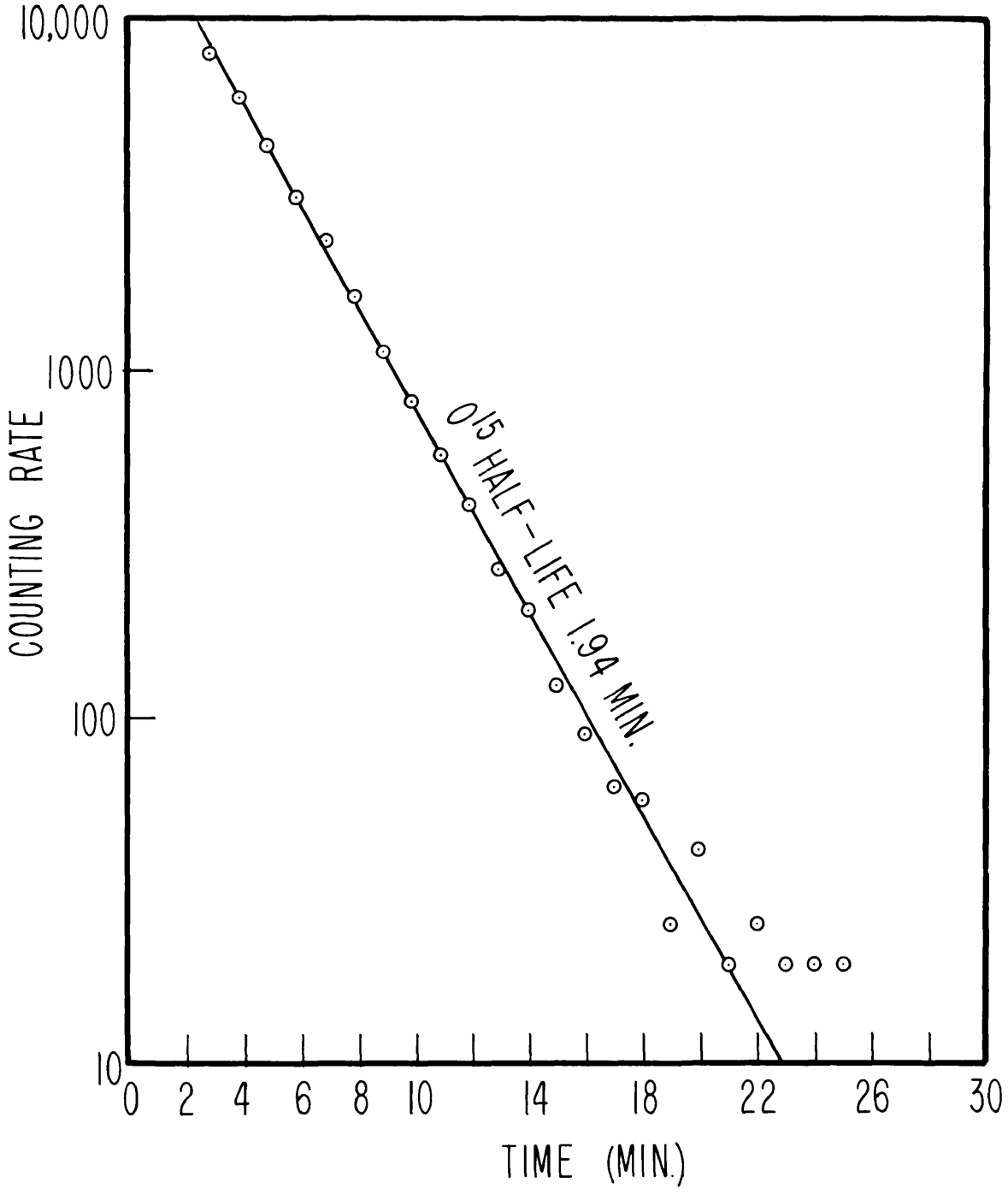

Fig. 22. O^{15} Decay Curve.

activity with a 2 min. half-life, three discs would suffice for the determination. As a further check on the equivalence of these discs, they were irradiated at a high energy where the statistical error due to the number of counts was about 2.6%. The activities were the same within the statistical error and thus confirmed what could have been inferred from the almost complete physical identity of the samples.

The decay curve of an irradiated boric acid disc (oxygen) is shown in Fig. 22. The measured half-life was 1.94 min. in agreement with the O^{15} half-life of 1.97 min. (20).

The procedure used was similar to that already described, except that the samples were not surrounded by cadmium during exposure. The exposure time was 4 min. during which the sample received about 13,000 roentgens. It was counted for 10 min. beginning 1 min. after exposure.

The data of threshold determination No. 1 are shown in Table 13. Column 3 lists the measured activities corrected for cosmic ray background. These data are shown graphically in Fig. 23. The portion enclosed within the dashed line is shown on an expanded scale in Fig. 24. It is seen on inspection of Fig. 24 that the threshold for the photoneutron reaction in O^{16} was at 1034 ± 1 h.u. A log-log analysis of the oxygen data revealed that a representation of the form $Y = k(H-H_0)^x$ is no longer valid over a 3-Mev (about 220 h.u.) portion of the activation curve. The data shown in Fig. 24 showed that from helipot 1070 down to threshold (about 480 kev) the activation curve was linear. The intersection of this line with that determined by the points below helipot 1033 is used as the

experimental definition of threshold for the reaction O^{16} (γ, n) O^{15}.

Analysis of the decay curves below helipot setting 1034 indicated the presence of a 5 - 10 min. activity. Only about 50 counts were obtained after subtraction of cosmic-ray background during the 10 min. counting interval. The poor statistics prevented a more reliable determination. An analysis of the decay curves for a series of oxygen runs ranging from helipot 1180 - 1040 indicated the 2 min. O^{15} half-life.

The helipot settings listed in column 2, Table 13 have all been normalized to a Cu control activity of 710 c/r. Most of the data near threshold were taken with a control of 710 c/r. The estimated precision of the helipot settings was $\pm$ 0.6 h.u. About 4 days were required to obtain the data of Table 13 and 25 control runs were taken. The spread in the control activities was 740 - 685 c/r or $\pm$ 1.4 h.u.

Not shown graphically are the data of Table 14. The threshold determined from a plot of this data was found to be 1040 $\pm$1 h.u. referred to a Cu control activity of 480 c/r. Sixteen control runs were taken with a spread in activity of 497 - 462 c/r or $\pm$0.8 h.u.

TABLE 13. O^{16} Threshold Determination No. 1

Run No.	Helipot	Activity (c/r)
869	1010	0.26
868	1020	0.25
873a	1025	0.30
871a	1028	0.14
867	1030	0.25
870a	1032	0.32
869a	1034	0.25
888	1034.5	0.42
886	1035.5	0.56
867a	1036.5	0.71
885a	1036.5	0.87
889	1037	0.65
886	1037	0.76
884a	1038	1.00
885	1039	0.95
865	1040	1.42
882a	1043	1.75
883	1044	2.08
881a	1048	2.40
882	1049	2.56
864	1050	3.17
890	1053	3.50
880	1054	3.45
879	1059	4.05
863	1060	4.49
892	1064	4.43
875a	1070	5.42
859	1080	7.97
879a	1080.5	8.82
858	1090	10.2
856	1100	17.7
855	1110	28.6
854	1120	57.6
853	1130	86.4
852	1140	112
850	1160	169
849	1180	218

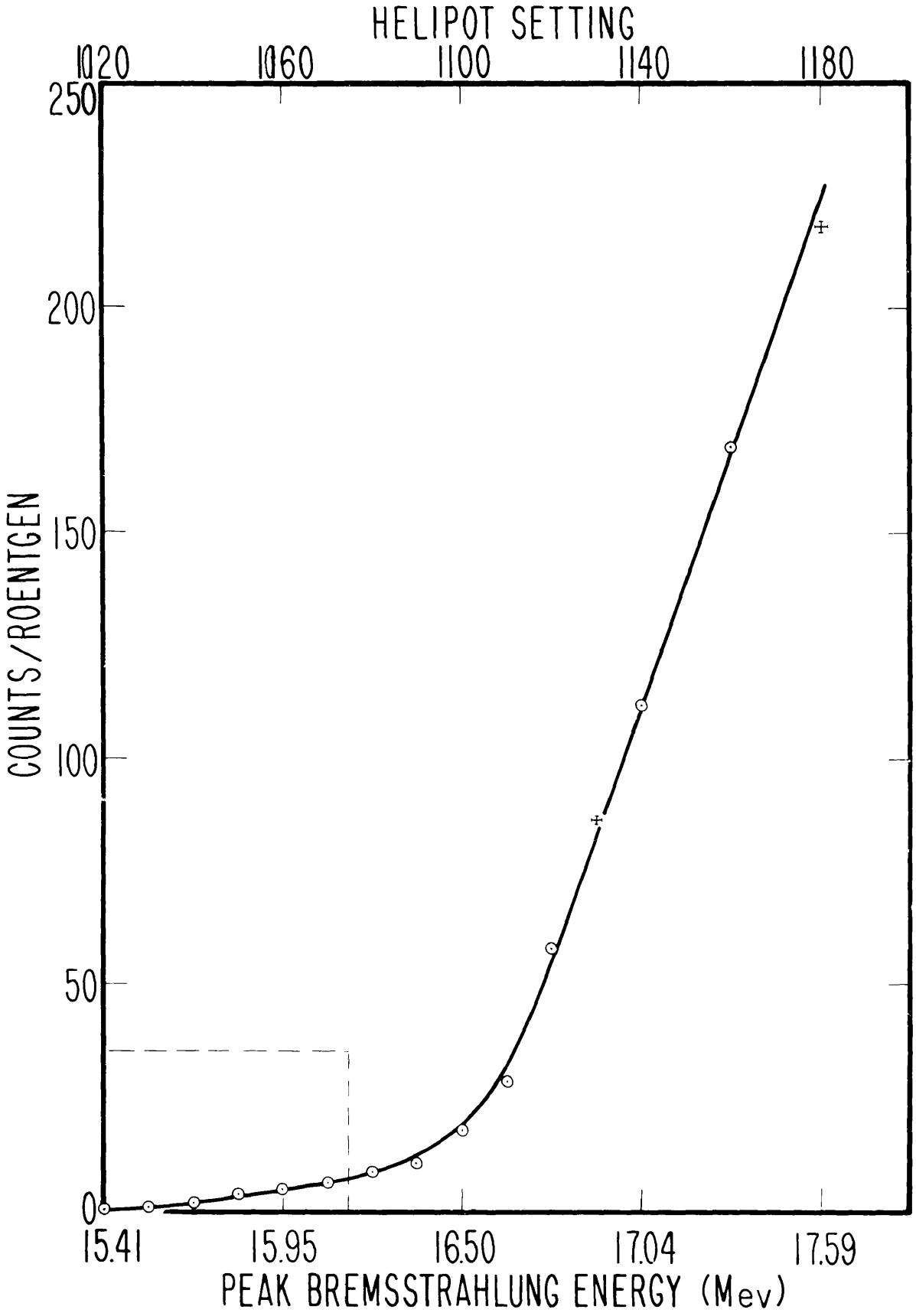

Fig. 23. O^{15} Activation Curve.

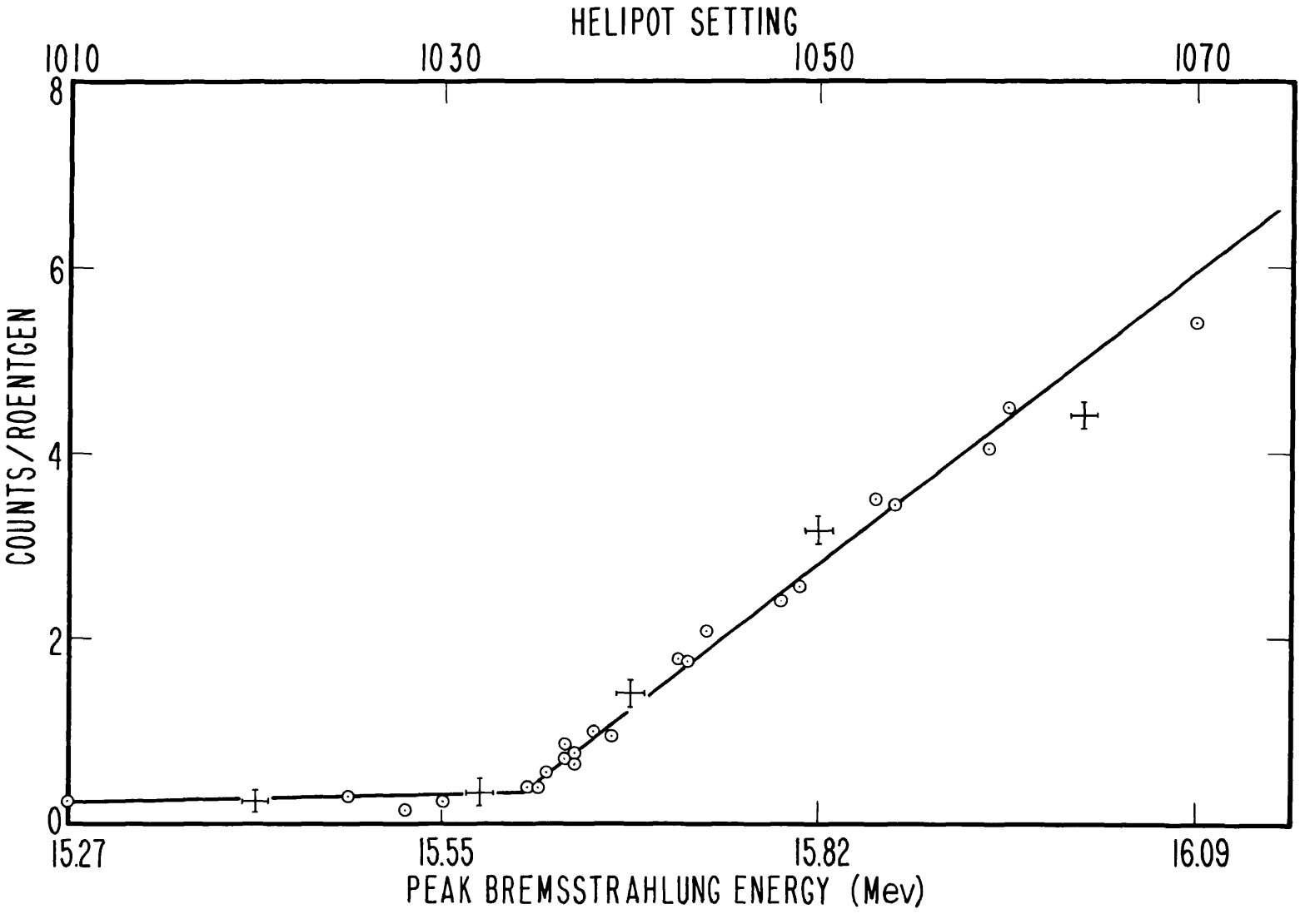

Fig. 24. O^{15} Activation Curve near Threshold.

TABLE 14. O^{16} Threshold Determination No. 2

Run No.	Helipot	Activity (c/r)
1103	1020	0.21
1102	1025	0.29
1101	1030	0.30
1105	1032	0.30
1106	1034	0.41
1099	1035	0.56
1110	1036	0.40
1111	1038	0.45
1126	1040	0.34
1098	1040	0.83
1114	1041	0.67
1115	1043	1.09
1097	1045	1.19
1121	1045	1.28
1119	1047	1.55
1117	1049	1.74
1095	1050.5	2.12
1118	1053	2.52
1094	1055.5	2.71
1133	1057	3.25
1127	1058	3.22
1092	1061	3.86
1128	1061	3.71
1134	1063	4.07
1123	1065	4.24
1137	1067	4.78
1135	1067	4.96
1125	1070	4.96
1131	1075	6.54

6.2 N^{14} Threshold Determination

The photoneutron threshold of N^{14} would also provide a calibration point for determination of the energy scale. Naturally occurring nitrogen consists of 99.62% N^{14} and 0.38% N^{15} and thus it is expected that irradiation will produce only the 10 min. N^{13} activity. Neutron absorption by N^{14} results in N^{15} which is stable. After a considerable search among the various solid compounds containing a high percentage of N by weight, it was decided to use melamine, $C_3N_6H_6$.[1] The presence of carbon does not interfere with the determination of the N^{14} threshold since its threshold is 8 Mev above that of N^{14}. About 20 discs of melamine were accurately machined to a diameter of 1.750 in. and a thickness of 0.125 in.

The decay of activity of an irradiated melamine disc is shown in Fig. 25. The measured half-life was 10.4 min. in agreement with the reported value of 10.1 min. (20).

The procedure employed was similar to that described for the O^{16} determination. The irradiation time was 15 min. during which time the sample received about 20,000 r. The sample was counted for 30 min. beginning 1.5 min. after the exposure.

The data of threshold determination No. 1 are listed in Table 15. The activities in column 3 have been corrected for cosmic-ray background. The N^{14} activation curve based on these data is shown in Fig. 26. In Fig. 27 is shown, on an expanded scale, the portion of the

---

[1] The author wishes to thank the American Cyanamid Co. for their cooperation in providing the pure melamine resin.

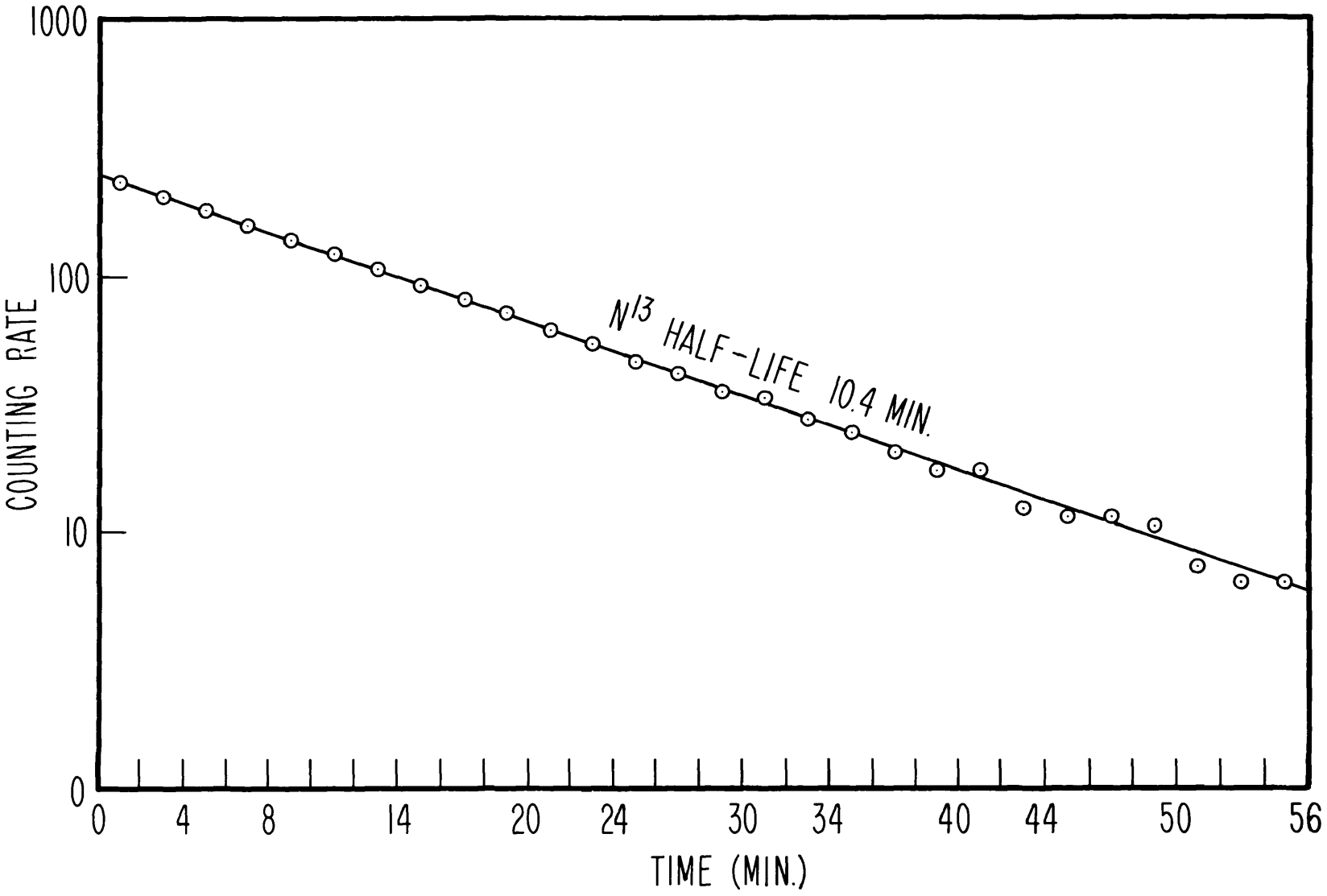

Fig. 25. N^{13} Decay Curve.

activation curve enclosed by the dashed line in Fig. 26. It will be remarked again that vertical bars represent the standard error due to counting statistics alone; the horizontal bar, the uncertainty in the helipot setting. Inspection of Fig. 27 showed the threshold to be 659 ± 2 h.u. Analysis indicated that the activation curve of Fig. 26 cannot be represented by a function of the form, $Y = k(H-H_0)^x$. The graph of Fig. 27 showed that from helipot 684 down to threshold (about 340 kev), the activation curve is linear. The threshold was determined by the intersection of this line with the line determined by the points below threshold. This was taken to be the experimental definition of threshold for the photoneutron reaction in N^{14}.

The activity of the points below the threshold was the lowest encountered and was so weak that it was not feasible to attempt a half-life analysis. On the average, 9 counts were recorded in the 30 min. counting interval for the points below threshold.

The helipot settings listed in column 2, Table 15 have all been normalized to a Cu control activity of 710 c/r. A precision of ± 0.6 h.u. was estimated for the helipot settings. The data of Table 15 was gathered during a 4 day interval and 25 Cu control runs were taken. These showed a spread in activities of 743 - 657 c/r or ± 2.1 h.u.

Not shown graphically are the data summarized in Table 16. The threshold determined from a plot of this data was found to be 659 ± 2 h.u. referred to a Cu control activity of 480 c/r. Fifteen control runs were obtained with a spread in activities of 502 - 465 c/r or ± 0.9 h.u.

TABLE 15. N^{14} Threshold Determination No. 1

Run No.	Helipot	Activity (c/r)
910	644	0.03
909	649	0.05
929	655	0.08
938	658	0.02
907	660	0.01
994	661	0.07
926	662	0.12
942	662	0.10
936	664	0.12
922	665.5	0.19
944	668	0.24
928	668.5	0.26
906	671	0.31
924	675	0.36
934	678	0.45
904	681	0.50
932	685	0.63
903	691	0.89
901	700	1.41
897	700	1.41
912	709	2.28
913	719	3.68
917	730	6.21
918	740	8.81

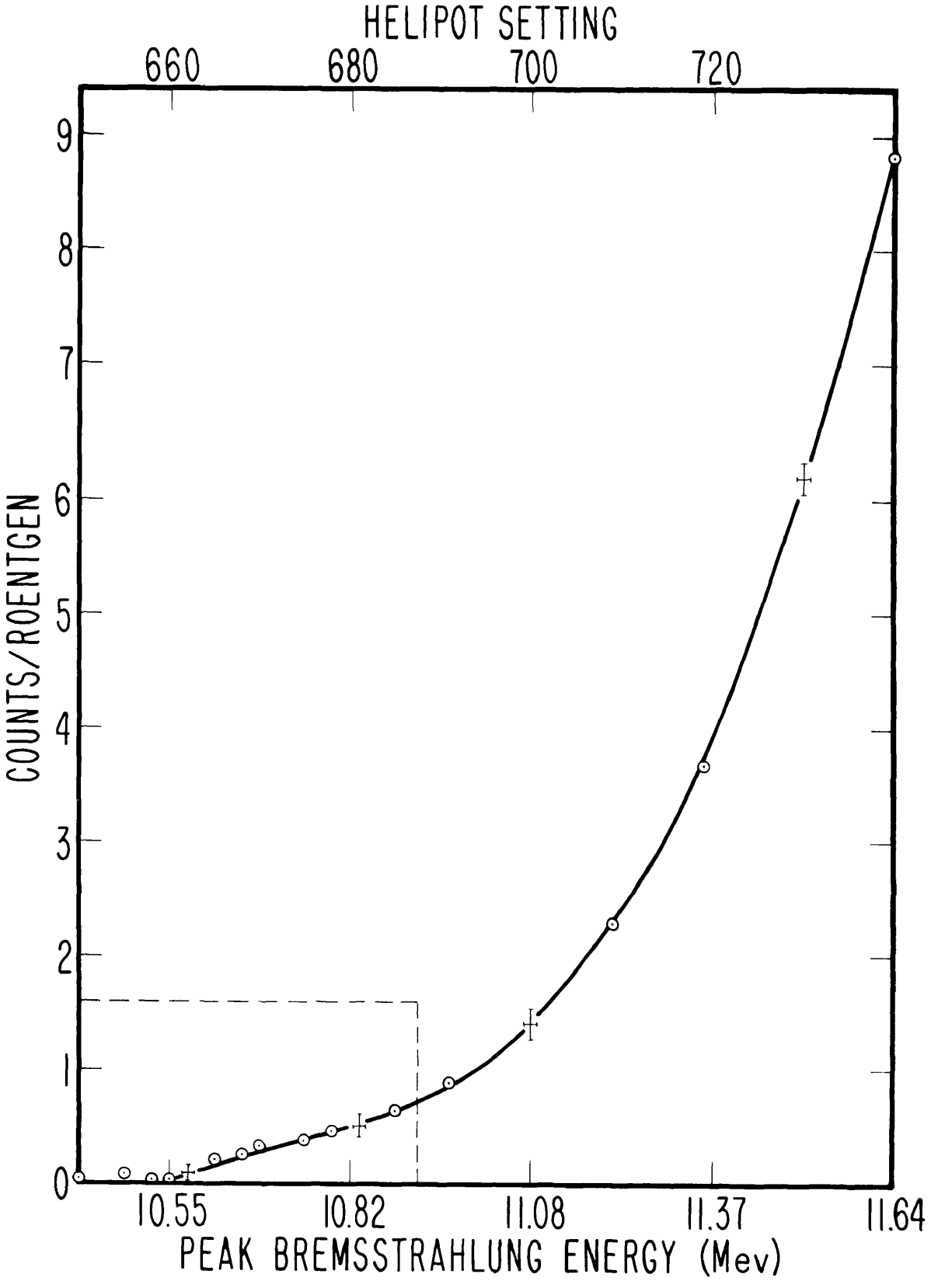

Fig. 26. N^{13} Activation Curve.

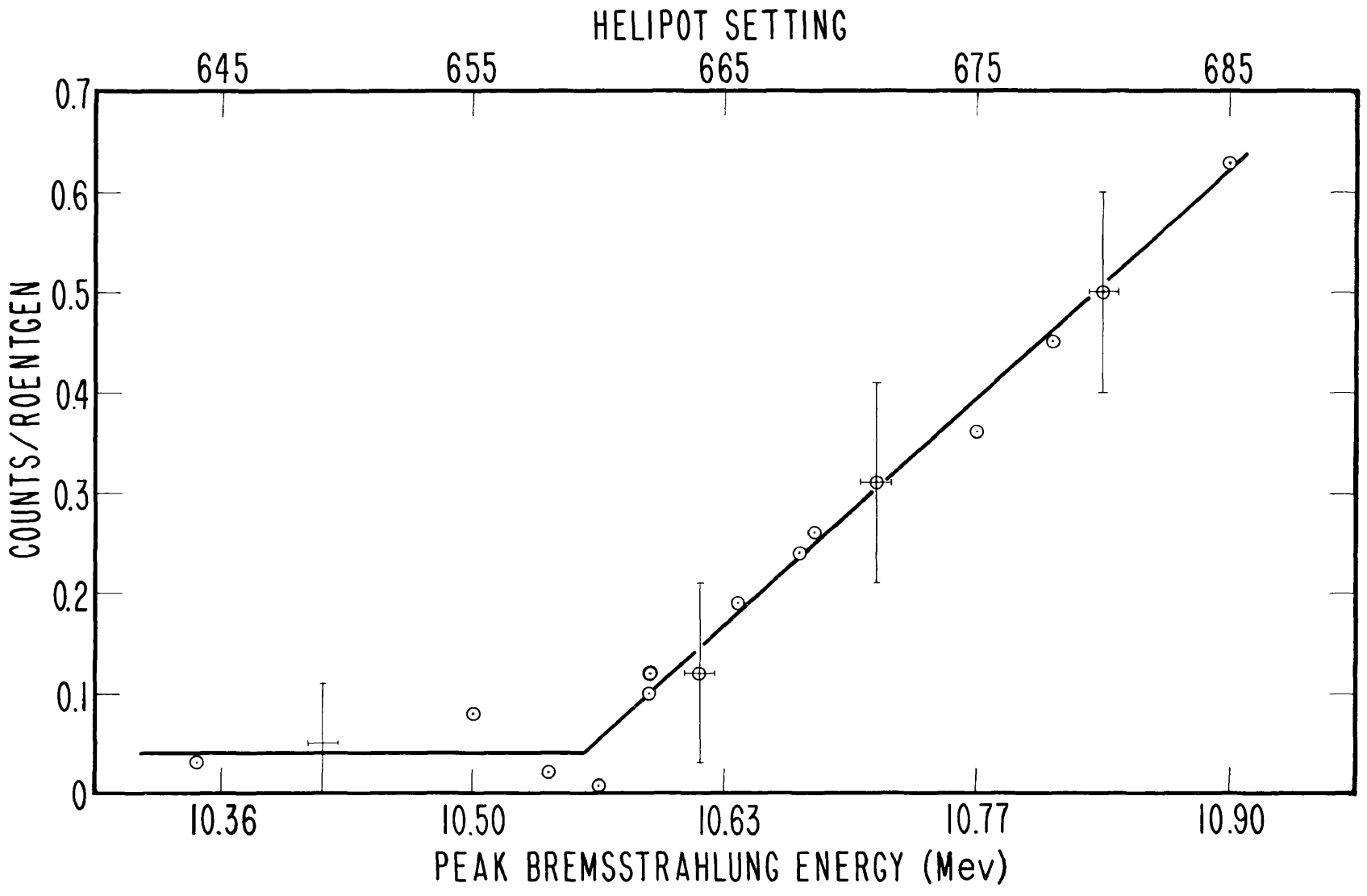

Fig. 27. N^{13} Activation Curve near Threshold.

TABLE 16. N^{14} Threshold Determination No. 2

Run No.	Helipot	Activity (c/r)
1087	668	0.06
1081	670	0.06
1061	672.5	0.14
1085	674.5	0.13
1057	675.5	0.20
1059	680	0.21
1076	680	0.24
1078	682.5	0.28
1051	684.5	0.33
1089	686	0.40
1080	687	0.41
1083	690	0.48
1049	690	0.40
1055	693	0.62

6.3 C^{12} Threshold Determination

In order to test the linearity of the energy scale determined by the thresholds of N^{14} and O^{16}, it was decided to investigate the photoneutron threshold of C^{12}, which could be accurately predicted from the mass data. Naturally occurring carbon consists of 98.9% of C^{12} and 1.1% of C^{13}. The only activity expected on irradiation is that of C^{11} with a half-life of 20 min. As a convenient solid material containing a high percentage of carbon by weight, polyethylene $(C_2H_2)_n$ was selected.[2] About 30 discs were machined to standard disc dimensions of 1.750 in. diameter and 0.125 in thick.

The decay curve of an irradiated polyethylene disc is shown in Fig. 28. The measured half-life was 21.0 min. in agreement with the value reported of 20.35 min. half-life for C^{11} (20).

The procedure employed was similar to that described in connection with the O^{16} and N^{14} thresholds. An irradiation time of 10 min. was used during which the sample received about 35,000 roentgens. The exposed discs were counted for 30 min. starting 1.5 min. after the irradiation.

The threshold data for C^{12} determination No. 1 are shown tabulated in Table 18. In column 3 are listed the activities corrected for cosmic-ray background. These activities were for a 20 min. interval beginning

---

[2] It was learned afterwards in a private conversation with Dr. H.W. Koch, who had previously investigated the C^{12} threshold, that polyethylene was the most suitable of the materials he had tried. Polyethylene had the smallest residual activity below threshold.

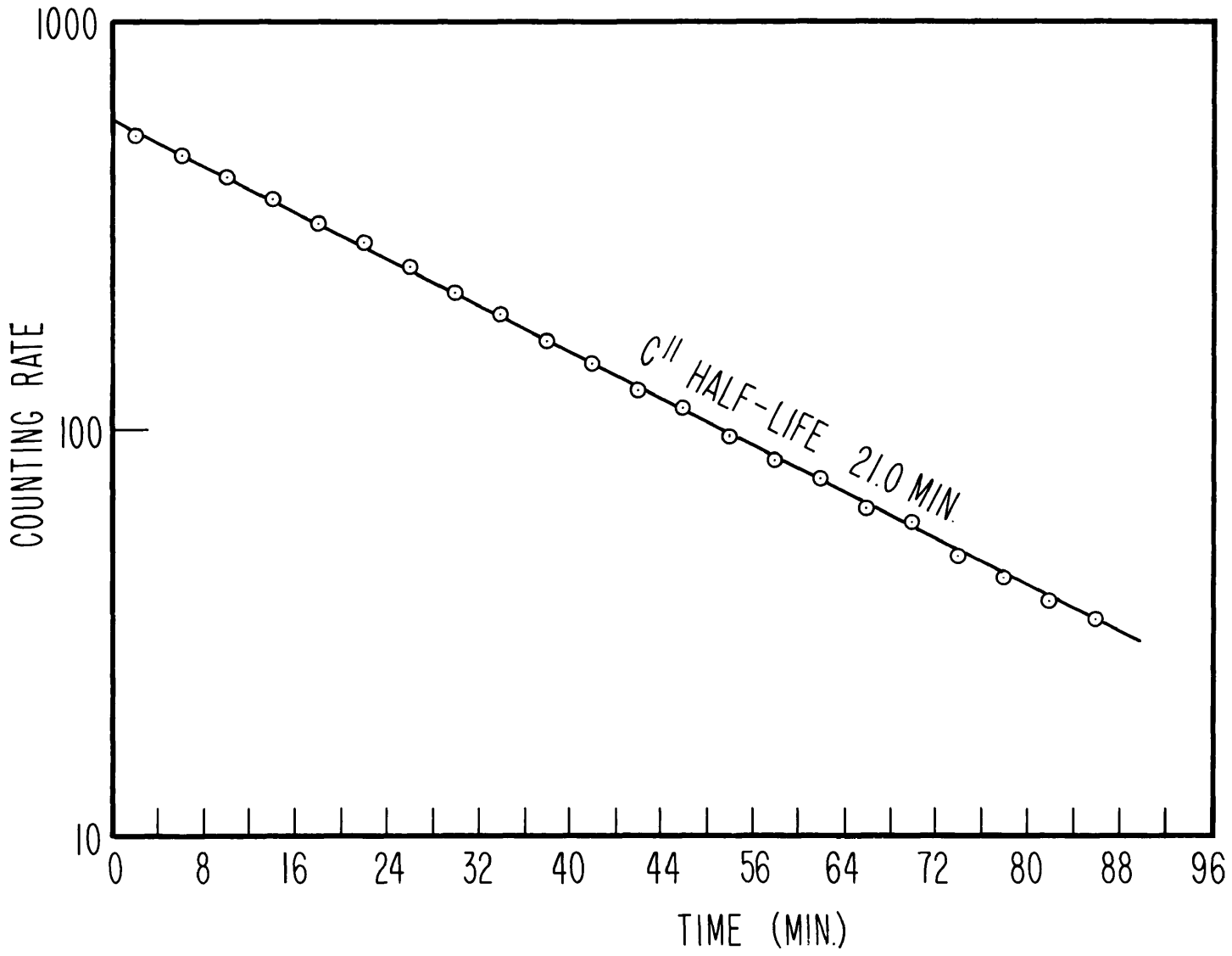

Fig. 28. C^{11} Decay Curve.

11.5 min. after the irradiation and corrected to an equivalent 6 min. irradiation (Sec. 4.3). The data of Table 18 is shown graphically in Fig. 29. The portion of the activation curve enclosed by the dashed line in Fig. 29 is shown on an expanded scale in Fig. 30. The threshold determined by inspection of Fig. 30 was 1232 $\pm$ 2 h.u. The data in the immediate neighborhood of threshold appear to be well represented by a straight line. This representation was good from helipot 1255 down to threshold (about 310 kev). As before, the threshold was determined by the intersection of this line with that determined by the points below helipot 1232. This was taken as the experimental definition of the photoneutron reaction in C^{12}.

The activation curve shown in Fig. 29 cannot be represented by a function of the form $Y = k(H-H_0)^x$ which holds for the 1-Mev interval shown. This result was similar to that obtained for the O^{15} and N^{13} activation curves.

The activity represented by the points below helipot 1232, the C^{12} threshold, was the strongest encountered in any of the determinations. This was not too surprising since the threshold of C^{12} occurs at about 18.7 Mev which is well above the photoneutron threshold for practically all other nuclei. Furthermore, the slope of the background points indicated an activity which was strongly energy dependent. In order to establish with greater certainty that helipot 1232 corresponded to the C^{12} threshold, a careful analysis of the half-lives of the activities represented by the points of Fig. 29 was instituted. The results are listed in Table 17 below.

TABLE 17. Half-lives of Polyethylene Discs near Threshold.

Helipot	Half-Life (min.)
1198	7
1209	11
1213	9
1219	11
1220	12
1225	13
1226	10
1228	13
1231	11
1234	14
1235	15
1236	16
1237	12
1239	18
1240	17
1243	16
1245	18
1248	15
1250	21
1252	22
1253	20
1254	19
1256	22
1259	20

A study of Table 17 indicated an activity below helipot 1232 with a half-life of approximately 10 min. and a sharp increase in the half-lives measured at helipot settings above 1232. The half-lives increased rapidly from 14 min. at 1234 to 20 min. at 1250. There could be little doubt that the sharp increase in activity at about helipot 1232 was due to the onset of the 20 min. C^{11} activity.

The residual activity below helipot 1232 was attributed to a very small nitrogen impurity giving rise to the 10 min. N^{13} activity. The cross-section for the photoneutron reaction in N^{14} increases steeply in the region between 18 - 20 Mev (22). This could account for the dependence of the residual activity on the peak x-ray energy.

The reason for counting the samples from 11.5 - 31.5 min. after irradiation rather than from 1.5 - 31.5 min. is now evident. The former counting interval discriminates more strongly against the 10 min. activity as compared to the 20 min. C^{11} activity.

The helipot settings of column 2, Table 18 have all been referred to a Cu control activity of 710 c/r with an estimated precision, in most cases, of $\pm$ 0.6 h.u. The data was gathered over an interval of approximately 1 week and 36 Cu control runs were obtained. These exhibited activities of 734 - 607 c/r or $\pm$ 3 h.u.

Not illustrated by means of figures are the results of C^{12} threshold determination No. 2, tabulated in Table 19. A 6 min. irradiation time and a 20 min. counting interval starting 1.5 min. after the exposure were employed. The activities listed in column 3, were obtained from

the counts accumulated in a 10 min. interval beginning 11.5 min. after the irradiation. As explained above, this counting interval discriminated against the interfering residual 10 min. activity. The threshold determined from the plot of the data of Table 19 was found to be 1243 ± 2 h.u. referred to a Cu control activity of 480 c/r. Sixteen control runs were obtained with a spread in activity of 516 - 466 c/r or ± 1.25 h.u.

6.4 Summary

The threshold determinations of the light nuclei C^{12}, N^{14} and O^{16} have several features in common. In all cases, the activation curves near threshold appeared to be linear functions of the peak x-ray energy. For carbon, this region extended from threshold to about 340 kev above, similarly for nitrogen, and for oxygen to about 480 kev above threshold.[3] In each case, the intersection of the straight line portion of the activation curve near threshold with the line determined by the points below threshold served to define experimentally the reaction threshold.

The activation curves for C, N and O over the measured intervals (0.8 Mev, 1.4 Mev and 2 Mev respectively) could not be represented by an expression of the form, $Y = k(H-H_0)^x$. Thus the shapes of the activation curves of the light nuclei were different from that of the medium weight nuclei of Cu^{63} and Ag^{109}.

---

[3] In a very recent piece of work, Haslam et al. (23) have found that the activation curve for the reaction $O^{16}(\gamma, n)O^{15}$ consisted of straight line regions with sharp breaks. These were taken to be levels in the O^{16} nucleus. The above results are consistent with these discoveries of the Saskatchewan group.

McElhinney et al. (3) found that the activation curves over a 3-Mev interval for all photoneutron reactions studied (including C^{12}, N^{14}, C^{63}) could be represented by a function, $Y = k(H-H_0)^2$. Sher et al. (10) found that over a 3-Mev interval, the activation curves could be represented by a function $Y = k(H-H_0)^x$ where the exponent, x, did not appear to be correlated with the characteristics of the nuclei. The present work seems to be in conflict with the previous work. However, it has to be pointed out that the previous investigations were so coarse that the shapes of the activation curves in the immediate neighborhood of threshold were never investigated. In the work of Sher et al. (10) the technique differed so drastically that perhaps comparison to the present work should not be attempted.

TABLE 18. C^{12} Threshold Determination No. 1

Run No.	Helipot	Activity (c/r)
1038	1287	8.45
1036	1276	5.80
1039	1272	4.71
1016	1265	3.25
1019	1264	3.46
1021	1259	2.84
1024	1256	2.20
981	1254	1.76
999	1253	2.08
1041	1252	2.03
1018	1250	1.94
1006	1250	1.82
1022	1248	1.46
1042	1245	1.45
1001	1245	1.34
961	1245	1.38
1025	1243	1.20
1003	1240	1.03
977	1240	1.01
982	1239	0.84
1028	1237	0.87
980	1236	0.93
985	1235	0.70
1005	1235	0.93
963	1235	0.74
1027	1234	0.75
1044	1234	0.75
1045	1231	0.56
1014	1228	0.59
965	1228	0.43
1010	1226	0.55
1032	1225	0.55
975	1220	0.38
987	1220	0.36
967	1219	0.27
1008	1213	0.28
969	1209	0.30
970	1198	0.16

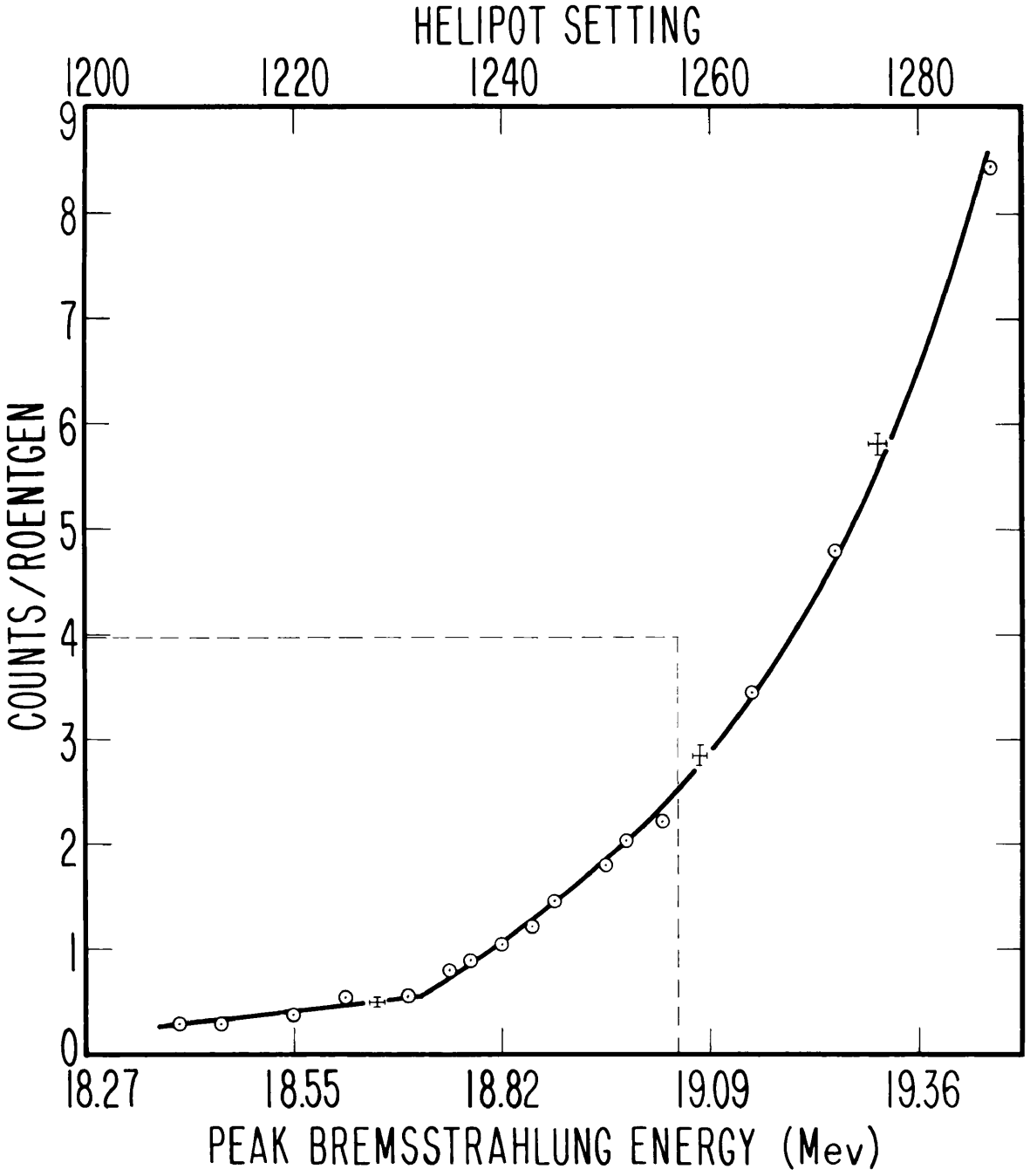

Fig. 29. C^{11} Activation Curve.

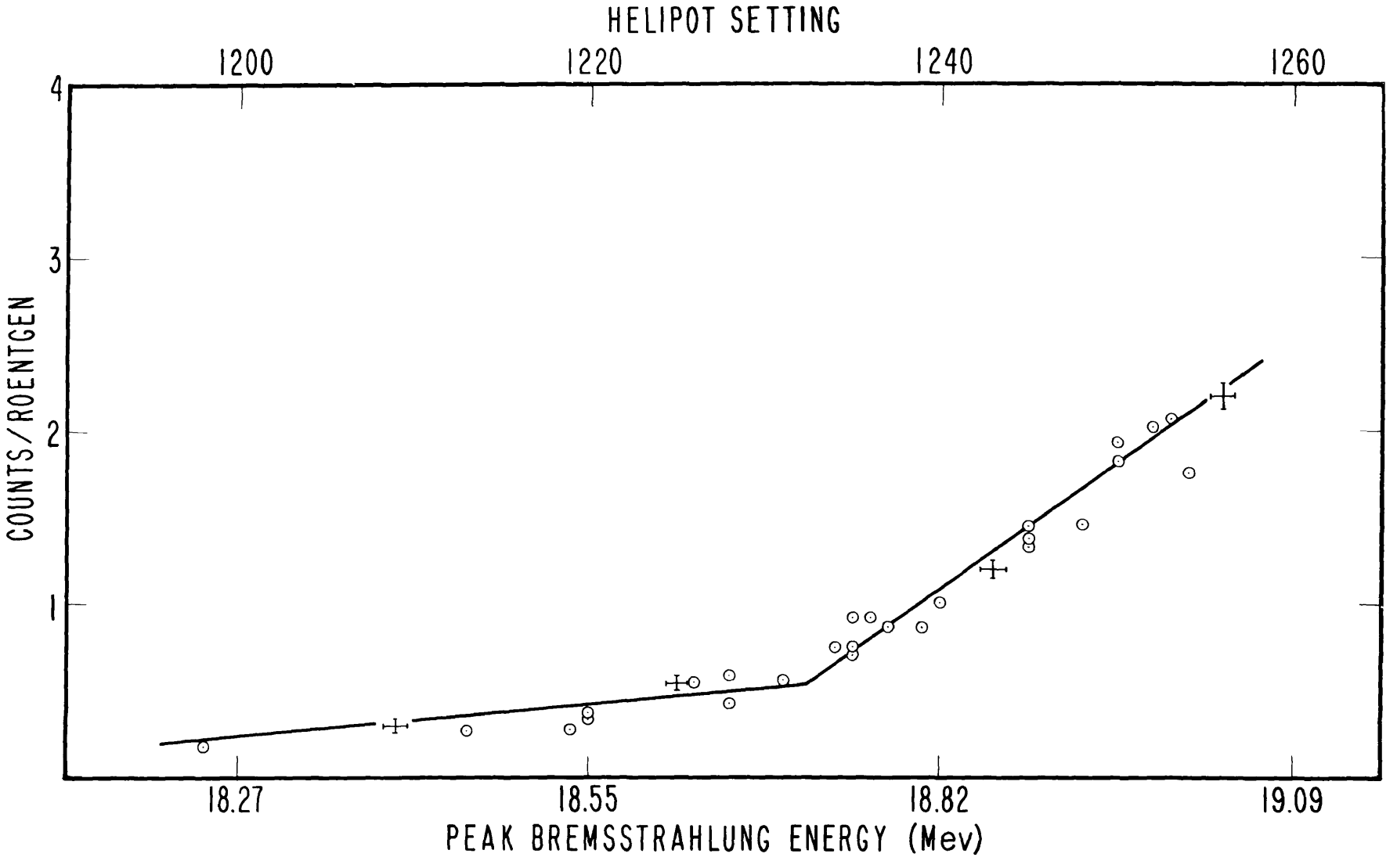

Fig. 30. C^{11} Activation Curve near Threshold.

TABLE 19. C^{12} Threshold Determination No. 2

Run No.	Helipot	Activity (c/r)
1155	1270	1.80
1156	1267	1.61
1255	1266	1.24
1152	1265	1.24
1041	1264	1.14
1305	1263	1.12
1154	1263	1.29
1254	1262	1.08
1253	1261	0.98
1252	1259	1.06
1158	1259	1.07
1240	1258	1.09
1145	1258	0.88
1042	1257	0.83
1241	1256	0.76
1243	1255	0.82
1303	1253	0.66
1244	1253	0.69
1150	1252	0.79
1245	1251	0.55
1144	1251	0.63
1247	1250	0.72
1248	1248	0.42
1302	1248	0.60
1148	1248	0.53
1159	1248	0.55
1249	1247	0.58
1147	1246	0.57
1306	1245	0.54
1250	1245	0.42
1045	1243	0.40
1151	1241	0.44
1307	1238	0.37
1032	1236	0.33
1309	1233	0.39

CHAPTER VII

EXPERIMENTAL RESULTS

7.1 Photoneutron Threshold Values of Cu^{63} and Ag^{109}

The method of calculating the threshold of the photoneutron reaction from the mass data will be illustrated by the following calculation for N^{14}. The reaction may be expressed

$$N^{14} + E_\gamma \longrightarrow N^{14*} \longrightarrow N^{13} + n \qquad (7\text{-}1)$$

where E is the photon energy and N^{14*} represents the excited N^{14} nucleus. The law of conservation of momentum requires the N^{14*} nucleus to have a momentum equal to the photon momentum, since the N^{14} nucleus initially can be considered at rest. As a result of this transfer of momentum, a kinetic energy is imparted to the N^{14*} nucleus equal to

$$E = p^2/2m = E_\gamma^2/2mc^2 \qquad (7\text{-}2)$$

where p is the photon momentum, m the mass of the nucleus and c the velocity of light. In general, the energy as computed by (7-2) for the case of particles as massive as nuclei will be small so that a very good approximation for the photon energy will be the value obtained from energy conservation considerations alone. From the mass data (energy conservation calculation) (21) the threshold energies for C^{12}, N^{14}, O^{16} were respectively 18.712 ± 0.03 Mev, 10.545 ± 0.02 Mev and 15.597 ± 0.01 Mev. Using the above values for the photon energy in (7-2) one obtains 0.016, 0.004 and 0.008 Mev for C^{12}, N^{14}, O^{16} respectively.

Adding these energies to the above, there result the following calculated threshold values: C^{12}, 18.728 ± 0.03 Mev; N^{14}, 10.549 ± 0.02 Mev; O^{16}, 15.605 ± 0.01 Mev.

The results of threshold determinations No. 1 for C^{12}, N^{14}, O^{16}, Ag^{109} and No. 2 for Cu^{63} were respectively 1232 ± 2, 659 ± 2, 1034 ± 1, 550 ± 1.5 and 662 ± 1.5 h.u. referred to a Cu control of 710 c/r. A linear energy scale can be determined using any pair of threshold values for the light nuclei. Here, nitrogen is always used as one of the pair since the thresholds to be determined were close to that of N^{14}. The results are summarized in Table 20 below.

TABLE 20. Thresholds Based on N^{14}, O^{16}, C^{12} Determinations No. 1.

Energy Scale Determination	Slope (kev/h.u.)	Thresholds (Mev)	
		Cu^{63}	Ag^{109}
N^{14}, O^{16}	13.5	10.59 ± 0.05	9.08 ± 0.07
N^{14}, C^{12}	14.3	10.59 ± 0.05	8.99 ± 0.07

The results of threshold determinations No. 2 for C^{12}, N^{14}, O^{16}, Ag^{109} and No. 3 for Cu^{63} referred to a Cu control of 480 c/r were respectively 1243 ± 2, 669 ± 2, 1040 ± 1, 562 ± 1 and 674 ± 1 h.u. Performing the same calculations as above, the results are shown in Table 21 below.

TABLE 21. Thresholds Based on N^{14}, O^{16}, C^{12} Determinations No. 2.

Energy Scale Determination	Slope (kev/h.u.)	Thresholds (Mev)	
		Cu^{63}	Ag^{109}
N^{14}, O^{16}	13.6	10.62 ± 0.05	9.09 ± 0.07
N^{14}, C^{12}	14.2	10.62 ± 0.05	9.03 ± 0.07

Although the respective threshold values quoted in Tables 20 and 21 have the same precision estimates, the results in Table 21 are considered to be somewhat more reliable than those of Table 20. The total spread in the values of the Cu control activity was 516 - 466 c/r or $\pm$ 0.017 Mev for the determinations of C^{12}, N^{14}, O^{16} and Cu^{63} so that corrections for shift of the peak x-ray energy was not required. The Ag^{109} threshold was referred to a Cu control of 520 c/r and was normalized to a Cu control of 480 c/r, the correction amounting to 0.027 Mev. In the cases of Cu^{63} and Ag^{109}, the corrections to the threshold values computed from equation (7-2) amounted to 1.0 and 0.4 kev respectively and were therefore neglected.

The fact that the slope was different (Tables 20 and 21) using N^{14} and O^{16} from that determined by N^{14} and C^{12} was an indication of a non-linearity in the relationship between helipot setting and peak x-ray energy. This non-linearity amounted to approximately 4% defined as the difference in slopes divided by the average slope. This non-linearity did not affect the threshold determination for Cu^{63} because its threshold is so

close to that of N^{14}. However, in the case of Ag^{109}, it results in a greater uncertainty in the threshold determination. The average value for the threshold of Ag^{109} was found to be 9.07 ± 0.07. This figure reflects the fact that more weight was given to the determinations using N^{14} and O^{16} than to those of N^{14} and C^{12}. This was reasonable since the N^{14} and O^{16} calibration points are closest to the threshold of Ag^{109}. The average value for the threshold of Cu^{63} was found to be 10.61 ± 0.05 Mev. A comparison of the threshold values obtained in this thesis as compared with those of other investigators is shown in Table 22 below.

TABLE 22. Cu^{63} and Ag^{109} Threshold Values.

Observer	Notes	Threshold Values (Mev)	
		Cu^{63}	Ag^{109}
Baldwin & Koch (2)		10.9 ± 0.3	9.3 ± 0.5
McElhinney, et al. (3)	Compared to N^{14}	10.8 ± 0.2	
McElhinney, et al. (3)	Aver. of 2 diff. methods (Sec. 1.5)	10.9 ± 0.2	
Sher, et al. (10)		10.85 ± 0.2	9.05 ± 0.2
Birnbaum		10.61 ± 0.05	9.07 ± 0.07

Thus, the high precision determination of the present work is in fair agreement with that of other observers and is lower, as might be expected from the improvement in precision. This determination indicates that the best value for the Cu^{63} threshold is about 0.3-Mev less

than the value in common use of 10.9 Mev. This suggests that all of the threshold determinations (3, 4) which used Cu^{63} as a calibration point at 10.9 Mev are likely to contain values which are high by about 0.3 Mev.

All of the figures showing activation curves have the activity plotted both against helipot setting and peak x-ray energy. The peak x-ray energy scales were obtained by taking the threshold values given in Table 22 for Cu^{63} and Ag^{109} and those calculated for N^{14}, O^{16} and C^{12} and using a slope of 13.6 kev/h.u.

7.2 Proof of Method of Cu Control Activity

A method of testing the absolute validity of the helipot correction method based upon the Cu control activity (described in Section 3.7) was afforded by the existence of two groups of threshold determinations; one obtained with a Cu control in the neighborhood of 710 c/r and the other with a control of 480 c/r. The method consists in comparing the change in threshold predicted by the Cu control data with the measured threshold changes. The comparison is tabulated in Table 23 below.

TABLE 23. Validity of Method of Cu Control Activity.

Nucleus	Threshold h.u.	Cu Control (c/r)	Predicted Diff. in Threshold (h.u.)	Actual Diff. in Threshold (h.u.)
Cu^{63}	674	480	4.8	5
Cu^{63}	669	565		
Ag^{109}	560	520	8.0	9
Ag^{109}	551	680		
N^{14}	669	480	11.5	10
N^{14}	659	710		
O^{16}	1040	480	11.5	6
O^{16}	1034	710		
C^{12}	1243	480	11.5	11
C^{12}	1232	710		

The first 3 sets of data offer the most significant proof of the method since the non-linearity of the scale will be insignificant over so small a range. It is evident that the numbers in column 4 and column 5 of the above table are in excellent agreement and thus establish the method with a precision of about 0.9 h.u. It is clear that this error is due mainly to uncertainties in the threshold measurements most of which were determined to within 1 - 2 h.u. On a relative basis the helipot correction method based on the Cu control activity can be expected to be much more precise. In fact, consideration of the results of Section 3.6 indicate a precision of the order of $\pm$ 0.2 h.u.

7.3 Non-linearity of the Energy Scale

There are many factors which could contribute to a non-linearity

in the helipot setting versus peak x-ray energy curve. Among these, two of the more likely hypotheses were: a time delay between the instant that electron orbit expansion is supposed to occur and the time at which it actually occurs, and the possibility of a phase shift between the flux integrator amplifier input signal and the magnetic field. Either of these effects (singly or together) could produce a non-linearity. If it is supposed that a constant time delay exists in the electron beam expansion process, then it is clear that the energy of the electrons will change during this time by an amount depending on the rate of change of magnetic flux at the time of expansion.

An experiment was performed in order to determine the presence of such effects. If a set of runs is taken at a constant helipot setting, but at different settings of the peak magnet amplitude, it is evident that this corresponds to expanding the beam at different values of rate of change of magnetic flux. An additional complication is present in that the response of the integrator amplifier may also be dependent on the rate of change of voltage at the voltage level (helipot setting) at which orbit expansion is called for.

The results of such an experiment are shown in Fig. 31. The ordinates are the activity (c/r) induced in Cu at helipot setting 730 plotted as a function of peak magnet amplitude (Mev). The change from an amplitude of 11 Mev to 21 Mev is equivalent to a shift in the peak x-ray energy of about 22 h.u. (300 kev). It was found that these results were consistent with the assumption of a constant time delay. However, when

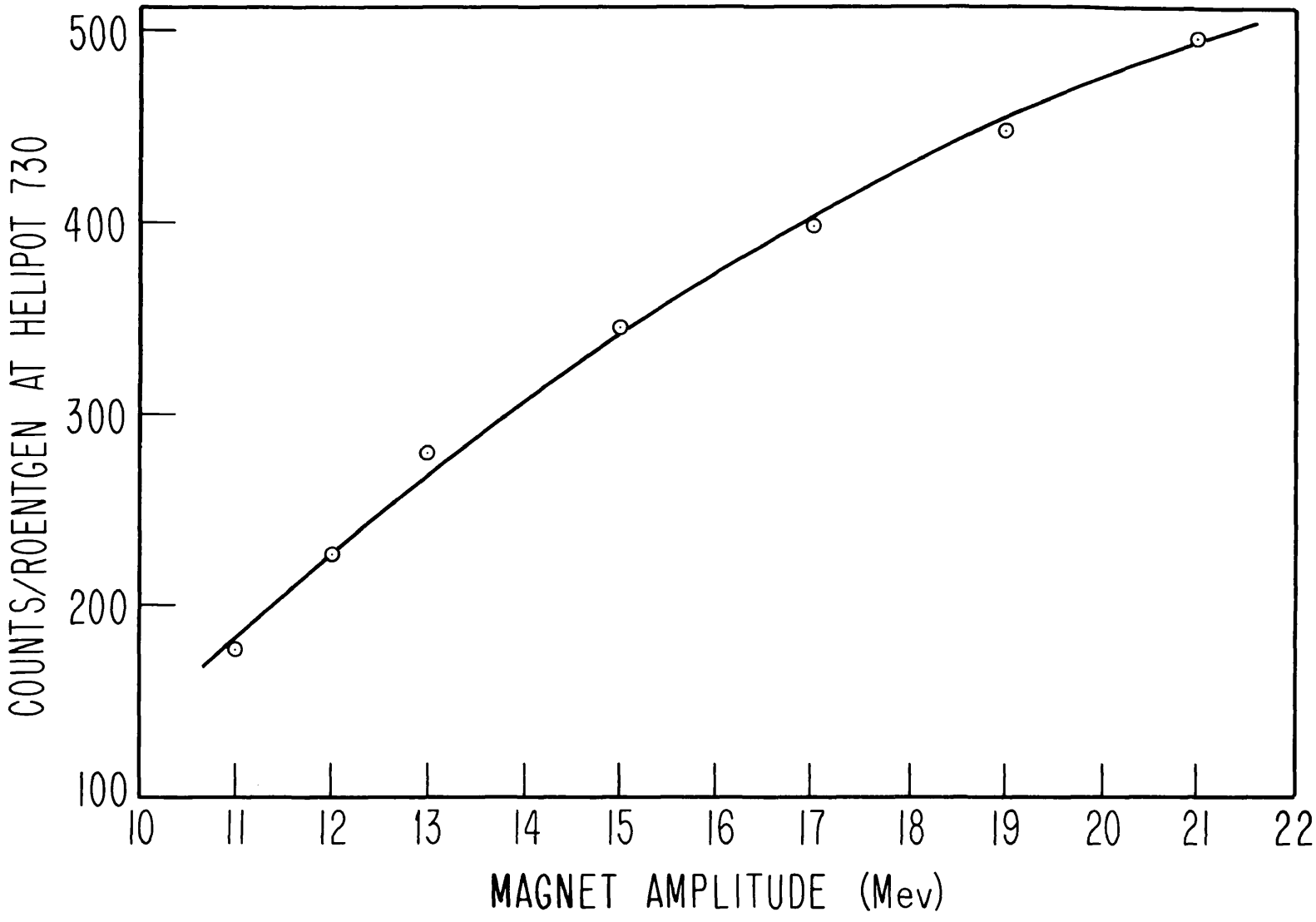

Fig. 31. Effect of Magnet Amplitude on Cu Activity at Fixed Helipot Setting.

a correction based upon these results was applied to the calibration points for the energy scale, the resulting scale possessed a non-linearity which was roughly the same as that which it had originally. It therefore appeared that the above considerations would not resolve the scale non-linearity.

One important conclusion of immediate consequence could be obtained from this experiment, namely, the degree to which the magnet amplitude must be held constant in order to eliminate this as an effect causing fluctuations in the peak x-ray energy. Reference to Fig. 31 shows that in the neighborhood of magnet amplitude 21 Mev, a 1-Mev change in the magnet amplitude can produce a change in the peak x-ray energy of 2 h.u. (28 kev). Thus if a stability of the order of $\pm$ 0.2 h.u. is desired, the magnet amplitude must be held constant to within $\pm$ 0.1 Mev. An electronic circuit has not been constructed with which precise regulation of the magnet amplitude can be achieved automatically.

7.4 Summary

New values have been obtained for the photoneutron thresholds of Cu^{63} and Ag^{109} which are considerably more reliable than previous determinations. The accurate determination of the Cu^{63} threshold is of particular importance because of the widespread use of this threshold as a substandard for the calibration of betatron energy scales. The new value of 10.61 $\pm$ 0.05 Mev is found to be approximately 0.3 Mev below the previously accepted value of 10.9 $\pm$ 0.2 Mev. It is suggested that those thresholds which have been determined relative to a scale based on

the Cu^{63} threshold at 10.9 Mev (about 38 threshold values) may be high by about 0.3 Mev.

It is necessary to remark that the precision with which thresholds have been determined in this experiment were in most cases of the order of ± 1 h.u. (14 kev). If the mass of the parent nucleus were known with great precision, then the mass of the daughter nucleus could be obtained with a precision of ± 0.000015 a.m.u. based upon a threshold determination of ± 1 h.u. This precision is comparable to the best precision by which masses of light nuclei can be measured by other methods. The precision of the measurement is independent of the weight of the nucleus involved.

It has been found that the scale determined by using the fixed points of N^{14}, O^{16} and C^{12} exhibited a non-linearity of about 4%. Experiments performed to determine the cause of the scale non-linearity have shown a dependence of the activity induced in Cu at a fixed helipot setting of 730 on the magnet amplitude. This effect appeared explicable in terms of the assumption of a constant delay in the expansion process. When a correction, based upon these data, was determined and applied to the calibration points, the resulting energy scale still exhibited a non-linearity of approximately the same magnitude. However, the effect of magnet amplitude on peak x-ray stability indicated the need for precise stabilization of the peak magnet amplitude, if very stable control of the peak x-ray energy is required.

It was shown by using two independent sets of threshold measurements

which were referred to different Cu control activities, that the method of monitoring the peak x-ray energy based on the Cu control activity has an absolute validity. The precision of this method was about ± 0.9 h.u. which is to be expected from the precision with which thresholds can be measured. On a relative basis the Cu control activity correction method should be valid to about ± 0.2 h.u. (about 3 kev).

APPENDIX I

ENERGY CONTROL OF A 22 MEV BETATRON

In a betatron, the acceleration of electrons is governed by Faraday's Law:

$$\oint \vec{E}\cdot\vec{dl} = -\frac{1}{c}\iint \frac{\partial \vec{B}}{\partial t}\cdot\vec{ds} \qquad \text{(I-1)}$$

Namely, the changing magnetic flux through the surface bounded by the electron orbit produces an electric field at the orbit. The energy gain per turn is

$$e\oint \vec{E}\cdot\vec{dl} = \frac{e}{c}\iint \frac{\partial \vec{B}}{\partial t}\cdot\vec{ds} = \frac{e}{c}\frac{\partial \Phi}{\partial t} \qquad \text{(I-2)}$$

where e is the electronic charge and $\Phi = \iint \vec{B}\cdot\vec{ds}$. If the electron moves with approximately the velocity of light, c, which is the case for all energies in excess of 1 Mev, then the time occupied by one cycle is $dt = 2\pi r/c$. The energy gain per second is

$$\frac{dW}{dt} = \frac{c}{2\pi r}\frac{e}{c}\frac{d\Phi}{dt} = \frac{e}{2\pi r}\frac{d\Phi}{dt} \qquad \text{(I-3)}$$

where W is the energy of the electron and r is the orbit radius. Integrating equation 3, there results

$$W = \frac{e}{2\pi r}\Phi \qquad \text{(I-4)}$$

taking W = 0 when $\phi = 0$. Equation 4 states that the instantaneous energy of the electrons is proportional to the flux passing through the surface bounded by the electrons.

The betatron magnet is operated well below saturation so that ϕ and B are proportional to I_m, the magnetizing current. It is assumed that B and hence ϕ are approximately in phase with I_m. The magnet coils are almost entirely reactive so that the voltage across the magnet coils leads by almost 90^o the current through the coils. If some method is used which taps and integrates this voltage, a signal is obtained which is in phase with I_m and hence ϕ and is proportional to the instantaneous electron energy. Use of a tapped integrated voltage, V_c as a measure of the electron energy implies a strict proportionality between V_c and ϕ. It is possible that the warm-up of the betatron magnet may cause small changes in this proportionality. However the calculation of this effect is at present beyond our means and for the purposes of this analysis, the strict proportionality between V_c and ϕ will be assumed. A circuit which provides a signal in phase with ϕ, is simply an integrator, namely, a large resistance in series with a capacitance (See Fig. 32).

The voltage V_c, whose magnitude is proportional to the instantaneous electron energy, serves as the input signal for the integrator amplifier. The first stage of the integrator amplifier consists of a cathode follower. The bias level of this stage is determined by the setting of the helipot energy control. Thus, the helipot sets the bias level of the cathode follower at some fraction of the standard reference voltage. In the NRL circuit, a fraction of the standard reference voltage was compared to that

of a Weston Standard Cell (Section 2.5). The output of the cathode follower is coupled to the initial stage of a d.c. coupled amplifier by means of a vacuum tube diode clamping circuit. In order for a signal to appear on the grid of the d.c. amplifier, it was necessary to raise the cathode voltage of the initial cathode follower to a leval which would just unclamp the diode. At this point, a signal appears on the grid of the first stage of the d.c. amplifier.

The basis of the energy control system is that a unique correspondence is established between the helipot setting and the magnitude of the input voltage which unclamps the diode. According to the above discussion, to this voltage there corresponds a definite electron energy and therefore a definite peak x-ray energy.

The signal which appears on the grid of the first stage of the d.c. coupled amplifier is amplified by a factor of about 100 and then used to trigger a multivibrator which, in the NRL circuit, is used to trigger a 2050 thyratron circuit similar to that of Fig. 8. The output pulse of the 2050 thyratron is used to trigger the high voltage 5C22 thyratron in the expander circuit. The expander system is shown in block diagram form in Fig. 33. A more detailed account of the peak x-ray energy control circuits will be found in (15).

In the block diagram of Fig. 33, is shown a connection between the trigger generator for the injector and the integrator amplifier. It was found that as a result of stray coupling between the injector and expander circuits, a signal was introduced into the integrator amplifier coincident

with the 60 kev injector pulse. This signal resulted in a triggering of the expander system with a consequent loss of the electron beam. In order to suppress this effect, a signal from the 2050 thyratron injector trigger circuit of Fig. 8 was applied to the multivibrator of the integrator amplifier which effectively blocked its operation during the time of injection. This eliminated the triggering of the expander system by the 60 kev injector pulse.

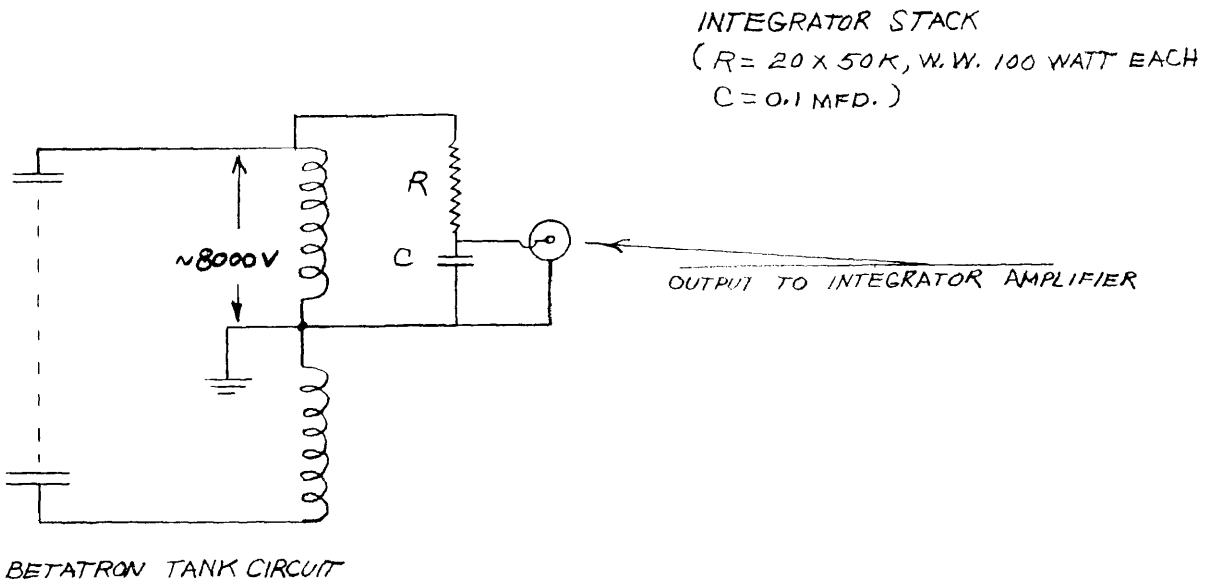

Fig. 32. Flux Integrator Stack Arrangement.

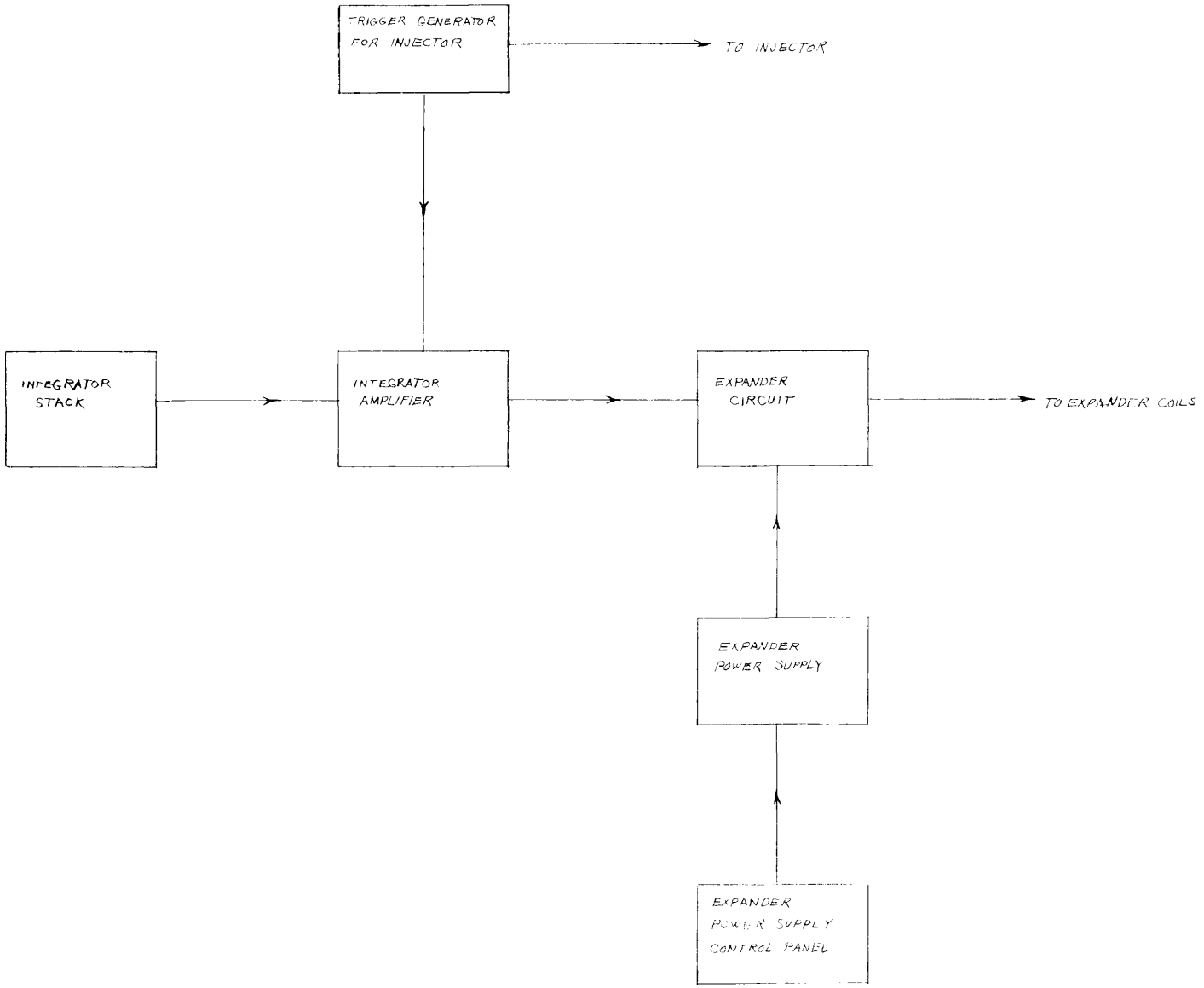

Fig. 33. Block diagram of Expander System.

LITERATURE CITED

1. J. A. Harvey, Phys. Rev. 81, 353 (1951).

2. G. C. Baldwin and H. W. Koch, Phys. Rev. 67, 1 (1945).

3. McElhinney, Hanson, Becker, Duffield and Diven, Phys. Rev. 75, 542 (1949).

4. Hanson, Duffield, Knight, Diven and Palevsky, Phys. Rev. 76, 578 (1949).

5. H. Palevsky and A. O. Hanson, Phys. Rev. 79, 242 (1950).

6. W. E. Ogle and R. E. England, Phys. Rev. 78, 63 (1950).

7. Ogle, Brown and Carson, Phys. Rev. 78, 63 (1950).

8. R. W. Parsons and C. H. Collie, Proc. Phys. Soc. A63, 839 (1950).

9. Parsons, Lees and Collie, Proc. Phys. Soc. A63, 915 (1950).

10. Sher, Halpern and Mann, Phys. Rev. 84, 387 (1951).

11. M. G. Mayer, Phys. Rev. 74, 235 (1948).

12. L. Katz and J. Goldemberg, post-deadline paper presented at the Washington meeting of the American Physical Society, May 1, 1953.

13. D. W. Kerst, Phys. Rev. 60, 47 (1941).

14. D. W. Kerst, Rev. Sci. Instr. 13, 387 (1942).

15. Katz, McNamara, Forsyth, Haslam and Johns, Can. J. Res. A28, 113 (1950).

16. H. W. Koch and R. E. Carter, Phys. Rev. 81, 815 (1951); Motz, Miller and Wyckoff, Phys. Rev. 89, 968 (1953).

17. E. Pollard and W. L. Davidson, Jr., Applied Nuclear Physics, (John Wiley & Sons, Inc., New York, 1942), p. 228.

18. Seren, Tobin and Burgess, "A Simple Reliable Direct-Current Amplifier" NRL Reprint No. 80-52.

19. W. A. Higinbotham and S. Rankowitz, Rev. Sci. Instr. 22, 688 (1951).

20. K. Way et al., "Nuclear Data", National Bureau of Standards Circular 499.

21. Li, Whaling, Fowler and Lauritsen, Phys. Rev. 83, 512 (1951).

22. Johns, Horsley, Haslam and Quinton, Phys. Rev. 84, 856 (1951).

23. Haslam, Katz, Horsley, Cameron and Montalbetti, Phys. Rev. 87, 196A (1952).

VITA

Milton Birmbaum

314 Livingston Terrace, S.E.
Washington 20, D. C.

Degree to be conferred: Ph.D. 1953

Date of birth: November 27, 1920

Secondary education: Tilden High School, Brooklyn, New York

Collegiate Institutions attended:	Dates:	Degree:	Date of Degree:
Brooklyn College	1938-42	A.B.	1942
University of Maryland	1946-53	M.S.	1948

Publications:

1. A Method for the Measurement of the Ionization and Deionization Times of Thyratron Tubes, Milton Birnbaum, T.A.I.E.E., 67, 209 (1948)

2. Prebunching: A Method Controlling Synchrotron Radial Oscillation Amplitudes, D.C. dePackh and Milton Birnbaum, J. Appl. Phys. 19, 795 (1948)

3. Theory of the Capture Process in a Betatron-Injected Synchrotron, D.C. dePackh and Milton Birnbaum, Rev. Sci. Inst. 21, 451 (1950)

4. Shape of Cosmic-Ray Star-Size Distributions in Nuclear Emulsions, Milton Birnbaum, M.M. Shapiro, B. Stiller, F.W. O'Dell, Phys. Rev. 86, 86 (1952)

Present position: Physicist, Nucleonics Division, Naval Research Laboratory, Washington 25, D. C.